MASTER THESIS

TRANSVERSE PRESSURE DEPENDENCE OF THE CRITICAL CURRENT IN EPOXY IMPREGNATED REBCO ROEBEL CABLES

Simon Otten

FACULTY OF SCIENCE AND TECHNOLOGY
CHAIR OF ENERGY, MATERIALS AND SYSTEMS (EMS)

EXAMINATION COMMITTEE
Dr. M.M.J. Dhallé
Dr. J.W.J. Verschuur
Prof. dr. ir. H.J.M. ter Brake

DOCUMENT NUMBER
-

UNIVERSITY OF TWENTE.

10-10-2014

Contents

Chapter 1

Introduction

1.1 Superconducting accelerator magnets

In circular particle accelerators such as CERN's Large Hadron Collider (LHC) and Tevatron, charged particles are accelerated to speeds close to the speed of light and collided. The collision creates many elementary particles which are analysed using particle detectors. Particle colliders such as these have been very important for research in high energy physics.

During acceleration, the particles are stored in a ring of magnets: The magnetic field results in a Lorentz force perpendicular to the travelling direction, keeping the particle beam in a circular orbit. The maximum energy of a particle stored in such a ring is limited by the magnetic field strength and by the radius of the ring. To achieve higher energies, very large accelerator rings have been constructed, of which the LHC is the biggest with a circumference of 27 km. On the other side, increasingly more powerful accelerator magnets are being developed. Here the use of superconducting materials has been crucial. When cooled below a certain critical temperature, these materials have zero resistivity and can carry currents without dissipation. The use of superconductors has been the only way to build magnets capable of fields well above 1 T, while keeping the cost and power consumption at an acceptable level.

In table 1.1, the most common superconducting materials and their critical temperatures are shown. NbTi and Nb_3Sn are "low-temperature" superconductors (LTS) and need to be cooled using liquid helium (T = 4.2 K). For a long time, these were the only materials that were used in superconducting devices on a large scale. More recently, materials with higher critical temperatures were discovered. *RE*BCO, Bi-2212 and Bi-2223 have a critical temperature above the boiling point of liquid nitrogen (T = 77 K) and are called "high-temperature" superconductors (HTS).

Material	T_c [K]	Discovery
NbTi	9	1962
Nb_3Sn	18	1954
MgB_2	39	2001
*RE*BCO	93	1987
Bi-2212	95	1988
Bi-2223	108	1988

Table 1.1: The most common superconductors, their critical temperatures and year of discovery.

The current that a superconductor can carry without dissipation has an upper limit, the critical current. Above this limit, the resistivity starts to increase. The critical current strongly increases with decreasing temperatures. For this reason, devices where a high current density is needed, such as high-field magnets, are cooled to T = 1.9 - 4.2 K using liquid helium, even if their critical temperatures are much higher.

Besides temperature, the critical current depends on the magnetic field. In figure 1.1, the critical current densities of several superconducting wires are shown as a function of the magnetic field. For practical applications, a current density of at least 400 A/mm^2 is needed [1]. This means that, at 4.2 K, the maximum field of a LTS magnet is limited to 9 - 10 T for NbTi and 17 - 18 T for Nb_3Sn. In order to achieve even stronger magnetic fields, HTS need to be used. Especially *RE*BCO conductors are promising, because they can carry a sufficient current density even in fields of 30 T and higher.

The magnets currently in use in the LHC storage ring are made of NbTi and have a maximum field of 8.3 T. There are plans to upgrade these magnets. A luminosity upgrade "High Luminosity LHC" is planned for 2020. In this project, part of the magnets will be replaced by 11 - 13 T Nb_3Sn magnets. For the more distant future (2030), a replacement of the entire ring by 20 T magnets is under consideration, the "High Energy LHC" [3]. Such magnets can only be realised with HTS materials. Alternatively, a new circular 80-100 km long tunnel may be built. This project is called the Frontier Hadron Collider (FHC) [4]. The accelerator magnets in this machine would be made of Nb_3Sn or HTS cables and generate 16 or 20 T.

In the coming years, a HTS demonstration magnet is to be built at CERN in the frame of the EuCARD-2, which stands for "Enhanced European Coordination for Accelerator Research & Development" [5]. The aim is to generate a 5 T field standalone, and 17 T in a 13 T background field. This magnet will likely be built from *RE*BCO-based conductors in a Roebel cable configuration. This type of conductor and cable is explained in the next section.

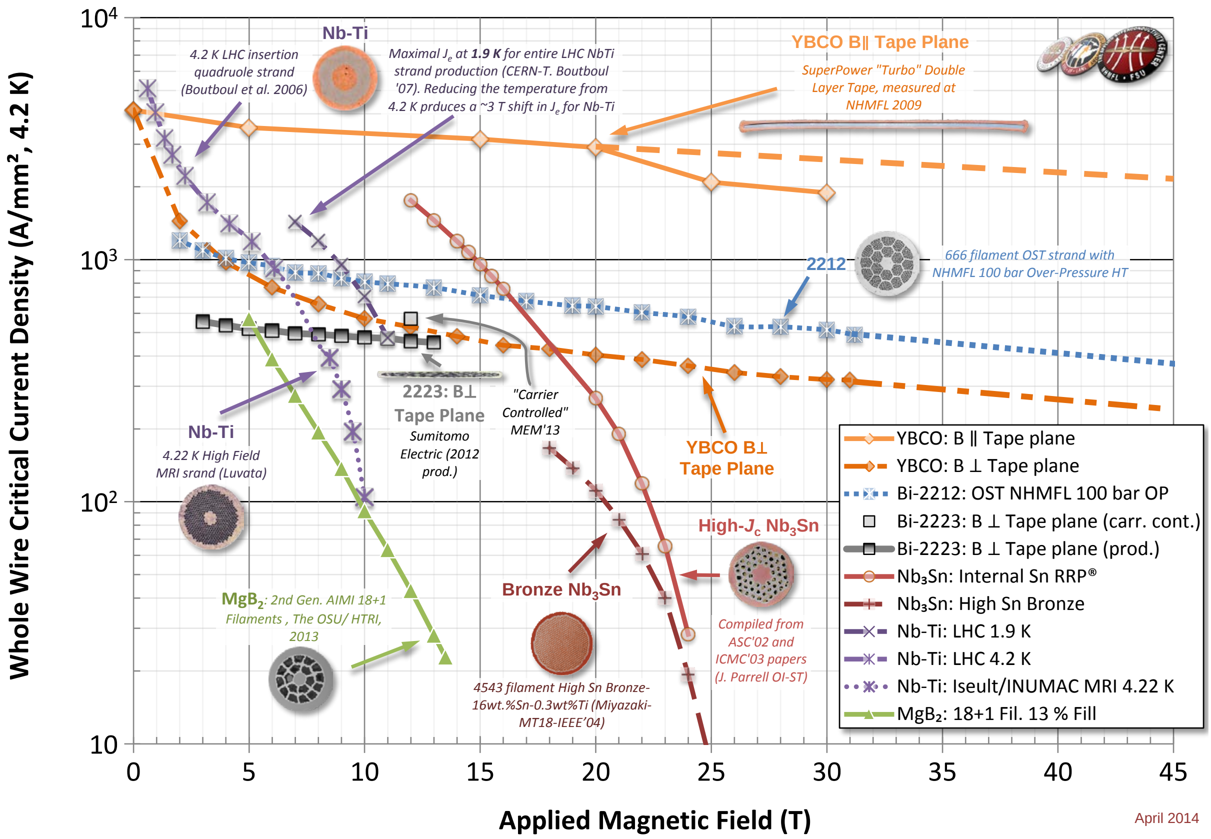

Figure 1.1: Engineering (whole wire) critical current densities of different superconducting wires at liquid helium temperatures (1.9 - 4.2 K). In strong magnetic fields, the high-temperature superconductors YBCO and Bi-2212 have the highest current densities. Chart by J. Lee [2].

1.2 *RE*BCO tapes and Roebel cables

*RE*BCO is short for Rare-Earth metal Barium Copper Oxide. It is a class of high-temperature superconductors that includes compounds with different rare-earth metals. Superconductivity above 77 K was observed for the first time in $Y_{1.2}Ba_{0.8}CuO_4$, with a critical temperature of 93 K [6]. The critical current of polycrystalline *RE*BCO, however, was initially very low due to weak links at the grain boundaries. A grain misalignment more than a few degrees strongly decreases the critical current [7]. Because of this, the powder-in-tube process is not suitable for *RE*BCO, as in that case the micro-structure is only slightly textured. Better alignment of the grains has been achieved by depositing *RE*BCO on a textured substrate [8]. Such coated conductors have been commercially available since around 2005 with increasing length and quality.

Figure 1.2 shows a cross-section of a typical *RE*BCO tape produced by SuperPower, which is also used in all experiments described in this report. The base of the tape is a 50 µm thick

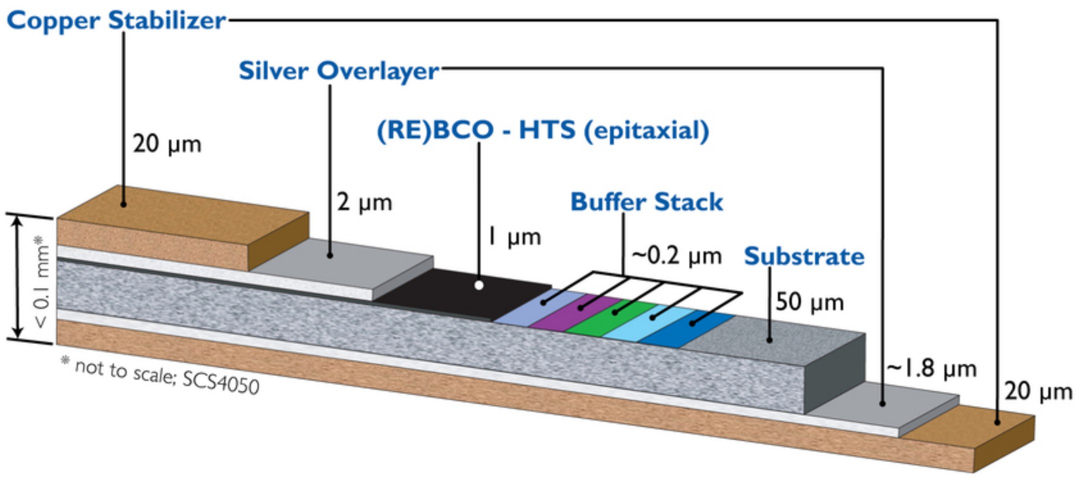

Figure 1.2: Cross section of a *RE*BCO coated conductor from SuperPower. Image by SuperPower [9].

Hastelloy substrate, a strong alloy that provides the mechanical strength. On this substrate a stack of buffer layers is deposited. The key element of the buffer is a biaxially textured layer of MgO, which is deposited using ion beam assisted deposition (IBAD). This textured layer ensures good alignment of the *RE*BCO grains that are epitaxially grown on top of it. Next, silver and copper layers are added to provide chemical protection and increase the thermal stability. The resulting tapes typically are 4 - 12 mm wide and 0.1 mm thick. The production process at SuperPower is described in more detail in [10].

Magnets for big particle accelerators and AC applications (transformers and generator armatures) cannot be wound from a single wire. A large number of turns would be needed, resulting in a prohibitively high self-inductance. Such a magnet could be ramped only slowly and under high voltage, and this would complicate safe shut-down after a quench. Instead, the magnet needs to be constructed from high-current cables consisting of 20 to 1000 wires and a smaller number of turns [11]. Cabling methods for round superconducting wires are well developed. Unfortunately, these techniques cannot be applied to *RE*BCO tapes because of their flat shape.

In figure 1.3 three of the most promising cabling architectures for *RE*BCO tapes are shown:

- The Twisted-Stacked Tape Cable (TSTC) was first proposed at the Massachusetts Institute of Technology. Like the name says, it is a stack of *RE*BCO tapes that is subsequently twisted. The tapes can be soldered together to improve the mechanical and thermal stability [12].

- The Conductor on Round Core (CORC) is developed and commercialised by Advanced Conductor Technologies. *RE*BCO tapes are wound onto a copper or aluminium cylindri-

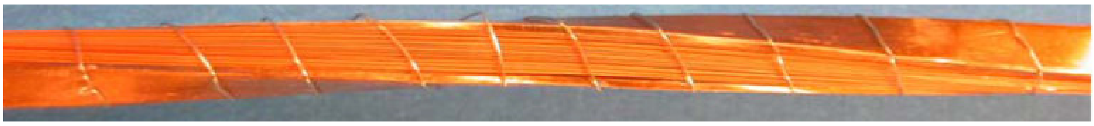

Twisted stacked-tape cable (TSTC) [12]

Conductor on round core (CORC) [13]

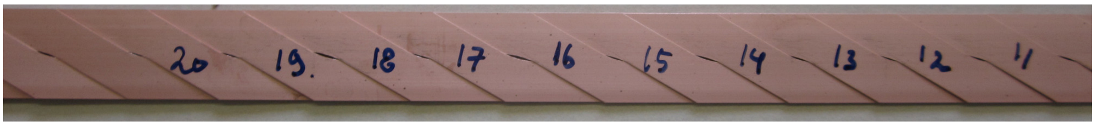

Roebel assembled coated conductor (RACC)

Figure 1.3: Different cables made of *RE*BCO coated conductors that have possible applications in high-field magnets.

cal former. Multiple layers can be added for higher currents [14].

- The Roebel Assembled Coated Conductor cable (RACC) is developed at Karlsruhe Institute of Technology [15] and at Industrial Research Ltd [16]. *RE*BCO tapes are punched into a meandering shape and assembled into a cable.

These cable concepts are still relatively new and a significant effort is ongoing to investigate their relative merits and drawbacks. Roebel cables have several advantages which make them an interesting candidate for AC applications and accelerator magnets: Unlike TSTC and CORC type cables, the Roebel cable is fully transposed. In other words, all strand of the cable are equivalent, in the sense that they experience the same magnetic field along their length. This ensures a homogeneous current distribution among the strands which is essential for the field homogeneity of accelerator magnets. Secondly, Roebel cables are densely packed, especially compared to CORC cables, resulting in a high engineering current density. Multiple Roebel cables can be efficiently stacked in a winding pack due to their flat shape. Another advantage is high mechanical flexibility for bending in the soft direction (out-of-plane), similar to single tapes (see chapter 5). On the other hand, in-plane bending of the cable is possible only for large bending radii.

The magnetic field dependence of the critical current of *RE*BCO tapes is highly anisotropic: a magnetic field perpendicular to the wide conductor surface has a much bigger influence than a similar field parallel to the surface (see figure 1.1). Roebel cables retain this anisotropy, because all strands have the same orientation. This can be an advantage if a magnet can be designed in such a way, that the magnetic field is always parallel to the surface.

A remarkable disadvantage of Roebel cables is that more than 50% of the material is lost in the punching process. In the future, this may be solved by punching the substrate before depositing the superconductor.

1.3 Transverse stresses in accelerator magnets and their effect on *RE*BCO conductors

For the EuCARD-2 demonstrator magnet, CERN is currently focusing on the option of so-called aligned block coils from *RE*BCO Roebel cables [17, 18]. Recent drawings are shown in figure 1.4. In an aligned block coil, the wide side of the Roebel cable is parallel to the magnetic field. This orientation has two advantages: In the first place, high current densities can be achieved, as the influence of parallel magnetic field on the critical current is small. Secondly, the design requires only little in-plane bending; Roebel cables are not very flexible in this direction.

In magnet design, the mechanical stresses due to Lorentz forces must be taken into account. The Lorentz force is perpendicular to both the current and the magnetic field. In an aligned block coil, it will be directed perpendicularly to the wide side of the Roebel cable. Calculations have shown that the transverse stress in the demonstrator coil can be as high as 110 MPa when operated in a 13 T background field [17]. In a 20 T accelerator magnet, the transverse stress

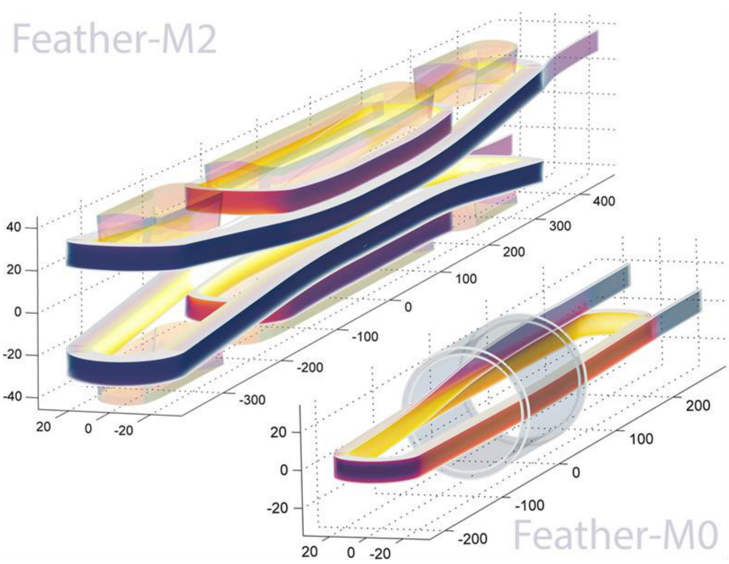

Figure 1.4: Aligned block HTS magnet designs from G. Kirby et al. [17, 18]. Feather-M0 is used for development of coil winding and quench detection, feather-M2 is the EuCARD-2 insert magnet.

can even reach 150 MPa. It is necessary to investigate if *RE*BCO Roebel cables can withstand these stresses.

The next two sections provide an overview of publications on the transverse strength of *RE*BCO tapes and cables.

1.3.1 Transverse strength of *RE*BCO tapes

There have been several investigations on the effect of transverse compressive stress on the critical current of *RE*BCO tapes. An overview is shown in table 1.2. For comparison, a transverse strength is defined as the stress needed to cause a critical current degradation of 5%.

The first transverse stress data were presented by J. Ekin et al. in 2001 [19]. The investigated tapes consisted of a 100 μm thick Inconel substrate (a nickel alloy) with a 0.9 μm YBCO layer. The samples were subjected to transverse stress in a liquid nitrogen bath, while the critical current I_c was repeatedly measured. After monotonic loading the I_c degradation was less than 5% at 100 MPa and 7% at 120 MPa. 2000 load cycles to 122 MPa resulted in less than 2% additional degradation.

In a study by N. Cheggour et al., *RE*BCO tapes with pure Ni and Ni-5%W substrates were subjected to transverse stress [20]. In the case of pure Ni substrates, a monotonic loading to 120 MPa did not cause I_c degradation. However, in load-unload mode, in which the stress is released after each measurement, an I_c degradation of 28% was observed at 100 MPa. The samples which had a harder Ni-5%W substrate were found to be more tolerant to transverse compression. They showed less than 6% degradation in load-unload mode with pressures up

Author	Year	Substrate	Transverse strength [MPa]	
J. Ekin et al. [19]	2001	100 μm Inconel 625	100	
N. Cheggour et al. [20]	2003	50 μm Ni	≥ 120	(monotonic)
			20	(load-unload)
		75 μm Ni-5%W	≥ 150	
N. Cheggour et al. [21]	2007	75 μm Ni-5%W	≥ 150	
		100 μm Hastelloy C-276	≥ 150	
T. Takao et al. [22]	2007	100 μm Hastelloy	≥ 300	
D. Uglietti et al. [23]	2013	50 μm Hastelloy	400	
L. Chiesa et al. [24]	2014	50 μm Hastelloy C-276	≥ 450	
		50-75 μm Ni-5%W	440	

Table 1.2: An overview of transverse stress experiments on *RE*BCO tapes. The transverse strength is defined as the stress needed to cause a critical current degradation of 5%.

to 150 MPa. In a follow-up, *RE*BCO tapes with Ni-5%W or Hastelloy C-276 (another nickel alloy) substrates were subjected to 20,000 fatigue cycles of transverse stresses up to 150 MPa [21]. No degradation of more than 1% was observed in any of the samples.

Monotonic loading experiments up to 400 MPa were reported T. Takao et al. [22]. All tested samples, which had a 100 μm thick Hastelloy substrate, did not show I_c degradation at pressures up to 300 MPa.

In 2013, D. Uglietti tested the effect of transverse stress on a commercial conductor from SuperPower [23]. 4 mm wide tapes (SCS4050) as well as a 2 mm wide Roebel strand punched from a wider tape (SCS12050) were measured. All samples had a 50 μm thick Hastelloy substrate. The critical current reduction was limited to 2% up to 200 MPa and to less than 8% at 550 MPa for all single tape samples. These results are of special interest as the same conductor is currently used for KIT's Roebel cables.

Recently, commercial tapes from SuperPower and AMSC were tested for use in TSTC cables by L. Chiesa et al. [24]. The SuperPower tape (SCS4050-AP), which had a 50 μm Hastelloy substrate, did not show degradation up to 450 MPa. The AMSC tape with a Ni-5%W substrate (344C) showed a slow degradation up to 13% at 480 MPa.

1.3.2 Transverse strength of Roebel cables

*RE*BCO tapes should easily be able to withstand the transverse stresses up to 150 MPa in a possible HTS accelerator magnet. In cable configurations, however, the stress may not have a homogeneous distribution over the entire surface. The stress at certain locations can be much higher than the average, and cause local damage.

J. Fleiter et al. subjected *RE*BCO Roebel cables manufactured by General Cable Superconductors (GCS) and KIT to transverse stresses [25]. Both cables were 12 mm wide. During compression, the cables were stacked with a pressure sensitive film from Fujifilm. This film becomes red when a pressure more than 40 - 50 MPa is applied. In figure 1.5, the stress patterns at 40 MPa are shown for two different Roebel cables. From the prints, the effective section that experiences transverse stress is estimated to be only 36% for the GCS cable and 23% for the KIT cable. This means that loading to 40 MPa leads to a local stress of at least 111 MPa for the GCS cable and 167 MPa for the KIT cable.

The cables were further loaded up to 45 MPa. Afterwards, the cables were disassembled and several strands were analysed at 77 K. No irreversible I_c degradation was observed [25].

Another transverse pressure test on Roebel cables was reported by Uglietti et al. [23]. The cables samples were provided by GCS and had a width of 4 mm. The strands of the cable

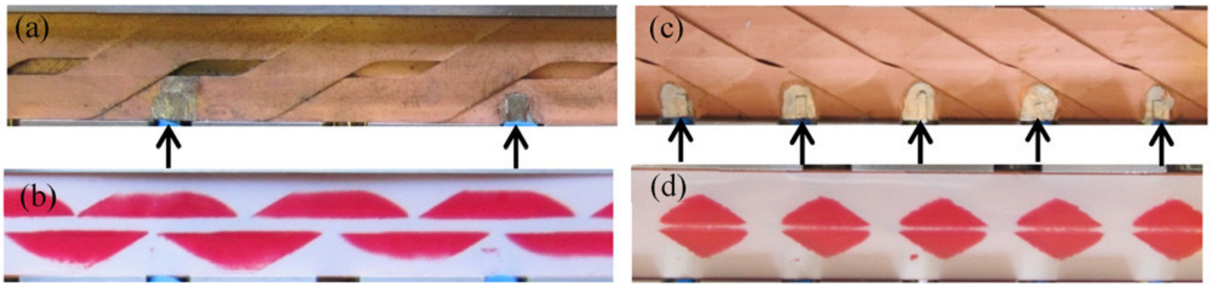

Figure 1.5: Roebel cables and corresponding stress patterns measured by J. Fleiter et al. [25]. (a) and (b) show a Roebel cable from General Cable Superconductors (GCS), (c) and (d) a cable from KIT.

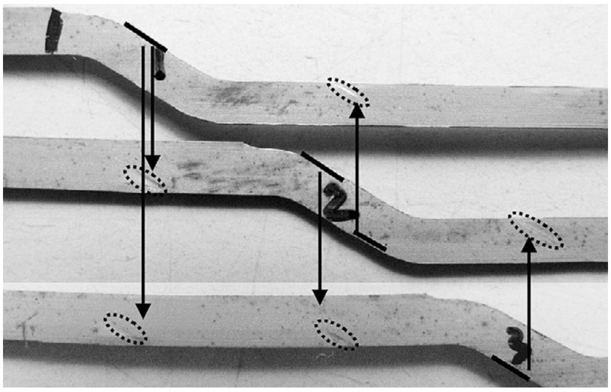

Figure 1.6: A cable that was disassembled after being subjected to 52 MPa transverse stress. The arrows indicate the relation between the tape edges and the damage on neighbouring strands. Image by Uglietti et al. [23].

were electrically insulated, allowing I_c measurements of the separate strands. Degradation was observed at pressures as low as 10 MPa, and most strands degraded by more than 20% at 40 MPa. In figure 1.6, three strands are shown of a cable that was subjected to a pressure of 52 MPa. Damage is visible where the strands are touched by the edge of the neighbouring strands. The damage location corresponds to the borders of the stress patterns measured by J. Fleiter (figure 1.5).

At similar pressures, D. Uglietti observed a more severe I_c degradation than J. Fleiter. There is so far no conclusive explanation for this difference.

Recently, G. Kirby et al. subjected a stainless steel Roebel dummy to 150 MPa transverse pressure, resulting in severe plastic deformation [17].

The above results indicate that there are stress concentrations at the tape edges, which will become problematic at stress levels expected in HTS accelerator magnets. It is therefore necessary to mechanically reinforce the cable and reduce stress concentrations.

1.4 Work overview

The goal of this master assignment is to investigate whether epoxy impregnation can reduce such stress concentrations and thus prevent critical current degradation at stress levels up to 150 MPa. To fulfil the assignment, these separate issues have to be addressed: an impregnation material and method need to be selected; a suitable sample holder needed needs to be designed, in particular the minimum bending radius of the investigated Roebel cables has to be determined; and the critical current of an impregnated cable sample needs to be measured at different transverse stress levels.

These different activities are reflected in the structure of this report:

Chapter 2: General experimental methods
This chapter discusses the preparation of Roebel cables and the general method used to measure their critical currents.

Chapter 3: Impregnation materials
An overview of impregnation materials is given, and their suitability for application in Roebel cables is discussed. The relevant low-temperature properties of several commercially available resin systems are measured. Based on these results, an epoxy resins filled with fused silica powder is selected as the most suitable material.

Chapter 4: Vacuum impregnation
The vacuum impregnation of dummy cables is described. The impregnation quality is evaluated using microscopic images of cable cross-sections. In this way, the impregnation process is improved without wasting expensive *RE*BCO cables.

Chapter 5: Out-of-plane bending of *RE*BCO Roebel cables
This chapter reports on measurements of the minimum bending radius for Roebel cables. These measurements are needed for the design of the sample holder for the transverse pressure tests.

Chapter 6: Transverse strength of a *RE*BCO Roebel cable
The test of an impregnated Roebel cable in a transverse press set-up is described.

This project was done within a cooperation between Karlsruhe Institute of Technology (KIT), where Roebel cables are developed, and Twente University (UTwente), which has facilities for mechanical tests of superconducting cables. The work described in chapters 3, 4 and 5 was done at KIT, the pressure tests described in chapter 6 were done at UTwente.

Chapter 2

General experimental methods

The aim of this short chapter is to explain experimental aspects that are referred to throughout the report. The production method and layout of *RE*BCO Roebel cables as well as the electrical analysis of those cables are discussed.

2.1 *RE*BCO Roebel cable preparation

First, the superconducting tape is punched into a meandering shape using a pneumatic punching machine (figure 2.1). The machine has two knives which can remove material from each side of the tape. A reel-to-reel system is used to automatically move the tape. The accuracy of the cuts

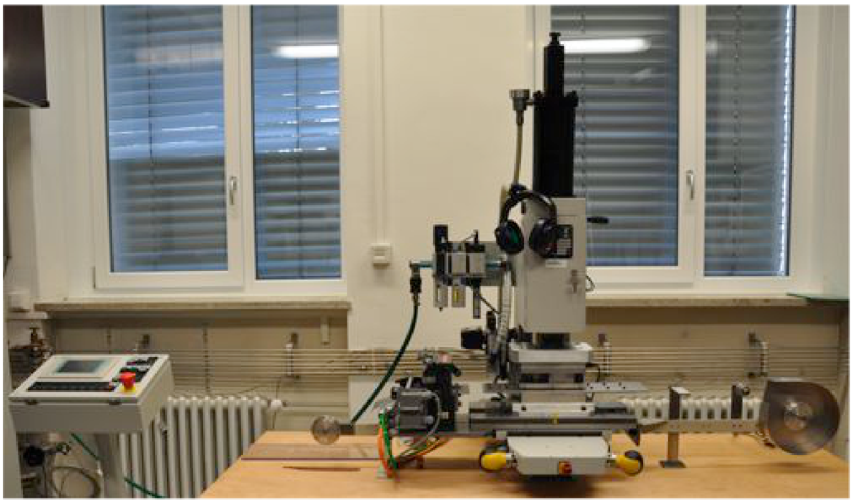

Figure 2.1: Computer controlled pneumatic punching machine that is used at KIT. It can be used to make Roebel strands of 4, 10 and 12 mm wide tapes with different transposition lengths. Image by W. Goldacker et al. [15].

is better than 50 μm [26]. After punching, the conductor has lost more than half of its critical current. Relative to the tape width, however, the critical current reduction is less than 3%. This indicates that the machine does little damage to the remaining part [26].

The machine is suitable for 4, 10 and 12 mm wide tapes. The standard transposition lengths are 115.7 mm for 4 mm wide tapes, and 126, 226, and 426 mm for 12 mm wide tapes. For this project, 12 mm wide tapes are punched with 126 mm transposition length. The punching pattern with dimensions is shown in figure 2.2.

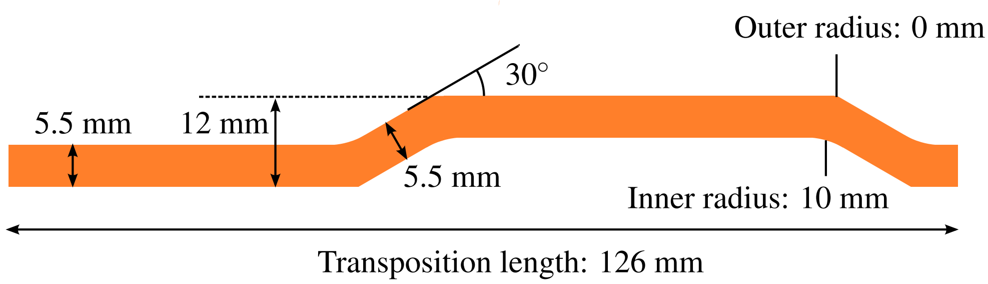

Figure 2.2: Shape of the Roebel strands after punching. The figure shows one transposition length in real size.

After punching, strands of the desired length are cut from the tape. The critical current is measured at 77 K (section 2.2) to check for any defects. If no defects are found, the strands are assembled into a cable by hand. All cables in this project consist of ten strands which all have the same orientation of the *RE*BCO-coated side.

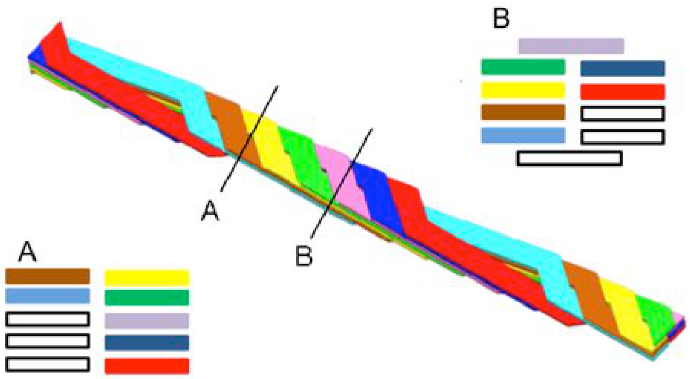

Figure 2.3: Computer drawing of an assembled Roebel cable, showing seven out of ten strands. Cross-sections are shown at the bridge (B) and between two bridges (A). The thickness of the tapes is exaggerated to better show the 3D structure. Image by W. Goldacker et al. [15].

2.2 Electrical characterisation

The goal of electrical characterisation is to determine the critical current and the n-value of the sample. The electric field E and the current I in a one-dimensional superconducting wire are often described by a power law:

$$\frac{E}{E_c} = \left(\frac{I}{I_c}\right)^n \tag{2.1}$$

In this equation, I_c is the critical current, which is defined as the current at which the electric field reaches a certain criterion E_c. In this report a criterion of $E_c = 10^{-4}$ V/m is used, as is usual for HTS conductors. The n-value describes the steepness of the superconducting transition, with $n = 1$ being a resistor and $n = \infty$ being an idealised superconductor. It is widely used as a measure of superconductor quality as it reflects both magnetic flux pinning and micro-structural homogeneity.

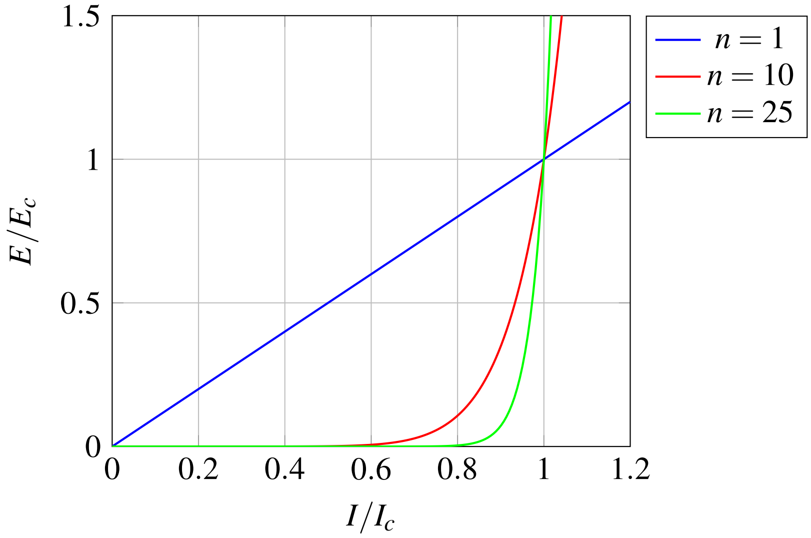

Figure 2.4: Superconducting transition for different n-values.

For electrical characterisation, the current-voltage characteristic is measured. This usually done by passing an increasing current through the sample and measuring the voltage over a well-defined length. The voltage is always measured with a separate pair of wires, connected at some distance from the current leads. This is done to avoid measuring the voltage associated with the resistive current contacts. In case of a cable consisting of multiple strands, the contacts are always connected to the same strand, to exclude potential differences between different strands. As the electric field criterion is relatively low, sensitive nano-voltmeters or pre-amplifiers need to be used.

The power law (equation 2.1) can be written as a linear relation between $\ln(I)$ and $\ln(E)$:

$$\ln\left(\frac{E}{E_c}\right) = \ln\left(\left(\frac{I}{I_c}\right)^n\right) \tag{2.2}$$

$$\Rightarrow \ln(E) = n\ln(I) + \ln(E_c) - n\ln(I_c) \tag{2.3}$$

To compute the critical current and the n-value, a linear fit is made. The n-value is equal to the slope. The critical current is determined from the n-value and the intercept with the vertical axis.

Chapter 3

Impregnation materials

3.1 Introduction

Epoxy resins are commonly used for reinforcement of resistive and low-temperature superconducting coils. These resins are processed by mixing two liquid parts (resin and hardener), followed by a curing cycle to harden it. As a liquid, uncured epoxy resin fills up small spaces inside a coil. It is applied using techniques such as wet-winding or vacuum impregnation. Additionally, most epoxy resins have good dielectric and mechanical properties.

In *RE*BCO coils, however, epoxy impregnation has been challenging: the first reported impregnated coils showed degradation of the critical current. After visual inspection of an impregnated coil, a separation of the layers (delamination) was observed by T. Takematsu [27]. Such damage is explained as a result of a mismatch in thermal expansion between the conductor and the epoxy: When epoxy is cooled down from room temperature to T = 4.2 K, it contracts by 1.33%, while the *RE*BCO tape contracts by only 0.25% [28]. This mismatch leads to tensile stresses perpendicular to the tape; in other words, the layers of the tape are being pulled apart. *RE*BCO tapes are very sensitive to such stresses, and degradation can occur at stress levels as low as 10 MPa [29, 30].

Several different methods to reduce tensile stresses have been proposed and tested successfully. The underlying principles are the following:

- Using no impregnation at all. This is possible in stacked cables and pancake coils, since the rectangular tapes form a good support themselves. Co-winding with an insulated steel tape has been done for additional support and electrical insulation between the windings [31].

- Avoiding epoxy penetration in between the winding and casing only the entire coil. By winding a pancake coil under high tension the tapes can be very closely packed. Epoxy impregnation of such a coil did not cause damage [32].

- Using a soft impregnation material. Beeswax and paraffin have been used to impregnate *RE*BCO pancake coils [27, 33]. Despite their high thermal contraction, these materials are too weak to build up high thermal stresses during cool-down; they crack instead.

- Using an impregnation material with low adhesive strength. Both beeswax and paraffin do not stick to metals. Cyanoacrylate resin does stick, but it still has a bonding strength several times lower than epoxy. A coil impregnated with this material did not show any degradation [34].

- Introducing a weak mechanical barrier between the conductor and the epoxy that absorbs the stress. This has been done by sticking the conductor in a polyester heat-shrink tube [35], and by coating it with a polyimide layer [36]. Both coils were then epoxy impregnated without any degradation.

- Using materials with low thermal expansion. Epoxy resins can be mixed with a powder of a low thermal-expansion material in order to decrease the overall thermal expansion. In a previous work at KIT, a Roebel cable was impregnated with a 1:1 mixture of epoxy and silica [28]. The critical current of the cable was measured at 77 K before and after impregnation, and no degradation was observed.

- Polyimide resins show a thermal contraction lower than epoxy even without any fillers [37]. Moreover, they are more resistant against radiation than epoxy [38], making them a promising candidate for impregnation of accelerator magnets. A bismaleimide resin has been used on a Nb_3Sn cable stack, which had decreased thermal contraction compared to one impregnated with epoxy [38]. However, such resins have not been applied yet to *RE*BCO coils and cables.

In order to reinforce Roebel cables and reduce stress concentrations under transverse loading, it is essential that the cable, and in particular the central hole, is filled with a strong material. The impregnation should prevent any movement of the wires, even under high pressures. Soft impregnation materials such as beeswax and paraffin are therefore not suitable. Likewise, weak mechanical barriers surrounding the tapes are undesirable as they allow for some movement. Using such a barrier around the entire cable is also not an option, as the cable itself would not be filled.

When choosing an impregnation material, one also needs to make some practical considerations. Both at UTwente and KIT basic equipment is available for vacuum impregnation with epoxy. Epoxy resins are generally processed at moderate temperatures ranging from room temperature to 100 °C, and maintaining this temperature is not critical. Polyimide resins need higher temperatures of 120 - 200 °C, and have a viscosity that strongly depends on temperature. This complicates the impregnation procedure; for example, syringes cannot be used to move the resin, as it will freeze in the tip and clog it. For this project we decided to stick to epoxy resins because of their ease of processing and proven good mechanical properties. Even so, polyimide resins remain an attractive alternative.

Many filled epoxy resins are commercially available, but their properties at low temperatures are not well-documented. In this chapter, epoxy resins with six different fillers are analysed specifically for low-temperature use. Their thermal expansion, thermal conductivity and electrical conductivity are measured for temperatures ranging from 4.2 to 300 K. Using the results, the most suitable resin is selected.

3.2 Tested filled epoxy resins

The tested epoxy resins are shown in table 3.1. Initially, the idea was to use a conductive resin to prevent the strands within the cable from becoming electrically insulated. In this way the stability may be improved. Silver- and graphite-filled epoxies (Duralco 125/127) were purchased from Polytec. Silver epoxy is the most common conductive epoxy. The electrical conductivity depends on a direct contact between silver particles, so a high filling ratio of 60 to 80% of the total weight is needed. Duralco 127, a graphite-filled epoxy, is a low-cost alternative.

Carbocond 171/6 and 471/6 from the company FutureCarbon are epoxy resin filled with a

	Filler	Filling ratio [wt%]	Product name
Electrically conductive fillers	Silver	60 - 80	Duralco 125
	Graphite	50 - 60	Duralco 127
	Carbon particles + CNT	4 - 8	Carbocond 171/6
	Graphite + CNT	4 - 8	Carbocond 471/6
Insulating fillers	Fused silica	50, 60, 66	Araldite CY5538/HY5571
	$Al(OH)_3$	56	Araldite CW5730N/HY5731

Table 3.1: Tested epoxy resins with several different conductive and insulating fillers.

mixture of carbon particles and single-walled carbon nanotubes (CNT). The carbon nanotubes provide a percolation path for the current even at very low filling ratios [39]. Resins with less filler have lower viscosity and are more easily processed. Carbon nanotubes also have been shown to increase thermal conductivity [40] and improve the mechanical properties [41]. Data on the thermal expansion of these mixtures was however not available, so we decided to measure it for two commercially available ones.

As discussed below, it was found that these conductive epoxy resins are not suitable for the impregnation of Roebel cables. Two additional insulating resins were offered for testing by Huntsman Corporation. Araldite CY5538 with hardener HY5571 is supplied unfilled. As filler, fused silica flour “Silbond FW600 EST” with a median grain size of 4 μm is used. Fused silica has a low coefficient of thermal expansion of $0.5 * 10^{-6}$ K^{-1} [42]. Araldite CW5730N is a resin pre-filled with 56 wt% aluminium hydroxide.

3.3 Thermal expansion

All filler materials investigated have a coefficient of thermal expansion much lower than epoxy (see table 3.2). Addition of these materials to the resin is therefore likely to reduce the overall thermal expansion. The thermal expansion of the filled epoxy resins were measured in the Cryogenic Material Test Facility Karlsruhe (CryoMaK) [43]. The measurements were done by Nadezda Bagrets.

Material	CTE [10^{-6} K^{-1}]	Source
Epoxy	87	[44]
Silver	18	[45]
Alumina	6.6	[42]
$Al(OH)_3$	?	
Graphite	2 - 6	[46]
Silica	0.5	[42]

Table 3.2: Coefficients of linear thermal expansion at room temperature for the investigated filler materials and unfilled epoxy.

3.3.1 Method

Samples are prepared by mixing the resin and hardener according to the instructions and curing in a Teflon form. The resulting samples have a size of 60 mm × 10 mm × 5 mm.

To measure the elongation of the sample, two extensometers are attached to the sample (figure 3.1). The extensometers consist of U-shaped bars of copper-beryllium. The sharp ends of the extensometer are fixed to the sample using steel clamps. On both extensometers strain gauges are attached which have a resistance dependent on the deformation. To obtain an accurate relation between the extension at the tips and the strain gauge resistance, the extensometers have been calibrated using a tensile machine. This calibration was done at different temperatures, as the calibration factor depends on the temperature.

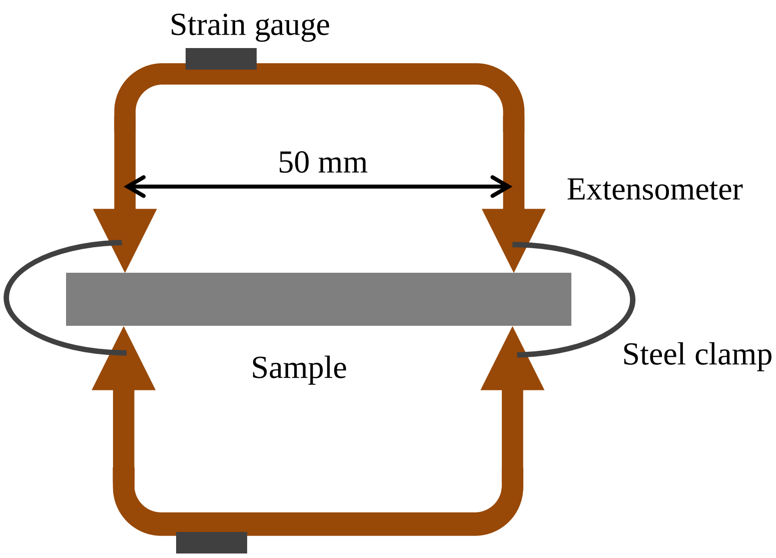

Figure 3.1: CryoMaK thermal expansion measurement setup.

The sample and extensometers are inserted into a cryostat and cooled to 4.2 K by filling the cryostat with liquid helium. Once the helium has evaporated, the temperature inside the cryostat slowly rises to room temperature in about ten hours. The slow temperature change ensures a homogeneous temperature in the sample area. During these ten hours, the strain gauge resistance is continuously measured. The temperature is measured as well using a Lakeshore cryogenic temperature sensor.

A correction needs to be made to compensate for the thermal expansion of the extensometer itself. For this reason, the measurement is repeated with a sample of Zerodur glass of which the thermal expansion is negligible. The difference in thermal expansion between the Zerodur and the actual sample measurements is taken as the final result.

3.3.2 Results

The total linear thermal expansion when cooling from room temperature to T = 4.2 K is shown in figure 3.2. The thermal expansion of an unfilled epoxy (Araldite DBF), alumina-filled epoxy (Stycast 2850 FT) and *RE*BCO tapes were measured before for a different project using the same equipment [28]. These values are added to the figure for comparison.

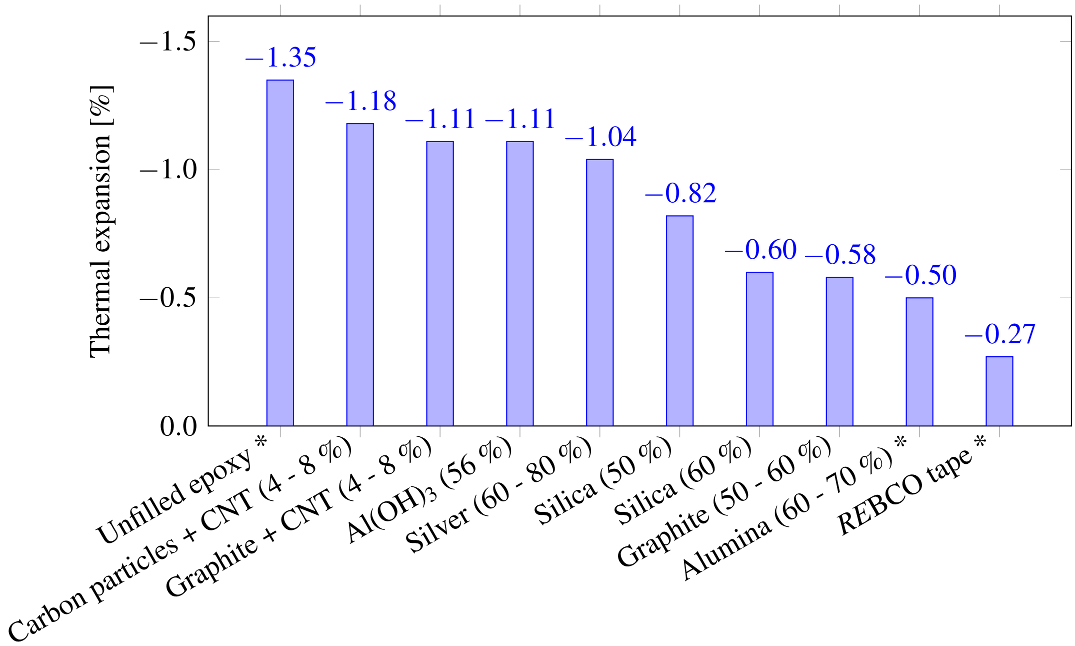

Figure 3.2: Thermal expansion for $T = 293 \rightarrow 4.2$ K for different filled epoxies. (*) The values for unfilled epoxy, alumina-filled epoxy and *RE*BCO tape were taken from Barth et al. [28].

The thermal expansion of unfilled epoxy is five times larger than that of *RE*BCO tape. All fillers decrease the thermal expansion to some degree. The mixtures with the lowest thermal expansions are heavily filled with silica, graphite, or alumina. This makes sense because silica, graphite and alumina are themselves materials with low thermal expansion.

3.4 Thermal conductivity

Apart from thermally induced stresses, another point of attention is the thermal conductivity of the impregnation mixture. A too low thermal conductivity will hamper heat removal to the environment and thus may endanger the thermal stability of the cable. For applications at temperatures above 0 °C, epoxy resins are commonly filled with silica, alumina or silver if an increased thermal conductivity is desired. But like many other material properties, the thermal conductivity changes with temperature. In this section, the thermal conductivity of several filled resins is analysed at cryogenic temperatures.

The thermal conductivity is measured in a Physical Property Measurement System (PPMS) from Quantum Design [47]. The setup features a 14 T magnet and a variable temperature cryostat for temperatures ranging from 1.9 to 400 K. The measurements described in this section were done by Sandra Drotziger and Nadezda Bagrets.

3.4.1 Method

The measurements principle is as follows: a known heat flux P is passed through the sample, which has a constant cross-sectional area A over its length. At the same time, the temperature difference ΔT is measured over a distance Δx parallel to the heat flow. The thermal conductivity k can then be calculated by dividing the heat flux density P/A by the temperature gradient $\Delta T/\Delta x$:

$$k = \frac{P\Delta x}{A\Delta T} \tag{3.1}$$

This method assumes a steady state; the temperature of the sample does not change in time.

Samples for the thermal conductivity measurements were cut from the larger thermal expansion samples. The new smaller samples are cylinders with a diameter of 6 mm. Cylinders with two different lengths (2 and 3 mm) were made from each resin. The measurements are repeated on these three samples and compared to rule out geometry effects.

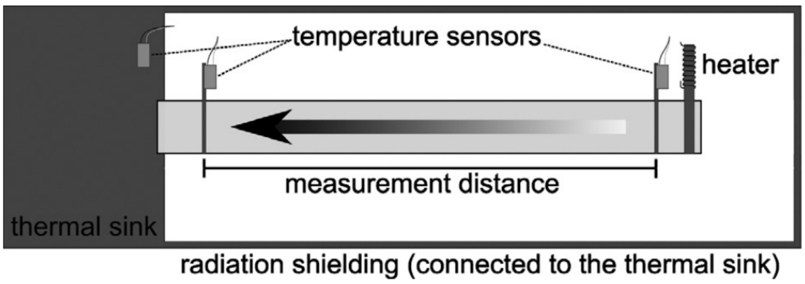

Figure 3.3: CryoMaK thermal conductivity measurement setup. Image by Bagrets et al. [48].

To establish a heat flux through the sample, one side of the sample is connected to a resistive heater using silver epoxy. The other side is glued to a thermal sink. Two temperature sensors are glued in between the heater and the sink. Next, the samples are inserted into a temperature variable cryostat. The chamber is evacuated to approximately 10^{-6} mbar to prevent heat transfer to the surrounding gas. Using the heater a temperature increase of 1 - 3% of the background temperature is created. Heat losses due to radiation are automatically estimated by the PPMS software.

A more detailed discussion of the thermal conductivity measurements at CryoMaK can be found in [48].

3.4.2 Results

The results of these measurements are shown in figure 3.4. The two samples of each resin show similar behaviour, indicating that the influence of geometry is small.

Three bar diagrams in figure 3.4 show the thermal conductivities at the most relevant cryogenic temperatures 77 K and 4.2 K. The values for unfilled, silica-filled (Araldite DBF) and alumina-filled (Stycast 2850 FT) epoxy resins are shown for comparison [49, p. 83]. These measurements were done in the same setup and are in agreement with literature values [50, 51]. At room temperature, all fillers increase the thermal conductivity, up to a factor 16 for the silver filler. At cryogenic temperature, however, this effect is much smaller. The thermal conductivities of the different epoxy resins at 4.2 K differ by no more than a factor four. For fillers other than silver the difference is even reduced to less than a factor two. These fillers will therefore have limited use for improving the stability of magnets operated at 4.2 K.

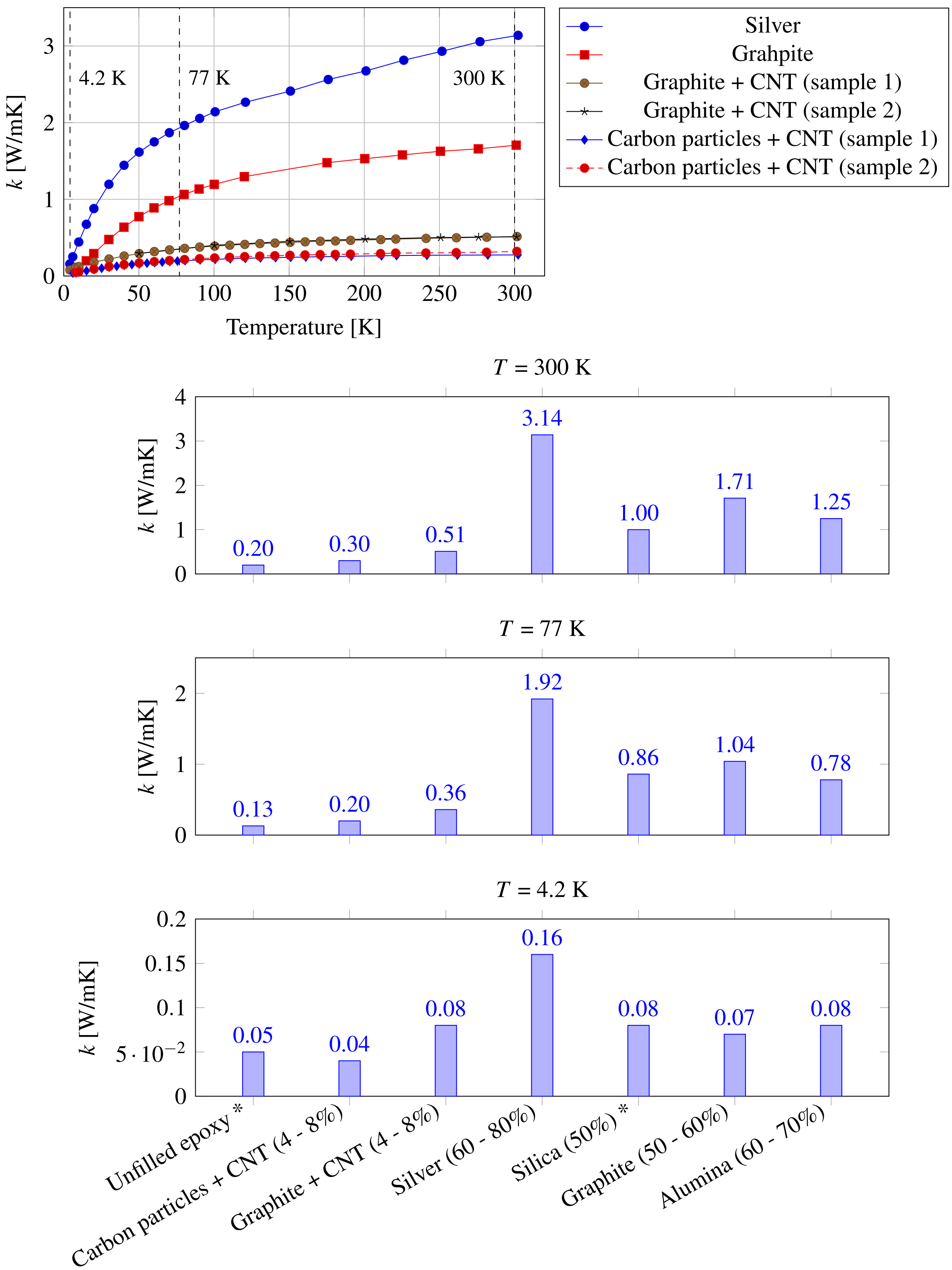

Figure 3.4: Thermal conductivity as a function of temperature for the different filled epoxy resins. Values with * are from C. Barth's thesis [49].

3.5 Electrical resistivity

At cryogenic temperatures, the specific heat of most materials is much lower than at room temperature. A relatively small amount of heat can therefore cause a large rise in temperature. If the temperature of a superconductor rises above the critical temperature a “quench” occurs: the superconductor suddenly enters its normal (resistive) state. If the subsequent resistive heating is lower than the cooling power, the superconductor can recover from the quench. Otherwise, the normal zone will become larger and larger and the current needs to be stopped. The energy needed to cause a quench is called the minimum quench energy. The higher the minimum quench energy, the better the thermal stability of the cable.

In a cable, multiple superconducting strands are connected in parallel. Suppose that one of those strands quenches and develops a normal zone. If the strands are electrically insulated (high inter-strand resistance), the current is forced to flow through the normal zone. If the inter-strand resistance is sufficiently low, the current can relocate to other strands of the cable. In this case, less current flows through the normal zone leading to a lower resistive heating. An increased minimum quench energy was shown for NbTi [52] and Nb_3Sn Rutherford cables [53] with a low inter-strand resistance.

If epoxy impregnation electrically insulates the strands, it can have an adverse effect on the thermal stability. Impregnation with a conductive silver-filled epoxy has been proposed for Roebel cables [54]. A cable impregnated with such material had a decreased inter-strand resistance compared to the one impregnated with unfilled epoxy. The effect on the thermal stability however has not been analysed yet.

In this work epoxy resins are analysed of which four have an electrically conductive filler. The electrical conductivity of those resins at low temperatures are described in this section. The measurements were done by Sandra Drotziger.

3.5.1 Method

For these measurements, new 4 mm × 4 mm × 15 mm samples were prepared. A small plug with four contacts in a line was inserted into the resin before it hardened. The two outer poles are connected to a current source which provides a current of a few mA through the sample. The voltage is measured over the inner two poles. The resistivity is then computed using the well-known formula

$$\rho = \frac{A}{l}R = \frac{AU}{lI} \tag{3.2}$$

in which A is the cross-sectional area and l is the distance between the two voltage contacts. The measurement is repeated at different temperatures in the temperature-variable cryostat of the PPMS.

3.5.2 Results

The results are shown in figure 3.5. The resins filled with carbon are electrically conductive but still have a relatively high resistance of more than 0.1 Ωm. Silver epoxy is much less resistive at about 10^{-5} Ωm. The temperature dependence of the electrical resistivity is not too strong: at cryogenic temperatures, the carbon-filled epoxy resins have slightly higher resistivities while the resistivity of silver epoxy is slightly lower.

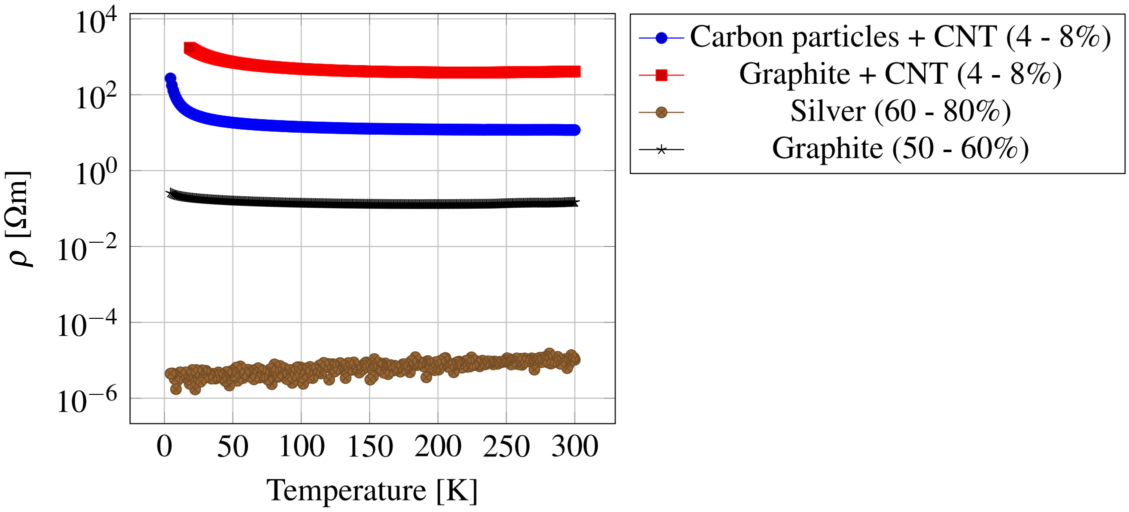

Figure 3.5: Electrical resistivity as a function of temperature for the different conductive resins.

To make inter-strand current redistribution in a cable possible, the inter-strand resistance must be comparable to or lower than the contact resistance at the current leads, which is usually in the range 1-1000 nΩ. Otherwise, current distribution will occur only at the current leads.

The following calculation estimates the upper limit to the resin resistivity, assuming a cable length of 1 meter and a 10 µm thick layer of epoxy resin between adjacent strands. The width of Roebel strand is 5.5 mm. The contact area of two adjacent tapes is therefore $5.5\ \mathrm{mm} * 1\ \mathrm{m} = 5.5 * 10^{-3}\ \mathrm{m}^2$. To achieve a inter-strand of 1 µΩ or lower the resin resistivity should be at most:

$$\rho = \frac{A}{l} R = \frac{5.5 * 10^{-3}\ \mathrm{m}^2}{10 * 10^{-6}\ \mathrm{m}} * 10^{-6}\ \Omega = 5.5 * 10^{-4}\ \Omega\mathrm{m} \tag{3.3}$$

Of course this is a very rough estimation, but as the resistivity of carbon-based conductive resins is 3 to 7 orders of magnitudes larger, they are not suitable for this purpose. On the other hand, silver-filled epoxy resins may have sufficient conductivity to allow current redistribution.

3.6 Chemical compatibility

When *RE*BCO tapes are punched into Roebel strands, the copper sheath is removed on one side. At this spot the *RE*BCO layer comes in direct contact with the resin during impregnation. Some epoxy resins contain corrosive components that can cause damage. For example, one of the Stycast hardeners has been shown to dissolve the *RE*BCO layer [55].

To rule out any chemical problems, the chemical compatibility of the separate epoxy components (resin and hardener) was tested. 10 cm long samples of conductor were used of which the copper edges had been removed by laser cutting. The samples were submerged in 10 ml of the component in a test tube for approximately 16 hours. The critical currents before and after exposure to the component were compared. No degradation was observed for the Carbocond and Araldite resins and hardeners. The Duralco resins were not tested because only a small amount was available.

In a future production method for Roebel cables, the copper stabilizer may be added after punching. In this case there is no direct contact between resin and superconductor, and chemical attack is no longer an issue.

3.7 Recommendation for Roebel cables

To achieve a large reduction in thermal expansion, the epoxy resin must be heavily filled (> 50 wt%) with low-CTE fillers. The lowest thermal expansions were indeed observed in the graphite- and fused silica-filled resins.

For impregnation purposes, there is another quantity that is important, and that is the processing viscosity: Adding particles to a resin strongly increases the viscosity and this impedes epoxy flow into the open spaces within the cable. The viscosities according to the datasheets are listed in table 3.3. Both the silver and the graphite-filled resins (Duralco 125/127) are heavily filled with particles and are a paste-like substance. The viscosity of these resins is too high for them to be used for cable impregnation. The tested resins filled with fused silica (Araldite CY5538) and $Al(OH)_3$ (Araldite CW5730N) are also heavily filled. However, these resins can be processed at an elevated temperature of 60 - 100 °C, while retaining a pot-life of several hours. In this way the viscosity is lowered and the heavily filled resin is suitable for impregnation.

Filler	Filling ratio [wt%]	Product name	Thermal expansion $T = 300 \rightarrow 4.2$ K	Viscosity [Pa s]
Silver	60 - 80	Duralco 125	-1.04 %	20 (20 °C)
Graphite	50 - 60	Duralco 127	-0.58 %	50 (20°C)
Carbon particles + CNT	4 - 8	Carbocond 171/6	-1.18 %	6 - 8 (20 °C)
Graphite + CNT	4 - 8	Carbocond 471/6	-1.11 %	1 - 2 (20 °C)
Fused silica	50 - 66	Araldite CY5538/HY5571	-0.82 % (50 wt%) -0.60 % (60 wt%)	$<$ 4.5 (80 °C)
$Al(OH)_3$	56	Araldite CW5730N/HY5731	-1.11 %	0.7 (60 °C)

Table 3.3: Tested epoxy resins with the measured linear thermal expansion and processing viscosity according to the datasheet. The temperature in brackets denotes the corresponding processing temperature. Values in red are problematic for application to *RE*BCO tapes.

The only resin that combines a low thermal expansion with low processing viscosity is Araldite CY5538/HY5571 with fused silica, and therefore it is the most suitable for impregnation of the Roebel cable.

In this chapter, six commercially available epoxy resins have been analysed. All but Araldite CY5538 are supplied pre-filled. Because of this, we cannot know exactly what and how much filler is inside. In addition to the filler material, the particle size and shape may also differ. Moreover, epoxy resins come in many different kinds for different purposes, all of which have different properties. One should therefore be careful when making comparisons. The conclusions made in this chapter do not generally apply to all epoxy resins with a specific filler. They are just a recommendation for the most suitable system out of the six tested.

Chapter 4

Vacuum impregnation

4.1 Introduction

To attain good reinforcement, all gaps in the cable or coil need to be filled with resin. Remaining gas bubbles in the cable or coil are highly undesirable, because they can lead to an inhomogeneous stress distribution. There are in principle two methods to do this: the wet-winding process, in which the resin is added to the cable just before coil winding, and vacuum impregnation, in which the resin is inserted into the coil after winding. Optionally, the cable can be stuck into a glass-fibre sleeve before impregnation. The resulting glass-fibre epoxy composite prevents successive windings from touching each other and thus provides electrical insulation between them.

Initially, we tried impregnation of a dummy cable using a simple method resembling wet-winding. The cable was stuck into a glass-fibre sleeve, and epoxy resin was added to the cable in a straight Teflon mould. Next, the cable was cycled to low pressure in a vacuum chamber, which should help air bubbles to escape. Earlier, a similar method had been used successfully on a less densely packed Roebel cable from General Cable Superconductors [28]. After curing (hardening) of the resin, cross-sections of the cables were made by cutting the cable in two with a diamond wire saw and polishing the sawed surface. The cross-sections were analysed with an optical microscope to check the impregnation quality. Cables impregnated in this way always ended up looking like the one in figure 4.1. There are air bubbles between the strands and the central hole is not totally filled. It is probably the geometry of the Roebel cable with many narrow openings and a relatively large open volume in the centre that allows air to remain trapped. From these try-outs its was concluded that wet-winding is not suitable for these densely packed Roebel cables.

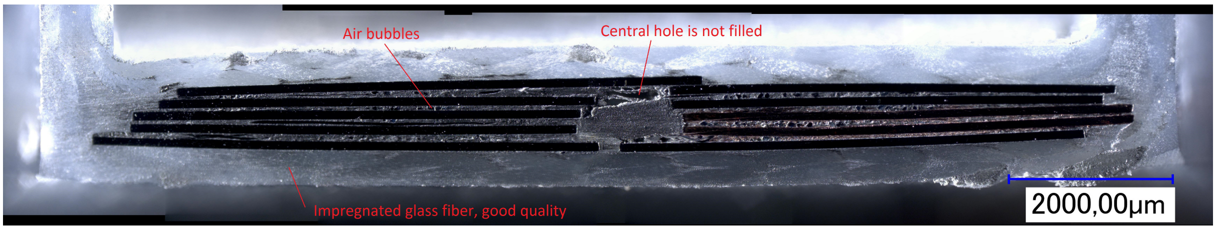

Figure 4.1: Cross-section of a cable impregnated by wet-winding, followed by cycling to low pressure in a vacuum chamber. The impregnation quality is poor: there are voids in the central hole and between the strands.

4.2 Vacuum impregnation principle

A more powerful method to get resin inside the cable is vacuum impregnation. The process consists of four basic steps (figure 4.2). A vacuum chamber is needed with the epoxy resin and the sample inside. First, the chamber this evacuated, removing all air from the sample. Next, the sample is submerged into the resin, and after some time the chamber is pressurised. This is the key step: the pressure pushes the resin into all openings of the cable that have not been filled yet by gravity or capillary suction. Any remaining gas bubble will shrink to a small fraction of its size. In our set-up, the atmospheric pressure is used, simply by opening the vacuum chamber. In more advanced set-ups, higher pressures can be used. Finally, the sample can be removed from the resin and cured.

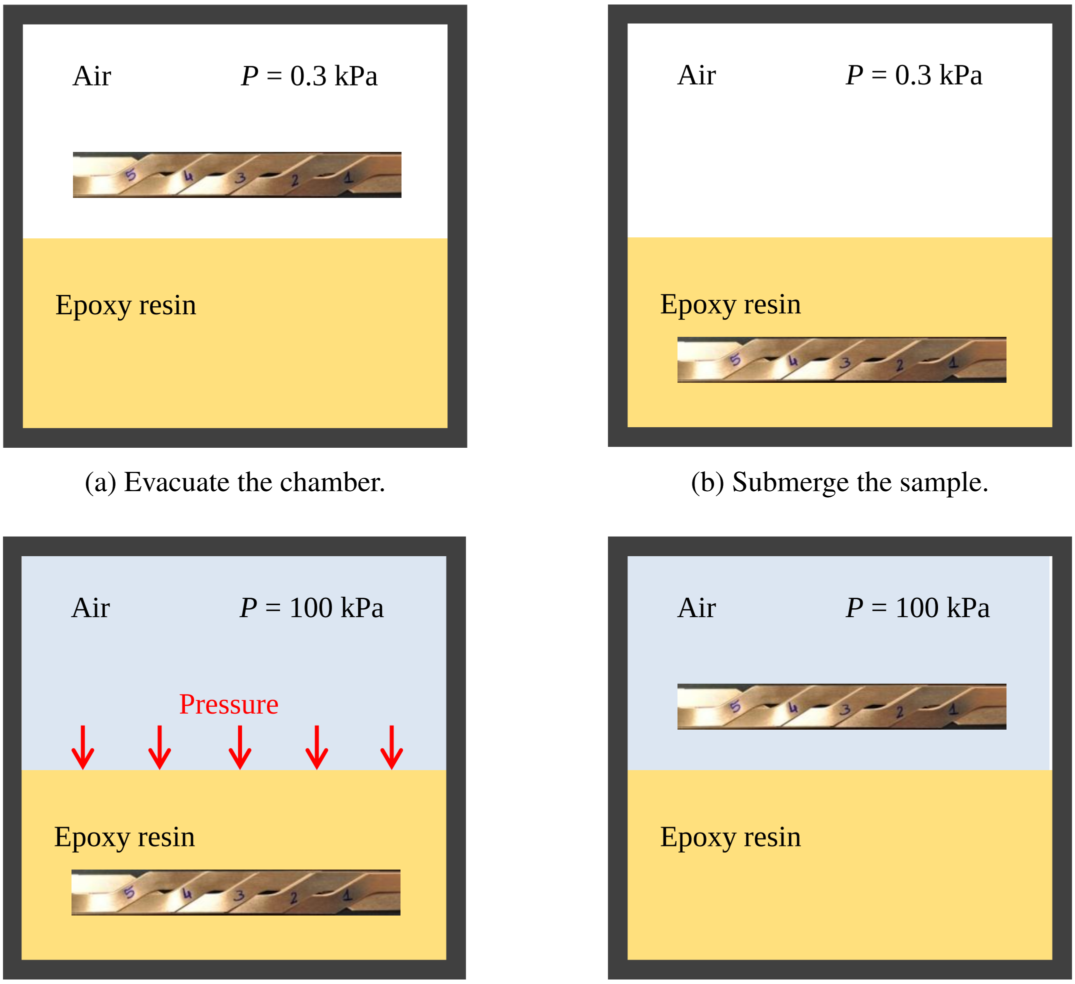

(a) Evacuate the chamber.

(b) Submerge the sample.

(c) Pressurise the chamber.

(d) Remove the sample.

Figure 4.2: Vacuum impregnation in four steps.

4.3 Vacuum impregnation set-up

A small impregnation set-up was already available at KIT which had been used for impregnation of *RE*BCO pancake coils with beeswax. This set-up was modified to make it suitable for impregnation of Roebel cables (see figure 4.3). The cable is fixed on the U-shaped outer surface of a Teflon sample holder, which has the same shape as the sample holder for the mechanical press at UTwente. The sample holder is fixed to the top flange of the vacuum chamber. Below the sample holder, there is a brass resin container that can be moved up and down from the outside by a steel rod. In this way, the sample can be submerged into the resin in vacuum conditions, without opening the chamber. Inside the container is a thermocouple necessary for controlling the resin temperature. The sample holder and resin container are inserted into the vacuum chamber, a glass tube of which the lower part is heated by an oven. The pressure in the chamber is controlled manually using a vacuum pump, a valve and a pressure sensor.

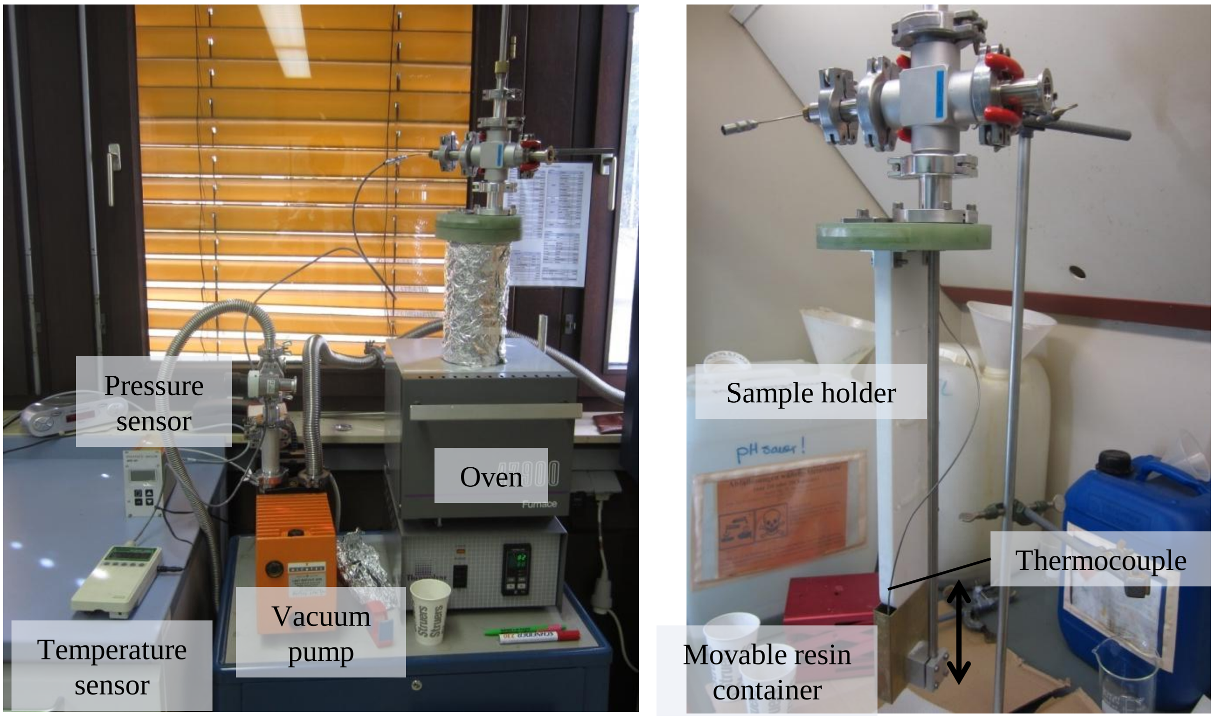

Figure 4.3: The vacuum impregnation set-up at KIT, modified for Roebel cables.

4.4 Vacuum impregnated dummy cables

As discussed in chapter 3, the epoxy resin needs to be heavily filled with silica or alumina to prevent degradation of the conductor due to a thermal expansion mismatch. These filler particles complicate the vacuum impregnation process. Many early attempts failed, and resulted in cables with voids, much like those in figure 4.1. These results, however, could be used for improvement of the process. The most useful observations were the following:

- Mixing epoxy with filler particles traps a big amount of air, visible as small bubbles. When the pressure in the vacuum chamber is decreased, the bubbles strongly expand and the mixture starts foaming. This effect can be so strong, that the entire vacuum chamber is filled with foam. Companies that use filled resins on a large scale use special equipment to mix the filler and resin under vacuum, and thus avoid trapping air in the first place. Unfortunately such equipment was not available in the group.

  We solved this problem by carefully degassing the resin after mixing: first, the mixture is heated in a flask to reduce its viscosity. Then the flask is connected to a vacuum pump, and the pressure is slowly decreased. At the same time, the mixture is constantly stirred with a magnetic stirrer. This breaks large gas bubbles and prevents the foam from becoming very large in volume. Mixtures degassed in this way did not cause foaming problems.

- Impregnation of cables in a glass-fibre sleeve always gave bad results. A possibly explanation is a filtration effect: the glass-fibres are very fine and can trap particles. More and more particles can get stuck, impeding the resin flow. Besides that, this effect can cause an inhomogeneous particle distribution. This could be observed in one sample impregnated with silica-filled resin: the resin looked transparent far away from the sides, whereas silica-filled resin is white and opaque. Based on these results we decided not to use glass-fibre for cables impregnated in this project.

- A high filler content is needed to achieve a sufficient reduction of the thermal expansion. However, fillers strongly increase the viscosity slowing down the flow of epoxy. It is therefore necessary to use a filler content which results in both an acceptable thermal expansion and viscosity. It is also necessary to use a resin that can be processed at high temperatures, as this decreases the viscosity and can (partly) compensate for the effect of the fillers.

Following these observations the impregnation method was adapted to the use of epoxy with fillers. Instead of using glass-fibre, the dummy cable was stacked in between two 100 μm stainless steel tapes. Araldite epoxy resin CY5538 with hardener HY5571 was used, following the recommendations of section 3.7. At 80 °C, this resin retains a pot-life of three hours, so processing at this temperature is possible. The resin is filled to 50 or 60 percent of the total weight with fused silica “Silbond FW600 EST” with a median grain size of 4 μm.

In brief, the impregnation procedure was as follows:

- Clean the sample in acetone using an ultrasonic cleaner.
- Mount the sample on the sample holder between stainless steel tapes, apply some pressure with a piece of Teflon and copper wires.
- Mix resin, hardener and fused silica powder by hand.
- Degassing: heat the contents in a flask to 60° C, mix with a magnetic stirrer and slowly evacuate to 1-2 mbar (30 minutes).
- Pour the mixture in the resin container, heat the impregnation set-up to 80 °C and evacuate to 3-5 mbar.
- Wait 5 minutes.
- Raise the container to submerge the sample.
- Wait 20 minutes.
- Pressurise the chamber.
- Wait 20 minutes.
- Lower the container.
- Cure the sample at 100 °C for 24 hours.

The impregnation takes about 80 - 90 minutes after mixing of the components, well within the pot-life of the resin. A more detailed procedure is given in appendix A.

Two dummy cables were prepared in this way, one using a mixture filled with fused silica to 50%, and one to 60% of the total weight. After curing, the dummies were cut in two parts with a diamond saw, and the cross-sectional surfaces were polished. In figure 4.4, microscopic images are shown. The sample impregnated using 50 wt% filler shows good impregnation quality: no voids are visible between the strands or inside the central hole. On the other hand, the sample for which 60 wt% filler was used has a void near the ceiling of the central hole. This is probably due to an increased viscosity of the resin, that results from the higher filling ratio. The use of 50 wt% filler can be recommended.

To check if the used method is suitable for *RE*BCO tapes, the impregnation with 50 wt% filler was repeated on a dummy cable of which one steel strand is replaced by a real superconducting strand. The critical current of this strand was measured at T = 77 K before and after impregnation. After that, the sample was measured once more after warming up and cooling down, to check the effect of thermal cycling. The results are shown in table 4.1. The critical current after impregnation was 170.2 A compared to 171.7 A before impregnation. The impregnation did not cause serious damage.

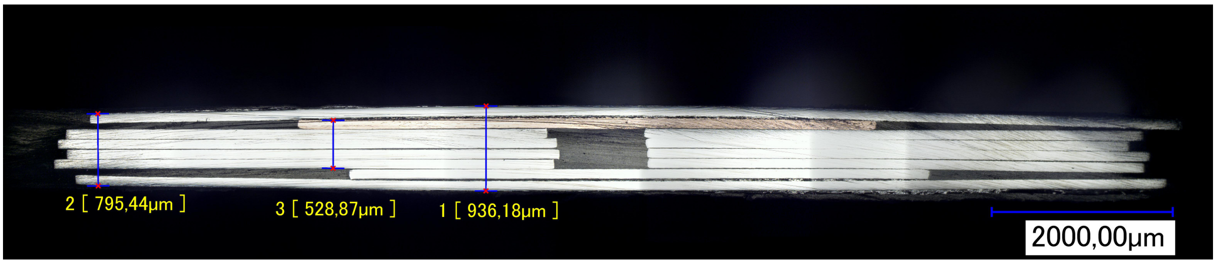

(a) Dummy cable impregnated with 50 wt% filled resin.

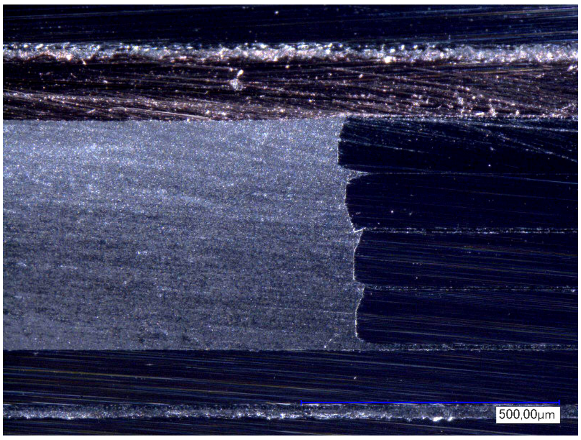

(b) 50 wt% fused silica

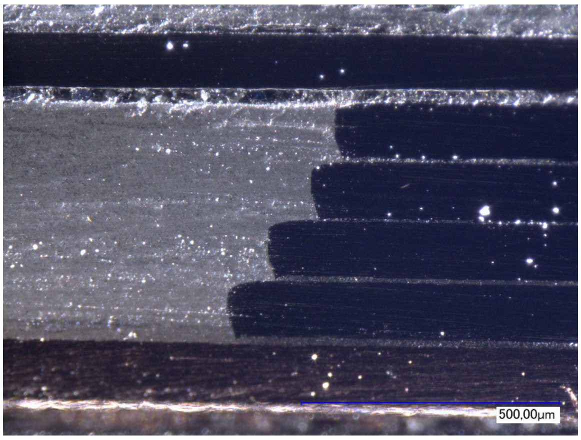

(c) 60 wt% fused silica

Figure 4.4: Cross-sections of dummy cables impregnated with epoxy resin filled with fused silica. Figure 4.4a shows the cross-section of a cable successfully impregnated with 50 wt% silica filler. 4.4b and 4.4c are close-ups of the central hole in sample impregnated with 50 wt% and 60 wt% filler. A void is visible in 4.4c where 60 wt% filler was used.

	I_c [A]	n
Before impregnation	171.7	28.1
After impregnation (cycle 1)	170.2	26.8
After impregnation (cycle 2)	170.9	28.5

Table 4.1: Critical currents and n-values of a Roebel dummy with one *RE*BCO strand.

4.5 Conclusion and discussion

Several dummy cables were impregnated and analysed. We found that vacuum impregnation is necessary in order to attain good impregnation quality (no voids). The use of filled resins together with glass-fibre results in voids and cannot be recommended. Good impregnation quality was achieved by replacing the glass-fibre by steel tapes, and vacuum impregnation at 80 °C using resin Araldite CY5538/HY5571 filled to 50 wt% with fused silica powder Silbond FW600 EST. The impregnation was validated on a dummy with one *RE*BCO strand, and no serious degradation of the critical current was observed.

The exact reason for the problems when using filled resin and glass-fibre together remains unclear. The simplest explanation is filtration by the fine fibres, which disrupts the distribution of particles. The forced flow of resin into the narrow openings between the strands may have a similar effect. This was not a problem in our case, in which only a single cable was impregnated. In larger structures such as coils, this may cause problems as the resin travels over a much longer distance, and meets many more narrow openings.

Also, the effect of thermal stresses in large coils needs more attention. The bigger the volume, the bigger the total contraction, and the more the stresses build up. It cannot be guaranteed yet that the used method will also be suitable for that purpose.

Chapter 5

Out-of-plane bending of *RE*BCO Roebel cables

5.1 Introduction

The original U-shaped sample holder of the cryogenic press (section 6.2.2) was designed for Nb_3Sn cables. These cables were shaped on the holder before heat treatment, when they where still ductile. Therefore, a small bending radius of 10 mm could be used. Roebel cables are assembled from ready-made *RE*BCO tapes that contain a brittle superconducting layer. A bending radius of 10 mm may be too small for such cables. Several alternative sample holders with larger bending radii have been designed. They are described in more detail in appendix B. In order to make a decision on the sample holder design, it is necessary to know the limitations on bending of Roebel cables.

Previous bending tests on single *RE*BCO tapes from SuperPower have shown that these conductors can tolerate bending to radii as low as 11 mm [56]. For Roebel cables, however, no such tests had been done. This chapter reports on experiments in which Roebel cables were bent in the out-of-plane (soft) bending direction.

As only one side of the substrate is coated with *RE*BCO, the layered structure of the tape is asymmetric. This may have an effect on mechanical properties. For example, different behaviour depending on the orientation of the *RE*BCO layer has been found in transverse stress experiments [22]. Therefore, bending was tested both with the *RE*BCO layer facing outward and inwards (figure 5.1).

Figure 5.1: Out-of-plane bending in two directions. For simplicity, only the Hastelloy, *RE*BCO and copper layers are shown. See figure 1.2 for a complete cross-section.

5.2 Experimental details

5.2.1 Sample description

SCS12050-AP REBCO tape from SuperPower was used (Table 5.1). The tape has 100 µm of copper stabilization instead of the usual 40 µm. As a result the total thickness of the conductor is 160 µm.

Spool I.D.	SP-KIT-20110913-9
Internal Tape I.D.	"M3-904-2 415.93-441.33"
Length [m]	25.4
Width [mm]	12.02
Thickness [µm]	160
Hastelloy substrate [µm]	50
Copper stabilization [µm]	*100*
Average I_c [A]	343
STDEV	0.82
Minimum I_c [A]	338

Table 5.1: Conductor specification as supplied by SuperPower

The tape had already been punched into Roebel strands with 126 mm transposition length for another project, but 12.6 meter had not been used. From this unused section 22 samples were cut with a length of 56.7 cm (4.5 times the transposition length). 20 strands were characterized and assembled into two Roebel cables. Because of cutting half twist pitches, every next strand is a mirror image and only even or uneven strands can be assembled into a cable. Cable 1 consists of the uneven strands 1 - 19, cable 2 of the even strands 2 - 20. The remaining two strands 21 and 22 were used for bending tests on single strands. Cable 1 and strand 21 were bent with the *RE*BCO layer on the inside (side with the lower bending radius); cable 2 and strand 22 were bent with the *RE*BCO layer on the outside.

5.2.2 Sample holder

A simple sample holder (figure 5.2) was designed and built to test the cable with various bending radii. The sample holder consists of a G10 support plate, a current lead assembly and a cylindrical former around which the cable is bent. The cylindrical part comes in 7 different radii: 50, 33, 26, 20, 16, 13 and 10 mm. In this way, the sample can be tested with decreasing bending radius. Both the cylinder and the current leads are movable to adjust for bending radius and sample length. The current leads are depressed so that the sample is directly supported by the G10 board.

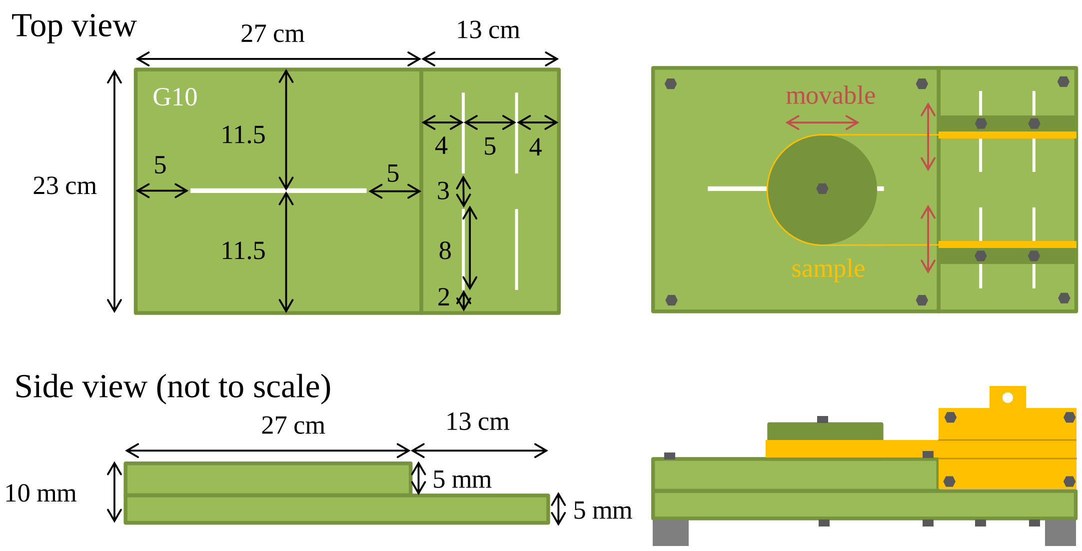

Figure 5.2: The sample holder used for cable bending. The cylindrical part comes in six different radii ranging from 10 to 50 mm. The sample and the current leads are in orange.

5.2.3 IV measurements

All four samples are soldered in copper current leads over a length of 13 cm. The cable section between the current leads has a length of 18.5 cm. Voltage taps are soldered to the ends of the cable that stick out of the backside of the current leads. In this way, no additional cable length is needed. The downside is that any defect related to the current leads will influence the measurements. The voltage is always measured over voltage taps soldered on the same strand. The voltage over single strands 21 and 22 is measured over one transposition length (12.6 cm) between the current leads.

All measurements were performed in liquid nitrogen ($T = 77$ K) with only the magnetic self-field present. As described in section 2.2, the critical current is computed from IV-data using the 1 μV/cm criterion (i.e. 18.5 μV for cables and 12.6 μV for the single strands).

5.3 Results

5.3.1 Individual strands before cable assembly

Strands 1 - 20 were characterized before cable assembly on a straight sample holder. The voltage was measured over 31.5 cm (2.5 transposition lengths). The computed critical currents and n-values are shown in figure 5.3.

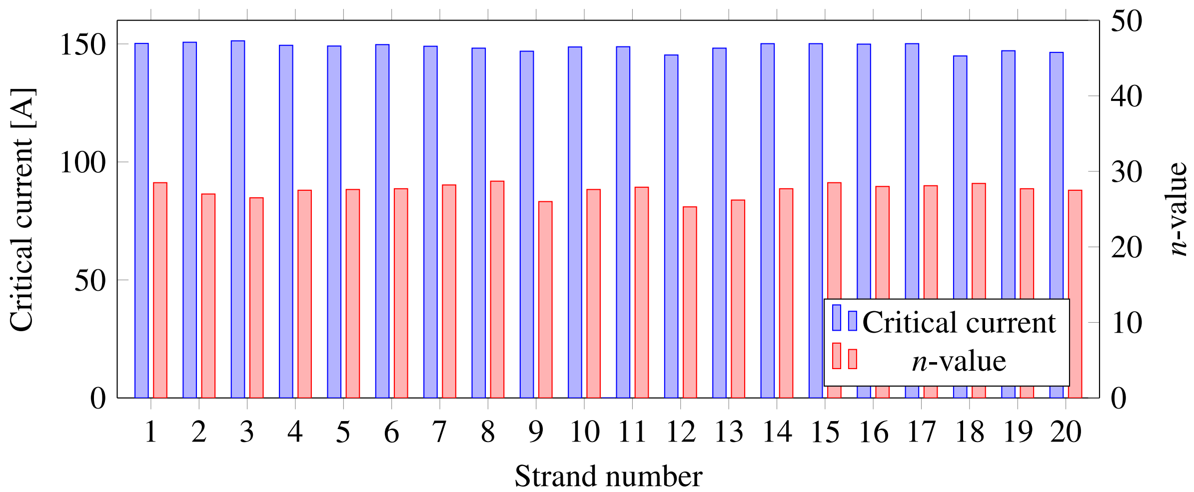

Figure 5.3: Critical current and n-value of the separate strands before cable assembly.

During the punching process, the width of the tape is reduced from 12 to 5.5 mm. The expected critical current for an ideally punched tape is therefore $5.5/12 \times 100\% \approx 45.8\%$ of the whole tape specification. The measurements show an average critical currents of 148.7 ± 1.8 A, which is 43.4 % of the average value as specified by SuperPower. No defects were observed.

5.3.2 Bending of single Roebel strands.

Single strands were bent in both possible orientations of the *RE*BCO layer (figure 5.1): *RE*BCO inside (Strand 21) and *RE*BCO outside (Strand 22). The bending radius was decreased step by step from 50 to 10 mm. In figure 5.4 the critical currents are shown.

No degradation of the critical current can be observed when decreasing the bending radius down to 10 mm. Strand 22 has a critical current lower than any of the other tapes. The damage was probably done during soldering of the current leads or mounting on the sample holder.

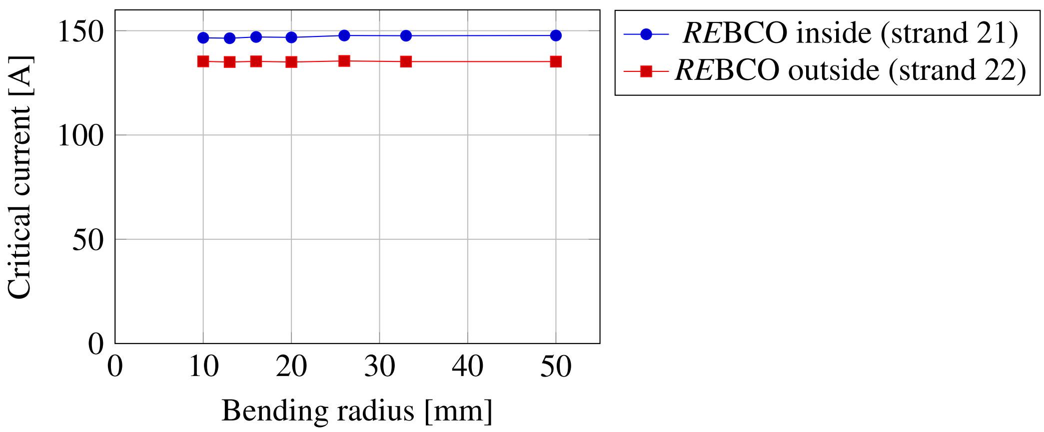

Figure 5.4: Critical current of the Roebel strands with decreasing bending radii.

5.3.3 Bending of Roebel cables

The voltage taps were soldered on the strands outside of the current leads (figure 5.5). This could be done only on six of ten strands in each cable, as the remaining four did not stick out of the current lead far enough. Critical currents and were computed for the measured pairs and averages are shown in the figure 5.6. Three of the strands in cable 2 (6, 8 and 16) showed resistive behavior for an unknown reason and were excluded from the average.

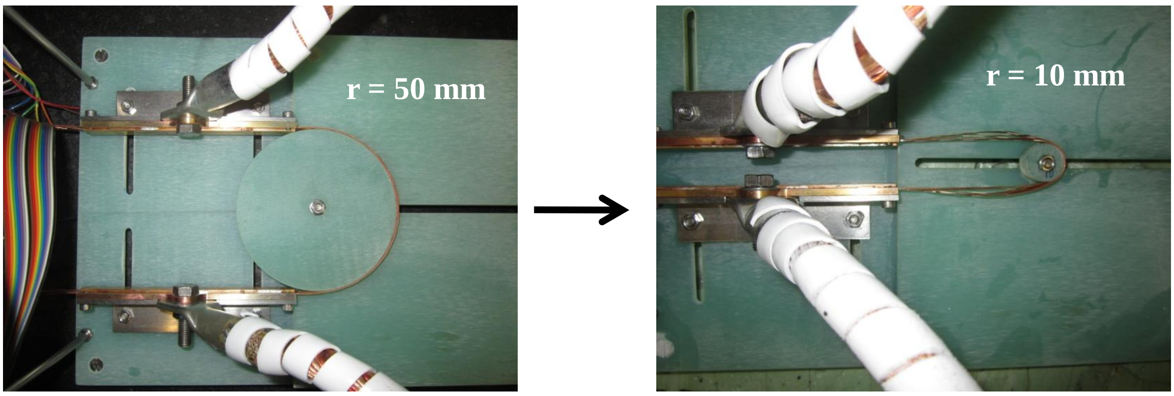

Figure 5.5: A Roebel cable mounted on the sample holder. The voltage taps are the thin colored wires visible in the left of the picture. They are connected outside of the current leads.

The critical current of cable 1, which had its *RE*BCO layer facing inwards, degraded by 63 A ($\approx 6\%$) when the bending radius was decreased from 26 to 20 mm. Cable 2 did not show any degradation during bending to this point. However, the number of data points is insufficient to conclude if this difference is related to the orientation of the tape (*RE*BCO inside/outside).

No degradation was observed when decreasing bending the bending radius further down to 10 mm. The critical currents even slightly increased for the lowest bending radii. So far no explanation for this behaviour has been found.

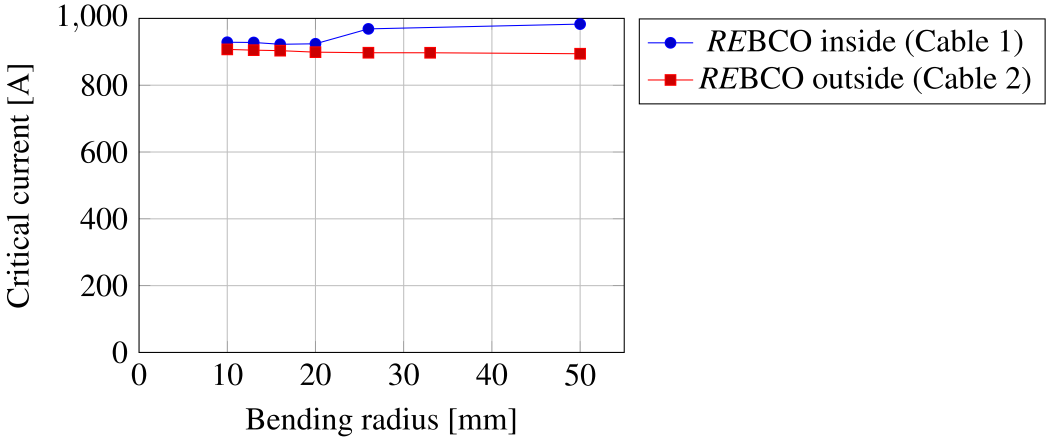

Figure 5.6: Critical current of the Roebel cables with decreasing bending radii.

5.3.4 Individual strands after cable disassembly

Since the voltage was measured over the entire cable length, including the soldered contacts, one cannot be sure about the location of any degradation. The cables were disassembled and the individual strands were measured once more, this time only over 10 cm length including the segment that was bent.

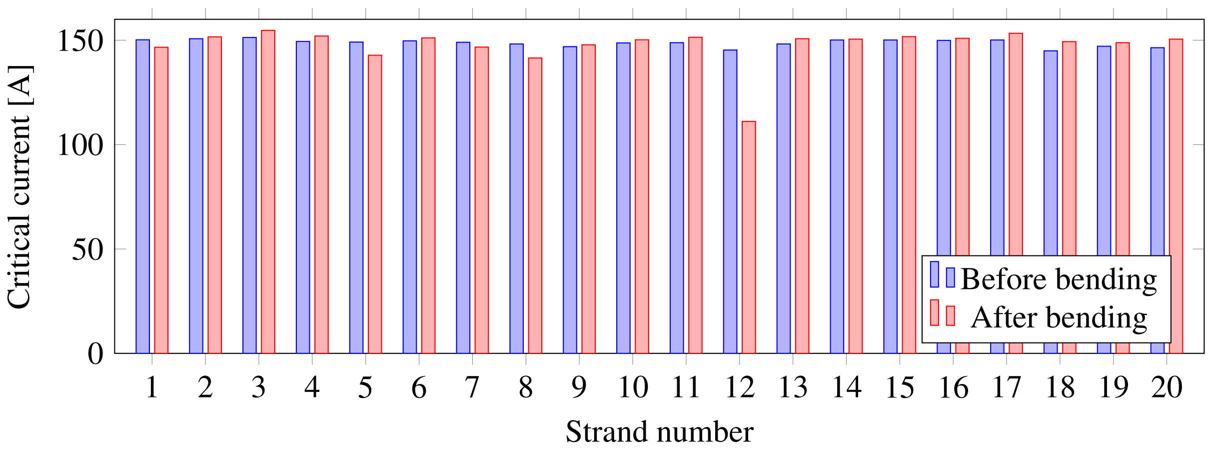

Figure 5.7: Critical currents of the single Roebel strands before and after bending.

Strand 12 shows a degradation of about 24%. Statistically, however, this strand is an outlier: the average critical current after bending is 147.7 ± 9.2 A, compared to 148.7 A before cabling. This is an average degradation of less then 1%. It can be concluded that cable bending to 10 mm causes hardly any degradation of the critical current.

5.4 Conclusion

Degradation due to bending strain was low (< 6.5 %) to zero for bending radii in the range 10 - 50 mm. To locate the damage, the cables were disassembled and the separate strands were measured once more, but this time only in the bent section. These measurements show that the average degradation in the bent section was less then 1%.

Based on this results a sample holder with 20 mm bends was constructed for the press at Twente University. The sample holder is discussed in more detail in section 6.2.3.

Chapter 6

Transverse strength of a *RE*BCO Roebel cable

6.1 Introduction

In this chapter, the central question of the master assignment is addressed: "Can impregnation reduce the transverse pressure sensitivity of *RE*BCO Roebel cables?" To answer this question, the critical current of a cable was measured at various pressure levels. The experimental details are destribed in described in section 6.2, the first results in section 6.3.

6.2 Experimental details

The measurements were done in a unique set-up at Twente University, which comprises a total of nine superconducting coils. It is capable of currents up to 50 kA, forces up to 250 kN and a background field of 11 T (figure 6.1). The system contains a lot of low-temperature superconducting wires, and it is therefore always operated in a liquid helium bath (T = 4.2 K). The transformer, the press and its geometry and sample preparation are discussed.

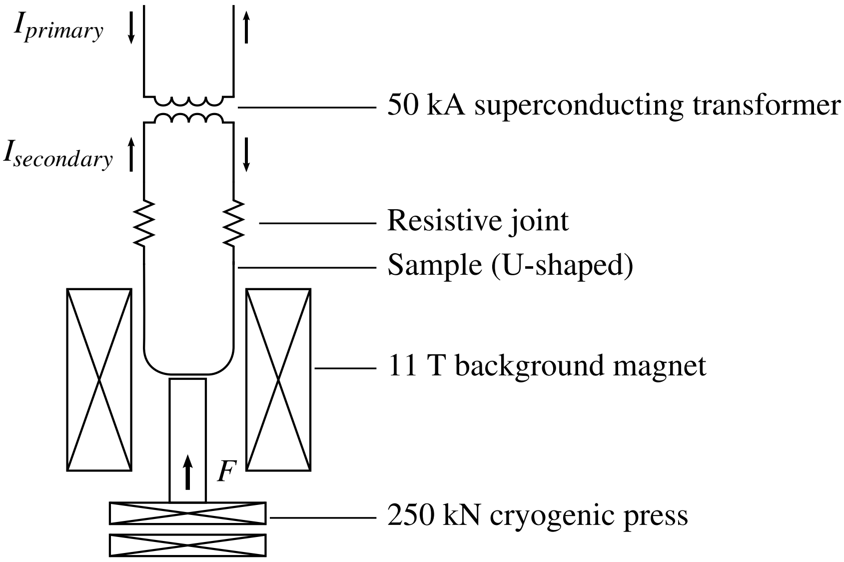

Figure 6.1: Scheme of the press set-up.

6.2.1 Superconducting transformer

The sample current is supplied by a superconducting transformer, which was built at Twente University [57, 58]. The transformer consists of a primary coil with a large number of turns, and a secondary coil with just one-and-a-half turns (see figure 6.2). Both coils are wound with NbTi wires. The secondary coil is connected to the sample, while the primary coil is connected to a current source. The transformer amplifies the current by a factor 1000. In this way, sample currents of 50 kA can be reached using only a small and relatively inexpensive 50 A current source. Another advantage is that the resistive current leads between the 4.2 K transformer and the room temperature power supply can be designed with a 1000 times smaller cross-section. This reduces the heat flow into the cryostat and saves liquid helium.

Transformers in resistive circuits can be operated only with alternating currents, since they rely on an induced voltage. In a superconducting transformer, the situation is different. The secondary coil is soldered to the superconducting sample, forming a loop with the soldered joints as the only resistive parts. Without an induced voltage due to flux coupling with the primary coil, the current decays exponentially with a time constant $\tau = L/R$, in which L is the self-inductance and R the resistance of the loop. A self-inductance of about 1 μH and a joint resistance of typically 2 nΩ result in a decay time of 500 s. This is a relatively slow decay, and can be compensated for by slowly increasing the primary current. In this way, the transformer can essentially be operated in DC mode for a limited time.

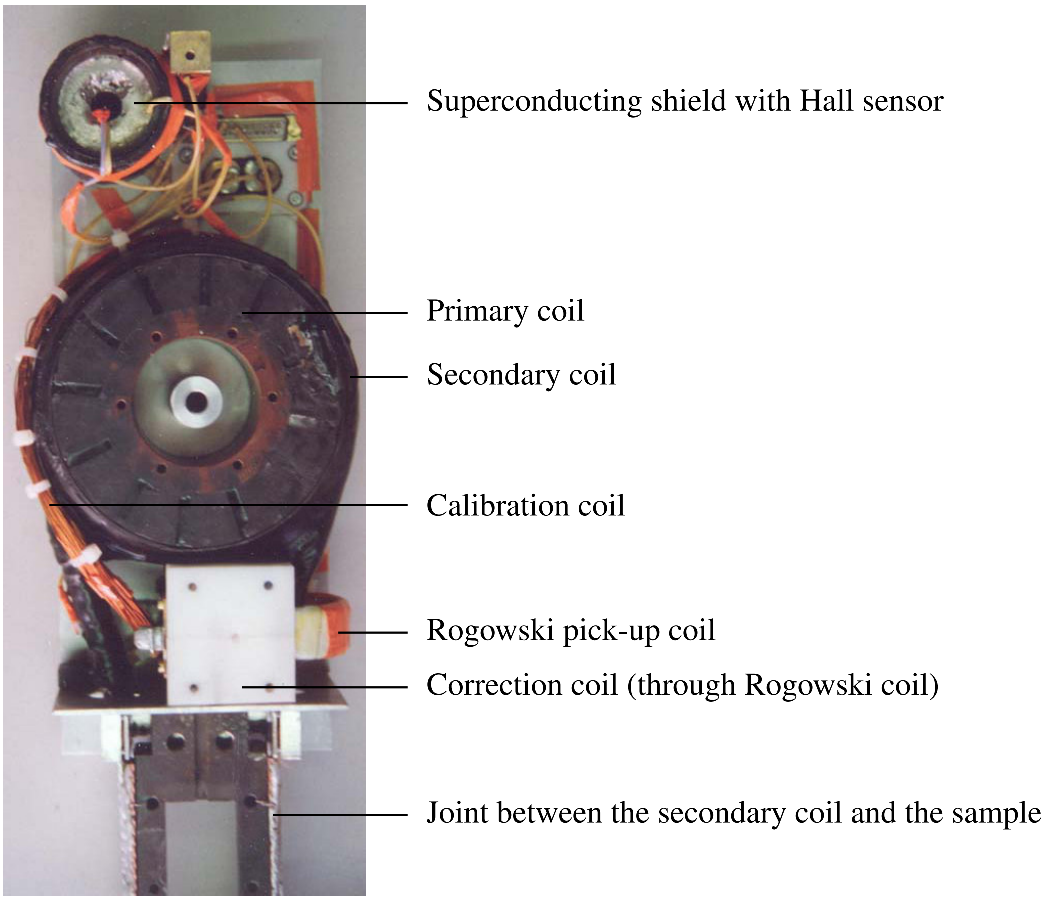

Figure 6.2: The superconducting transformer without its steel cover. Picture from W. Wessel [59].

Current meter

Measuring the current in the secondary coil is not straightforward. Adding a shunt resistor in series with the coil is not an option, as it would severely decrease the decay time and thus limit the measurement time. Direct magnetic measurements using a Hall sensor would be disrupted by the magnetic field of the many nearby coils. A new and accurate current meter was developed by H. ten Kate et al. specifically for use in these conditions [60, 61].

The electric scheme of the transformer is shown in figure 6.3. The core of the current meter is the purple superconducting loop consisting of the toroidal Rogowski coil and the Hall sensor coil connected in series. The Rogowski coil encloses the loop carrying the secondary current: the two loops are coupled and act like another transformer. A change in secondary current induces a current in the purple loop that does not decay. The loop current is detected by a Hall sensor, which is located above the transformer and shielded from all other magnetic fields

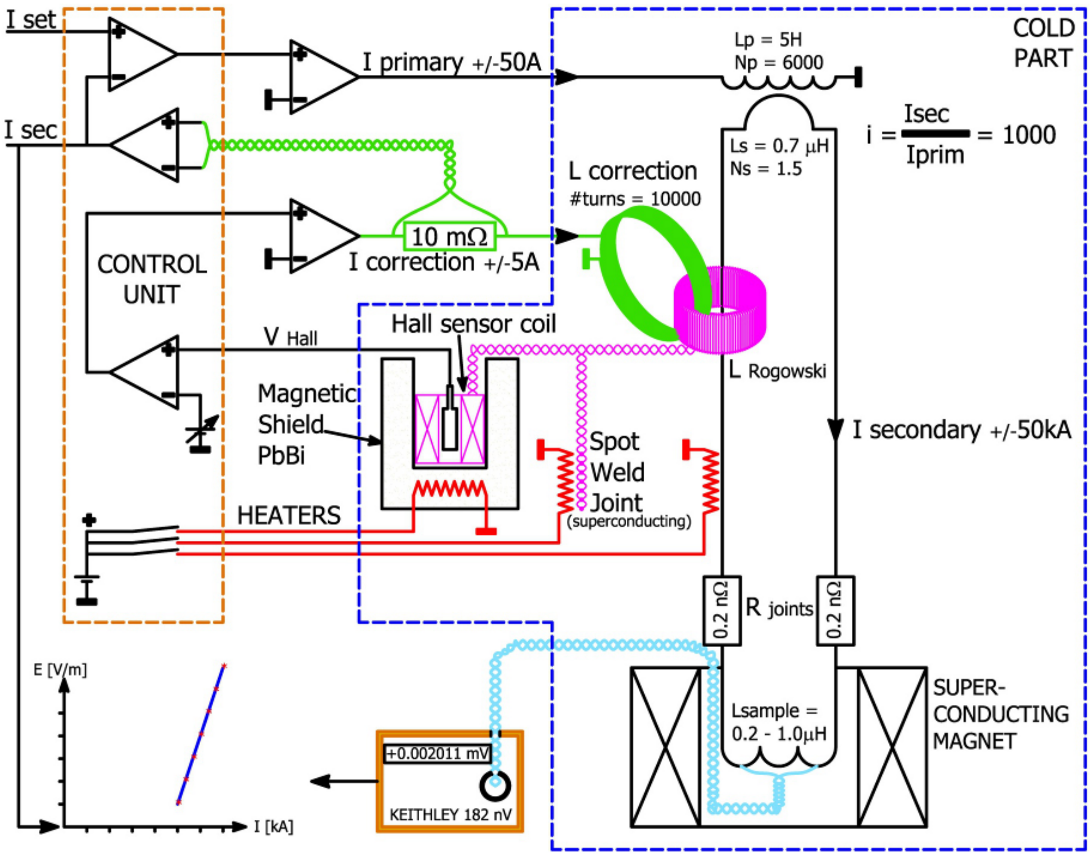

Figure 6.3: Electric scheme of the superconducting transformer [59].

by a thick superconducting layer of PbBi. The Hall voltage on its turn drives a power supply that sends a current through a correction coil with 10000 turns (in green). The correction coil is also enclosed by the Rogowski coil, but the direction of its flux is opposite to that of the secondary current. A rise in correction current will therefore decrease the loop current. A negative feedback loop has been formed: the correction coil current increases until the purple loop current is back to zero. At equilibrium, the correction current is equal to $1/10000$ of the secondary current. The correction current is passed through a 10 mΩ shunt resistor, and from this voltage the secondary current is computed.

The advantage of the correction system is that the Rogowski coil and the Hall sensor are operated around zero current so that the current measurement is no plagued by non-linear behaviour of the superconducting loop or the Hall sensor. The accuracy of the system has been shown to be better than 0.1% in its full range [61].

To test the current meter, the Rogowski coil also encloses a 125-turn calibration coil (see figure 6.2). The calibration coil emulates a current in the secondary loop that can be directly controlled using a current source. The current meter is tested before each series of measurements.

Feedback loop for the secondary current

Without an induced voltage, the secondary current will decay slowly due to dissipation in the soldered joints. The control unit of the transformer features a feedback loop that can keep the secondary current at a certain level. When enabled, the voltage over the correction shunt resistor is subtracted from a certain set voltage (I_{set} and I_{sec} in figure 6.3). The voltage difference drives the voltage over the primary coil, ramping it until the secondary current reaches the desired level. The set voltage can be controlled externally for automatized measurements with a computer.

Heaters and quench protection

There are electric heaters on the secondary coil, on the Rogowski coil loop and on the superconducting shield. These heaters are used to quench the respective parts and remove any current. The heaters can be switched on or off manually using the control unit.

The thermal stability of Roebel cables at $T = 4.2$ K has not been analysed yet. The cable might quench and the resulting temperature rise might cause damage. To prevent the cable from burning, a quench detector was installed that automatically turns on the secondary heater if its input voltage exceeds a threshold of about 7 mV. (Basically, the relay output of the quench detector was soldered in parallel with the switch in the control unit.) By quenching the secondary coil, part of the energy stored in the loop is dissipated there, and not in the sample. The temperature rise will therefore be smaller. In the experiments carried out for this assignment, the sample did not quench, and the quench protection had not been necessary.

6.2.2 Cryogenic press

The transverse stress on the sample is generated by a superconducting press built at Twente University [62]. The different parts of the press are shown in figure 6.4. On the bottom there are two NbTi “pancake” coils. The currents in both coils run in opposite directions, resulting in a repulsive Lorentz force between them up to 250 kN. The lower pancake coil is fixed to the sample holder by the stainless steel outer structure. The upper pancake coil lifts the inner cylinder which pushes against the sample. A pushing block with a sample-specific geometry can be attached on top of the inner cylinder. For our measurements, the pushing block is not attached here, but glued on the sample (see section 6.2.3). Three springs separate the upper coil from the outer structure, to prevent the inner cylinder from being launched at high speed.

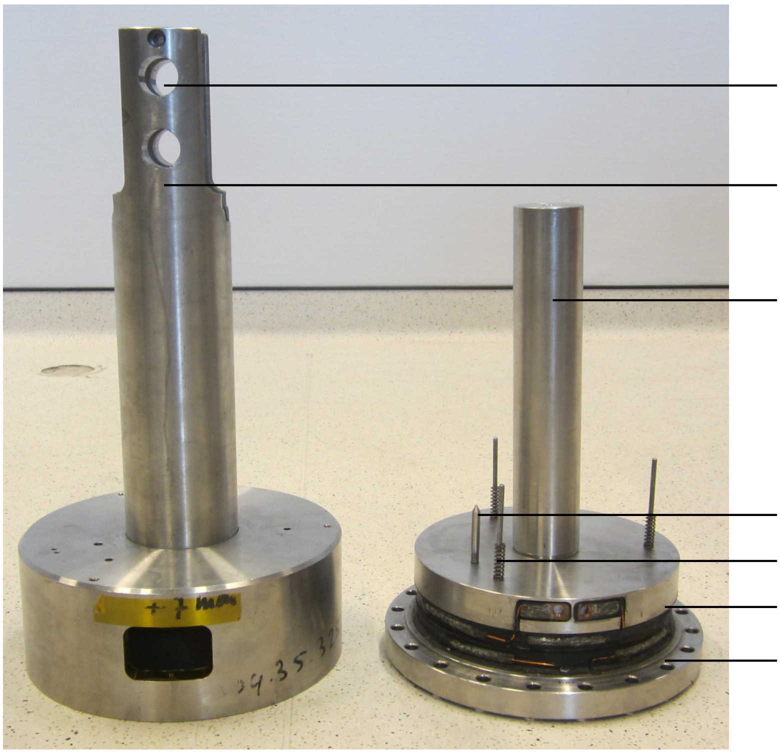

Figure 6.4: The disassembled cryogenic press.

The upward force on the inner cylinder is described by the following equation [62]:

$$F = I_p^2 \frac{\partial M_{12}}{\partial z} \pm I_p I_m \frac{\partial M_{m1}}{\partial z} - mg \tag{6.1}$$

In this equation,

- I_p is the press current in A
- I_m is the current of the background magnet in A
- M_{12} is the mutual inductance between the two pancake coils in H
- M_{m1} is the mutual inductance between the upper pancake coil and the background magnet in H
- $m = 11$ kg, the mass of the upper pancake coil and the inner cylinder
- $g = 9.81$ m/s^2, the gravitational acceleration
- z is the vertical dimension

The first term is the repulsive force between the two pancake coils. The second term describes the force on the upper pancake coil due to the background magnetic field. Its sign depends on the relative direction of the currents in the upper pancake coil and the background magnet.

During the measurements described in this report, the currents were anti-parallel, leading to a repulsive force. The background field of the main magnet pushed the upper pancake coil down and the force on the sample is decreased. The sign of the second term should therefore be negative. The third term is a correction for the gravitational force on the movable parts.

$\partial M_{12}/\partial z$ and $\partial M_{m1}/\partial z$ can be approximated by a linear expressions depending on the displacement of the upper pancake coil Δz [62]:

$$\partial M_{12}/\partial z \approx a_1 \Delta z + b_1 \tag{6.2}$$

$$\partial M_{m1}/\partial z \approx a_2 \Delta z + b_2 \tag{6.3}$$

With coefficients:

$$\begin{aligned} a_1 &= -2710\ \mathrm{H/m^2} \\ b_1 &= 82.47\ \mathrm{H/m} \\ a_2 &= 23\ \mathrm{H/m^2} \\ b_2 &= 2.277\ \mathrm{H/m} \end{aligned} \tag{6.4}$$

Extensometer

The derivative of the mutual inductances and thereby the force depend on the displacement of the upper coil Δz. It is therefore necessary to measure this displacement. This is done using an extensometer (figure 6.5). A cylinder with a sharp tip is fixed on the upper pancake. The tip pushes against a plate of a titanium-alloy. This plate is fixed to the outer structure of the press, to which the lower pancake coil is also fixed. Four strain gauges in a Wheatstone bridge configuration are glued onto the plate. The Wheatstone bridge configuration ensures a high sensitivity and a linear response. A current of 1 mA is used to excite the bridge.

The extensometer was calibrated by W. van de Camp [63, p. 76]. A linear calibration factor

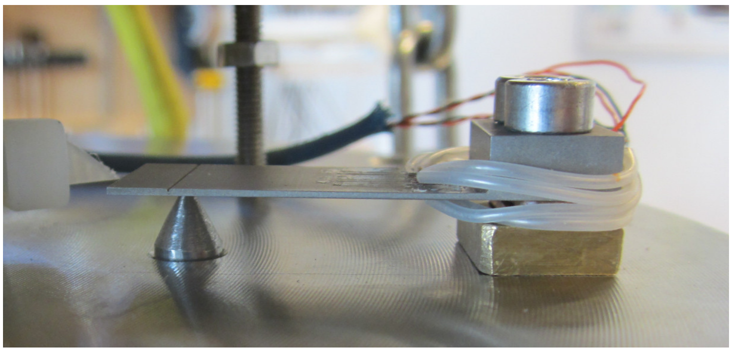

Figure 6.5: The extensometer.

was determined of 1.080 V/m at room temperature and 1.046 V/m at $T = 77$ K. For measurements at $T = 4.2$ K, the calibration factor 1.046 V/m is used.

6.2.3 Sample holder and pushing block

The background magnet has an inner bore of 8 cm. A U-shaped sample holder is used to attain a horizontal measurement section in the center of the magnet (figure 6.1). The original sample holder had 10 mm radius bends and a 46 mm straight section in between. This holder was used to test Nb_3Sn cables which were reacted in the required shape, so the low bending radius was not a problem. *RE*BCO cables are always made from ready-made tapes, which contain a brittle *RE*BCO layer. The bending properties of the cable therefore need to be taken into account. In chapter 5, we show that, at 77 K, Roebel cables can be bent down to a 10 mm bending radius without degradation. Still, we chose to use a sample holder with 20 mm bending radius to leave some margin for additional stresses, which could result from impregnation, further cool-down to 4.2 K or Lorentz forces. The bending radius of one sample holder was increased to 20 mm by spark erosion (see figure 6.6a). The remaining straight section has a length of 26 mm.

The pushing block is shown in figure 6.6b. The face that presses the cable has is 12 mm wide and 30 mm long, corresponding to 24.8% of the transposition length. The pushing block

(a) Sample holders

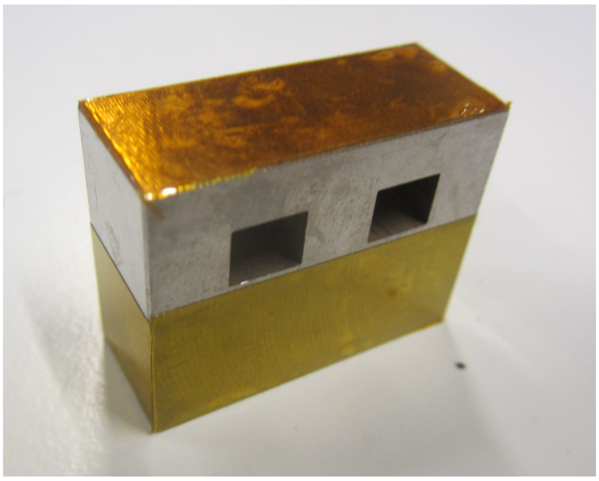

(b) Pushing block

Figure 6.6: (a) An original sample holder with 10 mm bending radius (left) and the modified sample holder with 20 mm bending radius (right). (b) The pushing block. The lower side is the side facing the cable.

is longer than the straight section of the sample holder. This is done to avoid a high local strain at the corners of the pushing block. The two rectangular holes are used to position the pushing block so that its surface is parallel to the inner cylinder of the press. This ensures that the pressure is evenly applied to the cable. The pushing block is then glued to the sample in this position over 30 mm. The sides of the pushing block are covered in Kapton polyimide tape, to prevent unwanted adhesion to the sample holder. The top is also covered in four layers of Kapton tape. The idea is that this soft layer will redistribute the force if the pushing block is still not properly aligned to the inner cylinder.

For calculation of the stress, a sample length of 30 mm is used, even though the straight section of of the sample is only 26 mm. As the pushing block is 30 mm long, this corresponds to the largest possible pressed surface, i.e. the minimum average pressure.

A 30 mm sample length is assumed as well of for determining the critical current. The critical current of a Roebel cable is strongly dependent on the orientation of the magnetic field (see figure 1.1). A voltage will therefore arise only in the cable section where the angle between the wide surface and the magnetic field is close to 90°. As the straight section of the cable is short compared to the bends, this length is not well-defined. For determining the critical current, a sample length of 30 mm is used, corresponding to the pushing block length. The motivation is that all damage due to pressing will occur in this segment.

More information about the sample holder design can be found in appendix B. Technical drawings can be found in appendix C.

6.2.4 Sample description and preparation

The cable was made from SuperPower SCS12050-AP *RE*BCO tape. This tape is 12 mm wide, has a 50 µm thick Hastelloy substrate, 2 µm silver and 40 µm copper stabilization. More

Spool I.D.	SP-KIT-20131011
Internal Tape I.D.	"M3-1081-2" 984.05-1049.05m
Length [m]	65
Width [mm]	12.00
Thickness [mm]	0.93
I_c average [A]	398
STDEV [%]	1.52
I_c minimum [A]	390

Table 6.1: Conductor specification as supplied by SuperPower. The critical current was measured at $T = 77$ K and in self-field.

conductor specifications are listed in table 6.1. A 75 cm long, 10-strands cable was prepared from this tape following the procedure in section 2.1.

Next, the cable was mounted on the sample holder. The *RE*BCO side of the cable faced the sample holder, as this side will be soldered to the transformer. This orientation is used for a lower contact resistance, as in opposite orientation the current would be forced to flow through the copper edges of the tape or through the highly resistive substrate and buffer layers. At the horizontal segment, the cable is supported against the sideways Lorentz forces by thick steel plates. In the vertical section, the cable experiences a small outward Lorentz force caused by its own magnetic field. The cable is supported by steel plates against this force too. All metal surfaces that can be touched by the cable were covered with Kapton polyimide tape for electrical insulation. Pairs of voltage taps were soldered on three strands over a distance of one transposition length (figure 6.7a). A block of Teflon was pushed against the horizontal segment to create a flat epoxy surface and prevent it from flowing out during the curing process (figure 6.7b).

The cable was impregnated using the same procedure that was successfully used on dummy cables. This method is described in section 4.4 and appendix A. The impregnation set-up used at UTwente is very similar to the one used at KIT. The main difference is that the sample holder and resin container are heated using heating resistors instead of an oven. Because the resin container is bigger, 280 g of resin needs to be prepared.

Figure 6.7c shows the cable after impregnation. The surface looks flat with the naked eye and no bubbles are visible in the resin. The big dark stain was already there before impregnation. Next, two layers of glass cloth with Stycast 2850FT/23LV epoxy were added to the cable. The pushing block was positioned in the epoxy using two spark eroded plates which were fixed to the sample holder with the 25 mm fixation cylinders. This method makes sure that the pushing block is properly aligned to the press. The distance between the lower side of the pushing block and the sample holder is 1.5 mm, leaving an approximately 0.8 mm thick layer of epoxy. The positioning plates were removed after the glue had become dry. Figure 6.7d shows the pushing block glued in place.

Then the sample holder was attached to the transformer. The Roebel cable was soldered between the transformer cable and a copper plate over a length of 126 mm with $Sn_{97}Ag_3$ solder. A hot plate was used to heat the cables.

Finally, the sample was fixed to the sample holder. At the current leads, this was done by wrapping it in glass fibre tape with Stycast epoxy. Below the current leads, the cable was fixed with four pairs of stainless steel plates screwed together, replacing the tie-wraps in figure 6.7b.

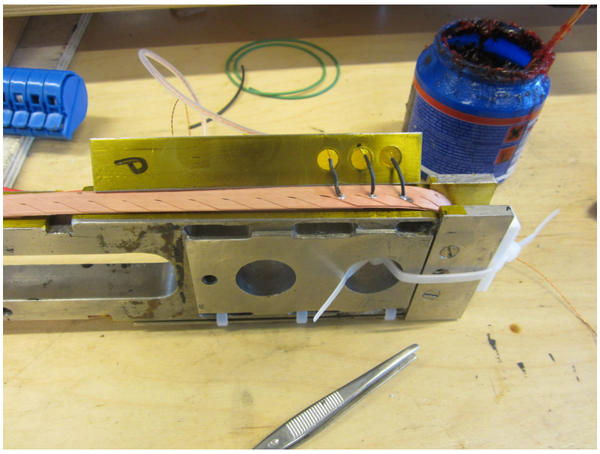

(a) Voltage taps on three strands.

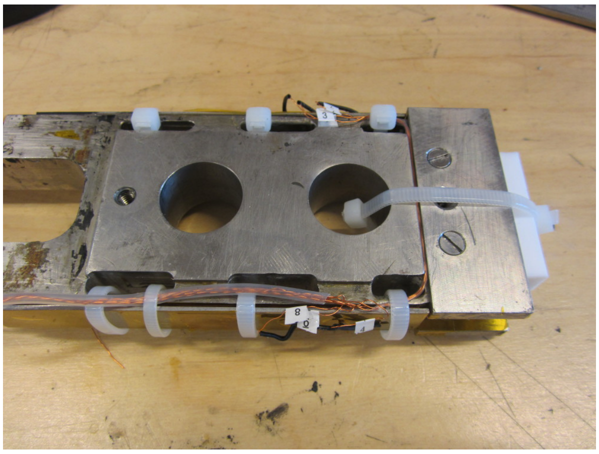

(b) Cable prepared for impregnation.

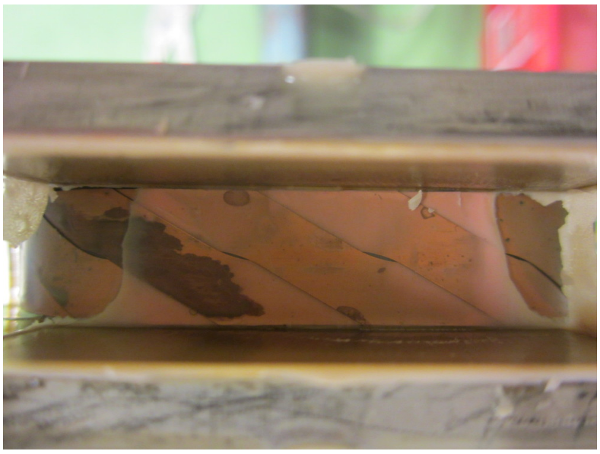

(c) After impregnation.

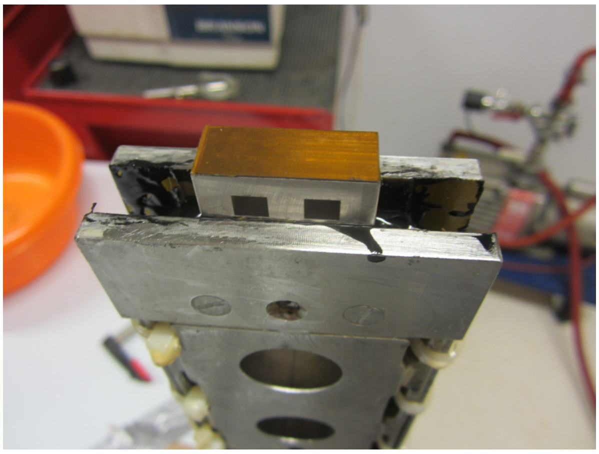

(d) Pushing block glued in place.

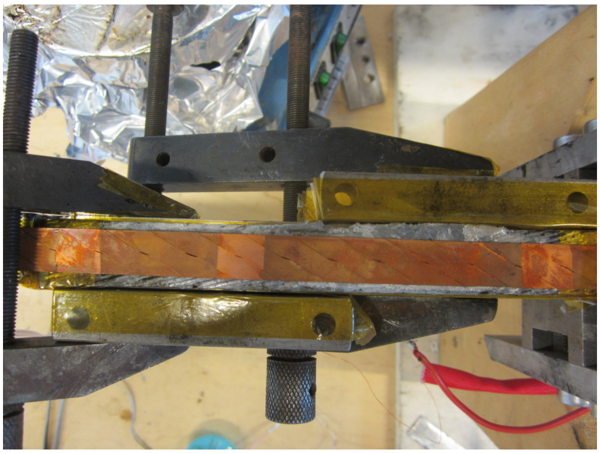

(e) Current contact before soldering.

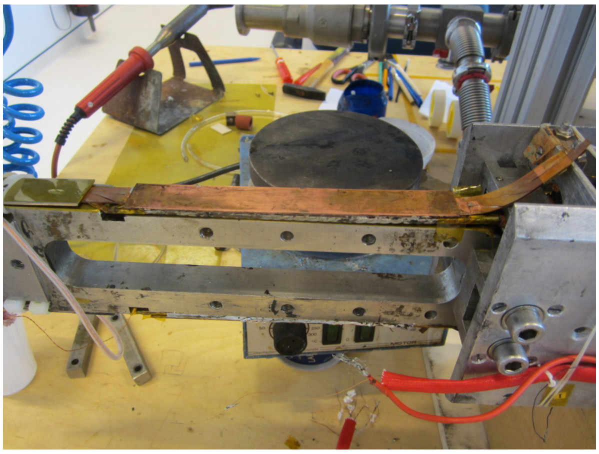

(f) After soldering.

Figure 6.7: Preparation of the sample.

6.3 Results

6.3.1 Critical current of separate strands

Before cable assembly, the separate strands were measured in a liquid nitrogen bath ($T = 77$ K) and no external magnetic field. The voltage was measured over a distance of 67 cm. The strands had an average critical current of 173.3 ± 2.0 A, 43.5% of the specification of the unpunched tape. For an ideally punched tape this value would be 45.8% (see section 5.3.1). The average n-value was 29.0 ± 1.0. No defects were found; all strands could be used for cabling.

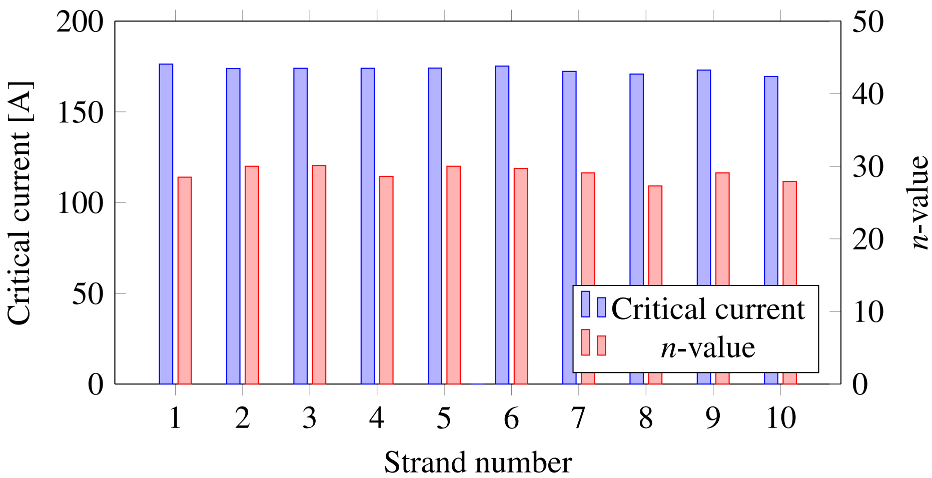

Figure 6.8: Critical currents and n-values of the separate strands.

6.3.2 Joint resistance

The secondary loop is basically an RL-circuit. Without an induced voltage from the primary coil, the current decays exponentially with a time constant τ:

$$I(t) = I_0\, e^{-t/\tau} \tag{6.5}$$

$$\tau = L/R \tag{6.6}$$

The self-inductance of the loop is approximately $L = 1$ µH. The loop resistance R can be computed from the time constant by observing the current decay when the feedback system is switched off.

A current of about 1 kA was induced, without external magnetic field and without applied pressure. The current decay over time is shown in figure 6.9. The current was found to decay

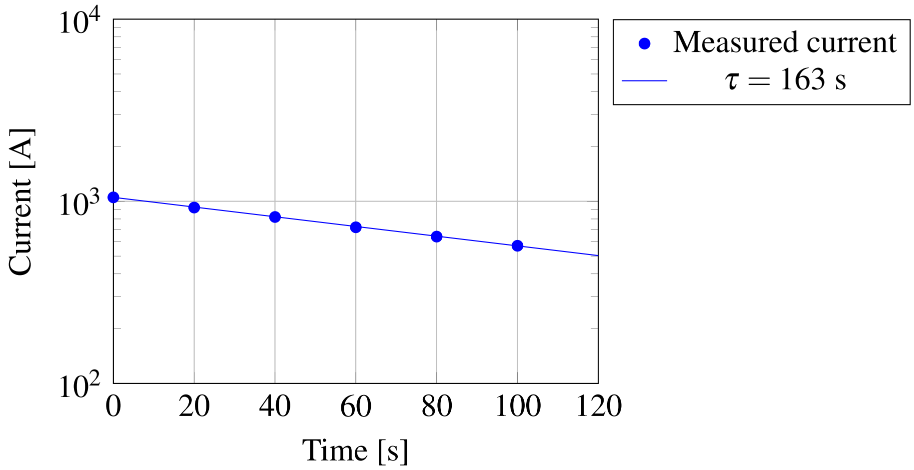

Figure 6.9: Decay of the sample current due to joint resistance.

exponentially with a decay time of 163 s. The loop resistance is therefore

$$R = L/\tau = 6.13 \text{ n}\Omega \tag{6.7}$$

or 3.06 nΩ per joint. The joints have an area of 12 mm × 126 mm, thus the surface resistivity is:

$$3.06 \text{ n}\Omega * 12 \text{ mm} * 126 \text{ mm} = 4.63 * 10^{-12} \ \Omega\text{m}^2 \tag{6.8}$$

This is a slightly lower value than the $8.92 * 10^{-12}$ Ωm^2 reported by J. Fleiter [25].

Since the self-inductance value is only an estimate, the computed joint resistance is not very accurate. The self-inductance for this specific sample geometry must be computed more accurately for a better determination of the joint resistance.

6.3.3 Initial pressure loading

Figure 6.10 shows the displacement of the upper pancake coil as a function of the upwards force. A force of about 966 N is needed to lift the coil and the cylinder. This is higher than the $mg = 108$ N force due to gravity mentioned in section 6.2.2. An explanation for the difference is the fact the the force due to the three springs (figure 6.4) is not included in the force equation. From now on, 966 N is taken as a zero point for force on the sample:

$$F = I_p^2(a_1\Delta z + b_1) - I_p I_m(a_2\Delta z + b_2) - F_0 \tag{6.9}$$

with the coefficients a_1, b_1, a_2 and b_2 as in equation 6.4 and $F_0 = 966$ N.

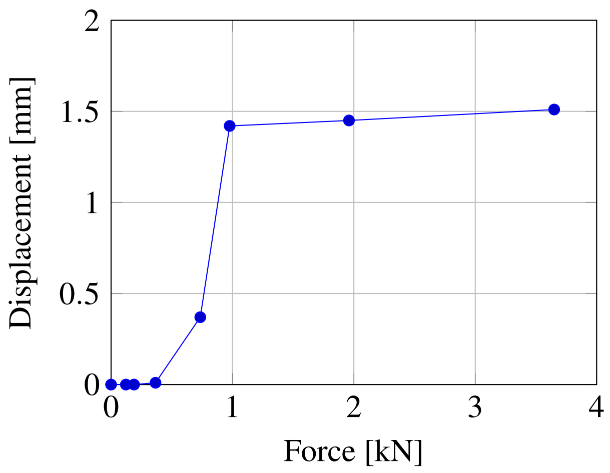

Figure 6.10: Displacement of the upper pancake coil at low forces.

6.3.4 Transverse pressure dependence of the critical current

After initial loading, the background magnet was ramped to 10.5 T ($I_m = 84.4$ A). In figure 6.11, the first successful IV-measurement is shown. The voltage could be measured over the current leads and over one strand near the horizontal section of the cable. Of the two remaining voltage pairs, one was used as input for the quench detector, and one did not yield useful data, possibly due to a short circuit. The voltage over the current leads shows a 6.5 nΩ resistive slope superimposed on the superconductor characteristic. This is consistent with the result from the current decay (6.3.2) and is hence likely due to the resistive joints. For computing the critical current, the voltage over the strand is used. As a sample length of 30 mm is assumed, the voltage

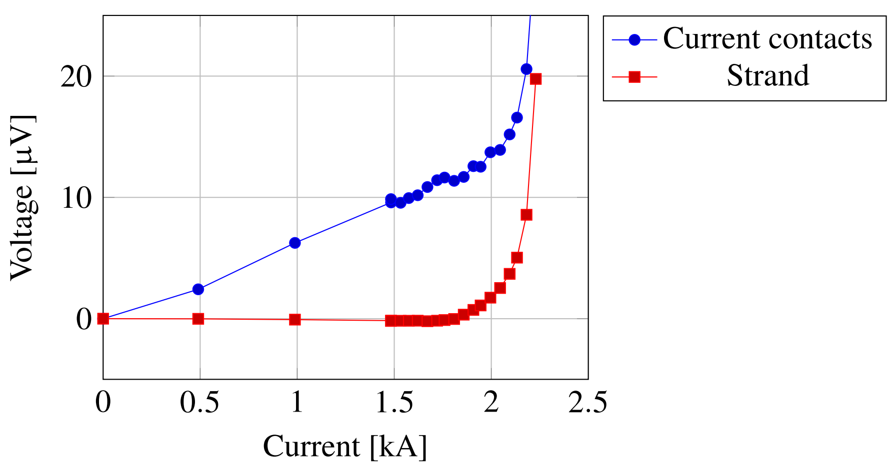

Figure 6.11: IV-curves made at a pressure of 4.09 MPa. The voltage was measured over the current contacts and over one strand near the horizontal section. The critical current is 2070 A.

criterion is 3 μV.

The initial critical current of the cable was 2.07 kA. For comparison, J. Fleiter measured a critical current of 2.4 kA in a similar cable in a 9.6 T magnetic field [25]. However, Fleiter's cable was made of a different batch of *RE*BCO tapes that had a lower critical current at 77 K. Also, the ratio of the critical current at $T = 77$ K, $B = 0$ T and $T = 4.2$ K, $B = 10.5$ T may be different for the two cables. This comparison can therefore not be used to verify that our cable was not damaged by impregnation.

Figure 6.12 shows the critical current as a function of the transverse stress. The transverse stress was calculated by dividing the force by the 12 mm × 30 mm sample area. The stress was increased in steps of about 10 MPa. At 262 MPa, the first degradation was observed, a decrease of about 4%. At 318 MPa, the critical current decreased by a further 21%. After the first degradation, each increase in pressure was followed by a measurement at 85 MPa. None of the degradation was reversible.

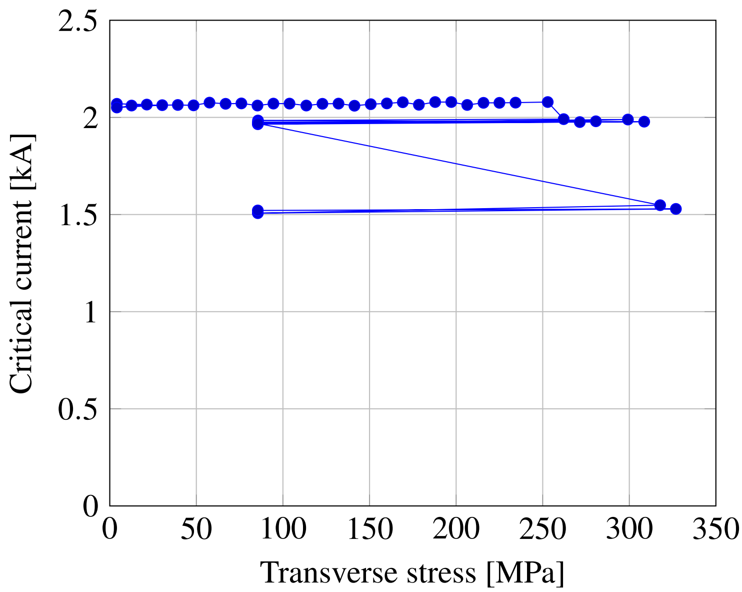

Figure 6.12: The critical current as a function of transverse stress.

The measurements show that the impregnated cable could withstand transverse pressures up to 253 MPa. This is a significant increase in strength compared to D. Uglietti's experiments [23], especially in view of the design requirement of approximately 150 MPa for accelerator magnets.

6.3.5 Microscopic analysis

In order to verify that also this impregnation went as planned and to check for possible damage due to the transverse stress, a cross-section of the sample was made for optical inspection. The cable and the pushing block to which it was still glued were cast in epoxy. Material was removed by sanding until the pressed section reached the surface. The surface was polished and pictures were made using an optical microscope.

Figure 6.13 shows an overview of the cable cross-section. The impregnation quality of the cable looks good; there are no bubbles visible. In the Stycast layer with which the block was glued to the cable, there are some holes because no vacuum was used. The thickness of the whole structure is close 1.45 mm over the entire width. Including the 50 µm Kapton insulation, the distance between the sample holder and pushing block was 1.50 mm, as designed.

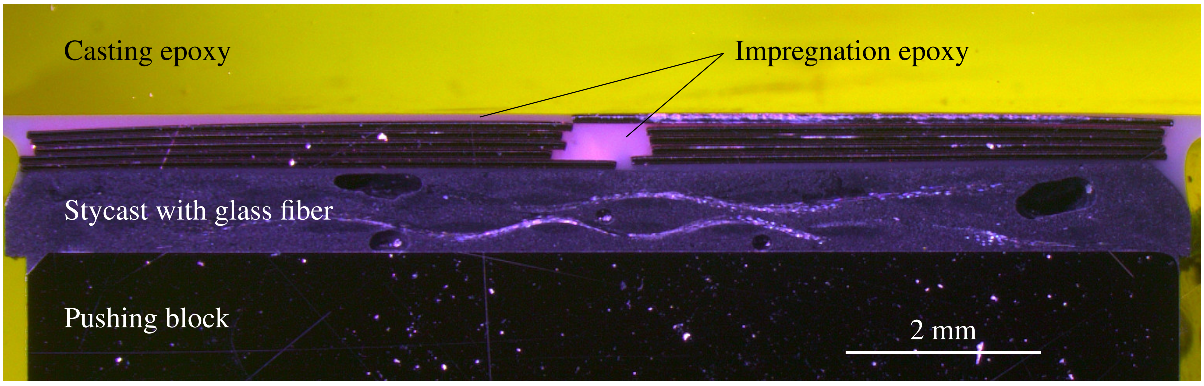

Figure 6.13: Overview of the cross-section. The upper surface was on the sample holder.

Note that the impregnated cable by itself is thicker on the left than on the right, probably because the Teflon block was not exactly parallel to the sample holder. The difference in height is corrected by glueing the pushing block using the positioning plates.

The only visible damage is delamination of the tapes closest to the sample holder. It's clearly visible in figure 6.14. The delamination may have occurred when the cable was removed from the sample holder. This was the only step in which a 'pulling' force was needed. Since the cross-section was made after many steps (cable assembly, impregnation, cool-down, pressure test, warming-up and finally removal from the sample holder), we cannot be entirely sure when the delamination occurred.

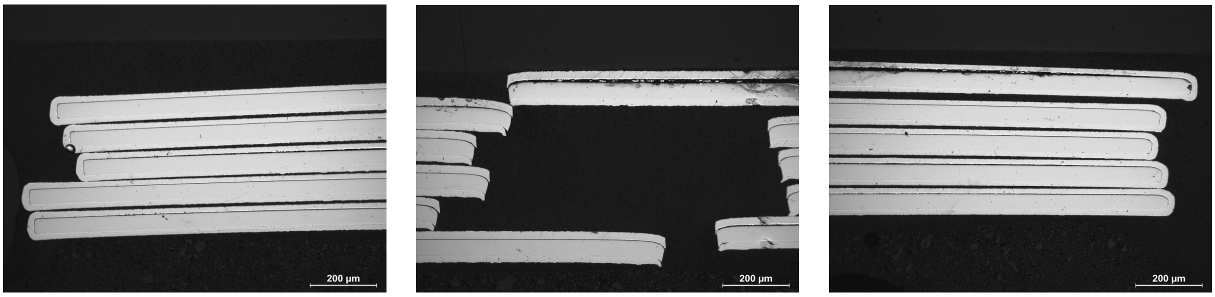

Figure 6.14: Close-ups of the left end, the central hole and the right end. Delamination is visible in the upper right tape.

6.3.6 Discussion

As shown in figure 6.7d, the pushing block is glued to the cable using Stycast epoxy. At the writing of this report, a remaining point of discussion is the bond between the pushing block and the stainless steel plates besides the sample. If the block is glued to these plates, a part of the force is directly transferred to the sample holder, leading to a lower pressure on the cable. To avoid a strong bond, both the pushing block and the plates were covered with Kapton polyimide tape. This tape has a silicone adhesive, which has a relatively low lap-shear strength of 1.7-3.4 MPa [64, p. 171]. On both sides of the pushing block, an area of 12 mm $\times$ 30 mm is facing the side plates. Assuming that the entire area is glued, the bond could transmit a force of:

$$2 * 12 \text{ mm} * 30 \text{ mm} * 3.4 \text{ MPa} = 2.5 \text{ kN} \tag{6.10}$$

This corresponds to a maximum error of 6.8 MPa in the sample pressure, 2.7% compared to its 253 MPa strength. In reality, not the entire area was glued, so the error should be lower.

A second discussion point is that the pressed section (30 mm) is shorter than the transposition length (126 mm). In the pressed section, only four out of ten strands have a ‘bridge’ from one side of the cable to the other, which is where stress concentrations occur. As a result, the measured degradation would be lower than in the case of a longer pushing block. This should however not affect the point of onset of the degradation.

6.4 Conclusion

A *RE*BCO Roebel cable was vacuum impregnated with a mixture of epoxy resin and fused silica powder. The impregnated cable was tested in a transverse press set-up at $T = 4.2$ K, $B_\perp = 10.5$ T. The initial critical current was 2070 A. Pressures up to 327 MPa were applied to a

30 mm long pushing block, which was glued onto the cable. No degradation was observed for pressures up to 253 MPa. After further loading to 327 MPa, the critical current decreased by 21%. The degradation was not reversible.

These results provide a first encouraging indication that suitably impregnated *RE*BCO Roebel cables can indeed withstand the transverse pressure levels occurring inside the winding pack of a dipole-type accelerator magnet.

Chapter 7

Conclusions and recommendations

The aim of this assignment was to find out whether impregnated *RE*BCO Roebel cables can withstand the transverse stresses up to 150 MPa in an accelerator magnet. Before the stress test could be done, a suitable impregnation material and method had to be found, and the effect of out-of-plane bending needed to be determined. A new U-shaped sample holder for the press was constructed according to the measured bending properties. A *RE*BCO Roebel cable was impregnated on this sample holder, and subjected to pressures up to 327 MPa.

In chapter 3 and 4, impregnation materials and techniques were discussed. A mixture of high-temperature processed epoxy and fused silica was found to be suitable for the cable examined in this work. Using vacuum impregnation, a dummy cable was successfully impregnated with this material. The critical current of a dummy cable with one superconducting strand was not affected by impregnation.

The out-of-plane bending experiments on two Roebel cables were described in chapter 5. Bending to radii as low as 10 mm hardly damaged the cable. Based on these results, a new sample holder for the transverse press was designed with bends of 20 mm radius.

The central question of the assignment was addressed in chapter 6. Here the measurements of an impregnated Roebel cable in a transverse stress set-up with superconducting transformer were described. A new technique was used to apply homogeneous transverse loads to samples with an inhomogeneous thickness. Transverse stresses up to 253 MPa did not damage the cable. This is a significant improvement compared to previous measurements of bare Roebel cables. Also, it is a first indication that a suitably impregnated Roebel cable can withstand the stress levels of 150 MPa in a future accelerator magnet.

At the time of writing, this project is still work in progress. One sample has now been finished, but at least two more will be measured. The next measurement will be a repetition of the first one, but with shorter side plates. This will be done to have more data and to address the discussion point described in section 6.3.6. Secondly, a cable with a different lay-out will be tested; it will consist of nine strands instead of ten. Recent work by J. Fleiter has shown that the number of strands influences the effective area of the cable under a transverse load [65]. A cable with nine strands was found to have a much smaller effective area than one with ten strands. With the test of a nine-strand cable we aim to determine whether the effective area can predict the transverse strength of impregnated cables.

Accelerator magnets need to function for many years, without degrading under their own Lorentz forces. Therefore, the effect of repeated loading on Roebel cables must also be investigated. This is in principle possible in the current set-up, but it would take a lot of time since the press is manually operated. For such measurements, some automation would be an improvement.

Acknowledgements

I would like to thank everybody who made this project possible. In particular I would like to thank my direct supervisors Marc Dhallé and Anna Kario. I would like to thank Wilfried Goldacker and Marcel ter Brake for giving me the opportunity to work in their groups. I also thank the technicians Brigitte Runtsch, Andrea Kling, Uwe Walschburger, Bernd Ringsdorf and Sander Wessel. Your work was essential for all experiments. Among other things, I thank Brigitte for help with optical microscopy, Andrea for preparation of the cables and the bending tests, Uwe for construction of the equipment for bending and impregnation, Bernd for the characterisation of strands at 77 K and Sander for the modifications to the transformer press set-up and help with operation. The measurements for the characterisation of epoxy resins were performed by Nadezda Bagrets and Sandra Drotziger, I thank them for that. Thanks Rainer Nast for preparation of the samples for the chemical compatibility tests. And thanks Peng Gao for all the measurements we did together. Finally, I would like to thank Hubert Wilbers from Huntsman corporation for providing free samples of their epoxy resins and Quarzwerke for supplying the fused silica powder.

Appendix A

Impregnation procedure

In this appendix the impregnation procedure is described which was used for successful impregnation of the sample discussed in section 4.4. The amount of filler is 50 wt% of the total mixture weight.

Materials:

- 30 cm Roebel dummy
- 2×5 cm of stainless steel tape with 12 mm $\times$ 0.1 mm cross-section
- 30 g Araldite CY5538 (resin)
- 30 g Araldur HY5571 (hardener)
- 60 g fused silica powder Silbond FW600 EST (4 µm median particle size)
- Copper wire and Kapton tape to fix the sample
- Vacuum equipment: pump, valve, tubes and pressure gauge
- Vacuum mixing set-up: flask with thermocouple and connection to a vacuum pump, heater with magnetic stirrer (figure A.1a)
- Spoon, cups, scale, ethanol, acetone, ultrasonic cleaner, paper towels etc.

Method:

- Set the "vacuum oven" to 105 °C, aim for 80 - 90 °C inside the vacuum chamber
- Set the chemical dryer to 100 °C
- Clean the sample and the steel tapes in acetone in the ultrasonic cleaner for 15 minutes
- Put the sample on the sample holder between the two steel tapes, lay the thick Teflon sheet on top of it
- Force the lower section of the sample into a straight shape with copper wire (figure A.1c)

- Fix the rest of the sample to the sample holder with Kapton adhesive tape
- Attach the sample holder to the flange and insert it in the vacuum oven (also heat the resin container)
- Mix the resin, hardener and silica powder in a beaker and heat to 40 - 60 °C. It is the easiest to add the powder in small portions and mix it before adding the next one.
- Pour the contents in the vacuum flask, connect the vacuum pump and the thermocouple
- Evacuate to 30 mbar, turn on the magnetic stirrer and heat again to 60 °C
- When the foam has gone down, lower the pressure slowly to 1 - 2 mbar (just above the vapour pressure)
- Mix for about 30 minutes, until only a few gas bubbles are visible
- Remove the vacuum, and pour the mixture into the beaker
- Heat the mixture to 80 °C
- Remove the sample holder and resin container from the vacuum oven
- Add 20 ml of resin to the brass container with a syringe (resulting in $\sim$15 mm liquid level)
- Move the container into position for insertion (red line on the rod, then the distance from flange to the bottom of the container is 40 cm)
- Insert the set-up into the vacuum chamber and evacuate to 5 mbar
- Wait at least 5 minutes to degas the resin for the second time, wait some more if the temperature has not reached 80 °C
- Slowly raise the resin container until the sample hits the bottom (in $\sim$1 minute)
- Wait for 20 minutes
- Remove the vacuum and wait 20 minutes
- Remove the sample holder from the vacuum chamber
- Wait until the temperature has dropped to $<$ 60 °C
- Remove the sample slowly from the resin container,
- Add Teflon pieces on both sides to prevent the resin from falling out. You can stick them behind the copper wires used to straighten the cable (figure A.1d).
- Impregnation is finished: put excess resin in a cup
- Clean up the mess with ethanol/acetone/soap and paper towels. The flask and the resin container are best cleaned with acetone in the ultrasonic bath.
- Cure 24h/100°C in the chemical dryer

For the first few samples a curing temperature of 130 °C was used. This led to buckling of a tape in a sample not described in this report. After correspondence with Huntsman it was

(a) Vacuum flask with magnetic stirrer and thermocouple

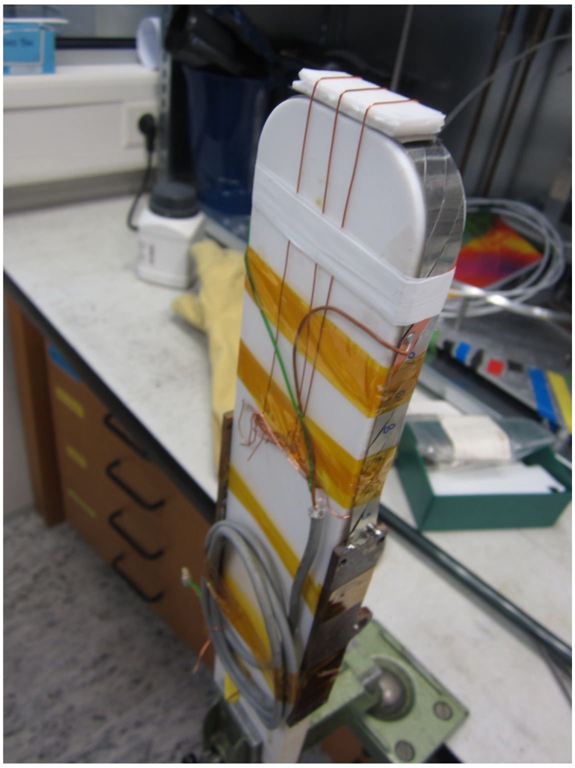

(b) Fully fixed sample

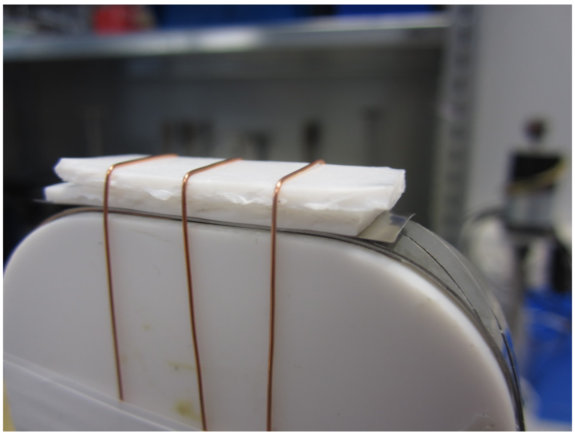

(c) Pressure is applied using piece of Teflon and copper wire

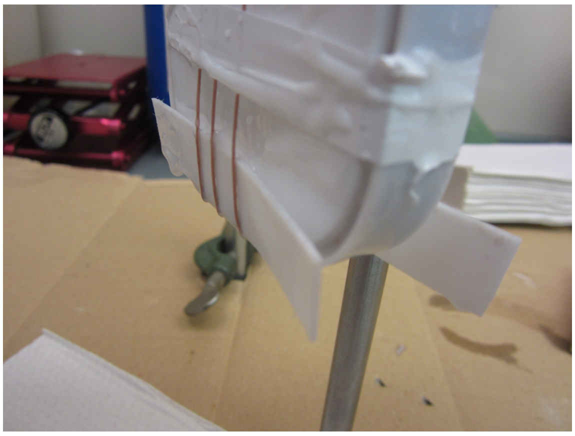

(d) Pieces of Teflon to prevent epoxy leaking out

Figure A.1

decided to use a lower curing temperature of 100 °C, to reduce thermal stresses after cool-down.

Appendix B

Press design

Note: The following appendix was written in an early stage of the project. It is therefore not totally up-to-date: for example, the use of glass fibre is still assumed. After measurements of the minimum bending radius of Roebel cables, it was found that a press geometry with a flat anvil should not pose problems. After that, the calculations done in this section were not very useful anymore, and I decided not to update them.

The original sample holder is not suitable for Roebel cables, as its bending radius of 10 mm is too low. The minimum bending radius for SuperPower *RE*BCO tapes is 11 mm [66]. At the start of this project is was forseen that for Roebel cables this value would be somewhat larger because the strands are already subjected to some torsion strain due to cable assembly. As shown in chapter 5, these expectations were overly pessimistic, which measured cables showing no significant degradation down to bending radii of 10 mm.

Several new designs with larger bending radii were considered (see table B.1 and figure B.1). Designs 1, 2 and 3 have a shorter straight section to increase the bending radius; 4, 5, 6 and 7 have no straight section at all and need a cylindrically shaped anvil. All designs have a total sample holder width of 66 mm, and the thickness of the sample is assumed to be 1.5 mm. The cable geometry is periodic over 12.6 mm. All anvils press over a whole number times this length.

Sample holders without straight section allow for a large bending radius, but they have some other problems:

- The perpendicular magnetic field component is not homogeneous over the pushing length, which means that the critical current is also not homogeneous over this section.

- The force is not perpendicular to the cable surface everywhere. This will lead to shear stress additional to transverse compressive stress. Shear stresses are undesirable because

Design	Bending radius [mm]	Straight section [mm]	Maximum angle	Anvil length [mm]	Pushing length [mm]
Original	10.0	46.0	0°	45.0	45.0
1	13.6	38.8	0°	37.8	37.8
2	19.9	26.2	0°	25.2	25.2
3	26.2	13.6	0°	12.6	12.6
4	33.0	0	41.9°	46.0	50.4
5	33.0	0	31.4°	35.9	37.8
6	33.0	0	20.9°	24.6	25.2
7	33.0	0	10.5°	12.5	12.6

Table B.1: Parameters for the seven new press designs.

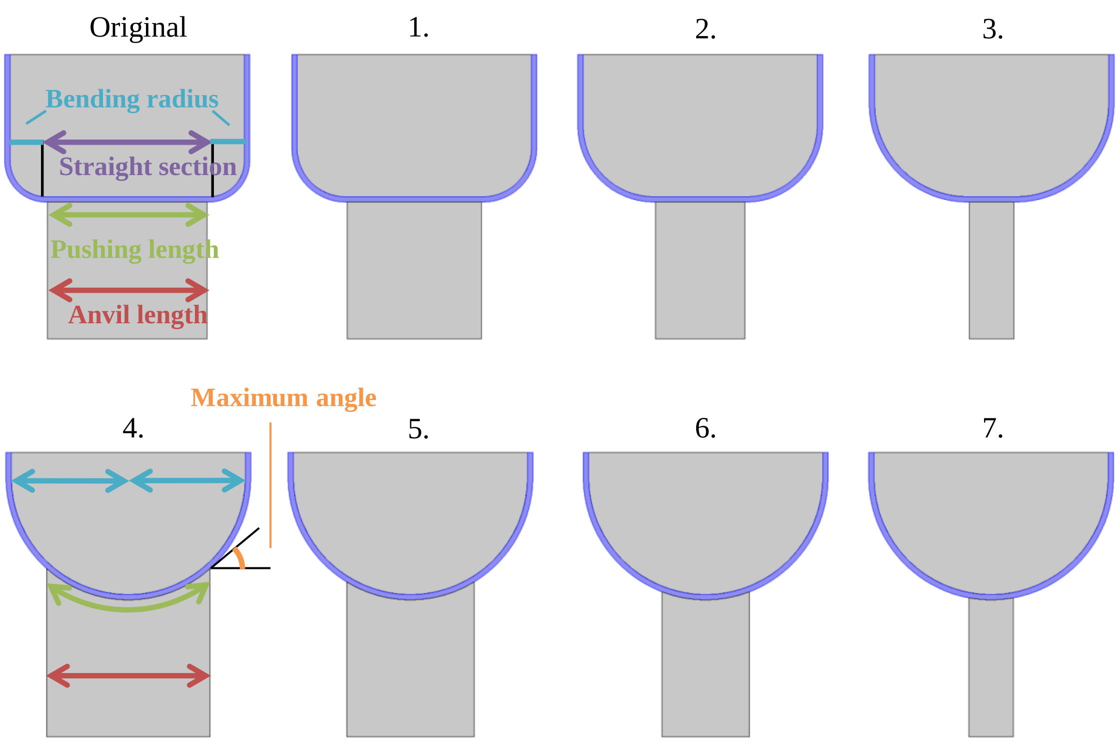

Figure B.1: Sketches of the different press designs. The 1.5 mm thick sample is in purple.

we want to assess the effect of pure transverse pressure. The shear stresses are computed using Comsol.

- The outside of the curved cable will have a slightly larger bending radius than the inside. This means that, in order to make a good fit, the anvil needs to have a slightly larger bending radius than the sample holder. This radius depends on the thickness of the sample, so once the anvil is made it can be used for only one specific thickness. If there is no good fit, the pressure will be concentrated in the center or at the ends of the anvil.

All these effects can be reduced by using a shorter anvil, decreasing the maximum angle between the surface of the cable and the force and magnetic field (e.g. design 7). However this will lead to a shorter section subjected to pressure.

A flat anvil seems much preferable. If we can prove that 19.9 mm bending radius does not destroy the cable, we can use design 2.

Comsol calculations on round-anvil designs

Geometries 4 to 7 were inserted into a 2D Comsol model. For the sample holder and the anvil, the material properties of stainless steel 304 at 4 K were used. Our cables will probably consist largely of fiber glass and epoxy resin, so I used the properties of G10 fiber glass epoxy for the sample.

Material	Density [kg m^{-3}]	Young's modulus [GPa]	Poisson's ratio
Stainless steel 304 (T = 4 K)	7860	210	0.279
G10 (room temperature)	1650	28	0.2 [1]

Table B.2: Relevant material properties from Ekin [67]

More details about the simulation:

- The linear elastic model is used from the structural mechanics module.
- A free triangular mesh is used with the element size set to "extremely fine" near the pressing surface and "finer" everywhere else.

[1] This value is not from Ekin but it is an educated guess. Because of the anisotropic nature of fiberglass-epoxy, the Poisson's ratio is actually dependent on the angle relative to the glass fibers. It ranges from 0.06 to 0.32 at room temperature, for T = 4 K I could not find any value.

- A stationary solver is used.
- The top of the sample holder has a fixed position. A pressure of 100 MPa is applied to the lower surface of the anvil part.

Comsol evaluates the Cauchy stress tensor $\boldsymbol{\sigma}$ in the entire geometry. The normal stress $\boldsymbol{\sigma_n}$ at the outer surface of the sample is computed by taking the dot product with the normal unit vector $\boldsymbol{n}$.

$$\boldsymbol{\sigma_n} = \boldsymbol{\sigma} \cdot \boldsymbol{n} = \begin{bmatrix} \sigma_{xx} & \sigma_{xy} \\ \sigma_{xy} & \sigma_{yy} \end{bmatrix} \begin{bmatrix} n_x \\ n_y \end{bmatrix} = \begin{bmatrix} n_x\sigma_{xx} + n_y\sigma_{xy} \\ n_x\sigma_{xy} + n_y\sigma_{yy} \end{bmatrix} \tag{B.1}$$

The magnitude of the normal stress is:

$$|\sigma_n| = \sqrt{(n_x\sigma_{xx} + n_y\sigma_{xy})^2 + (n_x\sigma_{xy} + n_y\sigma_{yy})^2} \tag{B.2}$$

The shear stress $\boldsymbol{\tau}$ is the stress parallel to the surface, so normal to the normal vector:

$$\boldsymbol{\tau} = \begin{bmatrix} \sigma_{xx} & \sigma_{xy} \\ \sigma_{xy} & \sigma_{yy} \end{bmatrix} \begin{bmatrix} n_y \\ -n_x \end{bmatrix} = \begin{bmatrix} n_y\sigma_{xx} - n_x\sigma_{xy} \\ n_y\sigma_{xy} - n_x\sigma_{yy} \end{bmatrix} \tag{B.3}$$

The magnitude of the shear stress is:

$$|\tau| = \sqrt{(n_y\sigma_{xx} - n_x\sigma_{xy})^2 + (n_y\sigma_{xy} - n_y\sigma_{yy})^2} \tag{B.4}$$

The computed normal and shear stresses for the different geometries are shown in figure B.2. The normal stress is close to the expected 100 MPa in the middle of the anvil, especially for the wider designs 4 and 5.

Both the shear stress and normal stress are the highest at the edges of the anvil, because of high local deformation. This effect is probably weaker in reality, because the edges are not “infinitely sharp” as in this model. Anyway, it makes sense to round the edges of the anvil slightly before using it.

The computed shear stress may be exaggerated in this model because the sample cannot move with respect to the sample holder and the anvil. It is as if the sample is glued between both parts. In reality the sample is not fixed to the anvil, and this will relieve part of the shear stress.

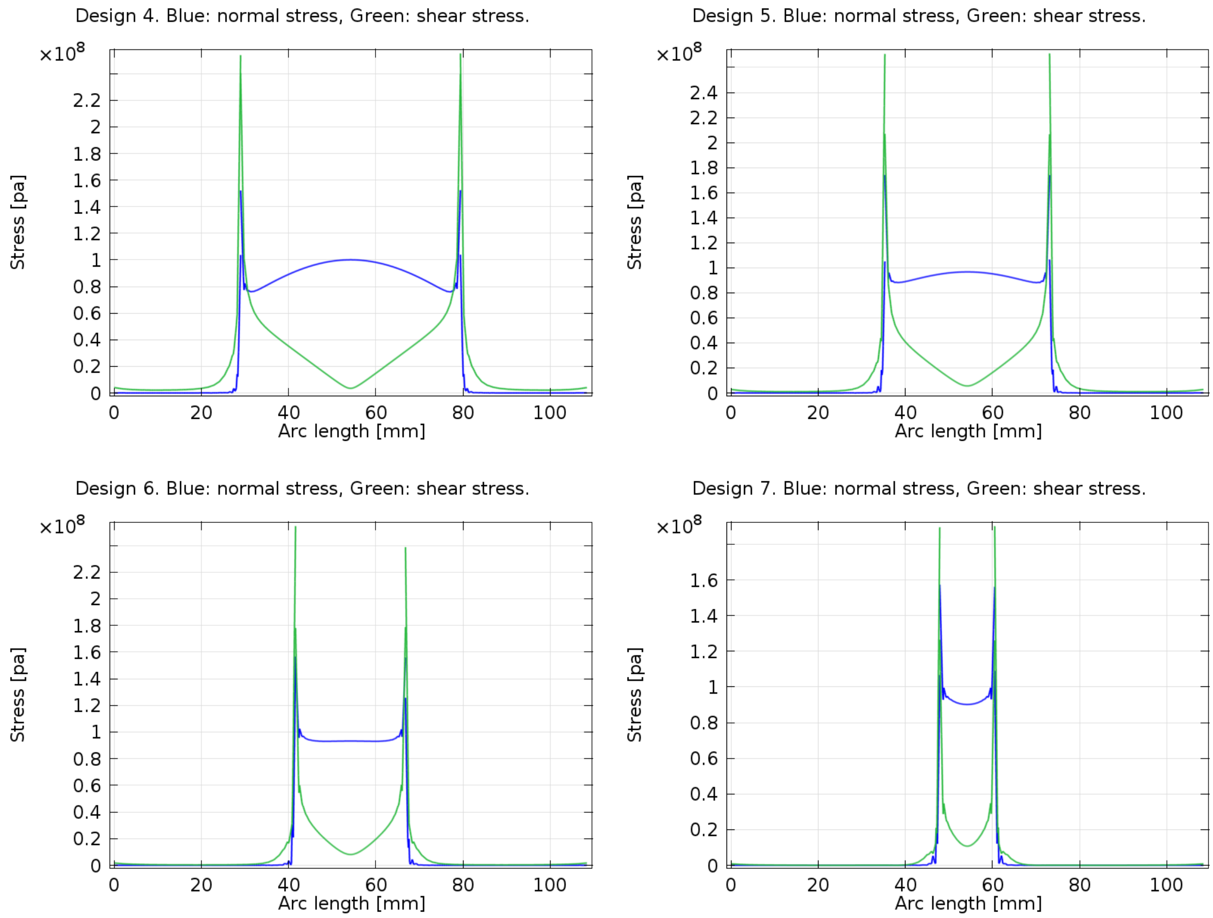

Figure B.2: Normal and shear stresses at the interface of the sample and the anvil for the different cylindrically shaped anvils, calculated using Comsol. The applied pressure is 100 MPa.

Appendix C

Technical drawings

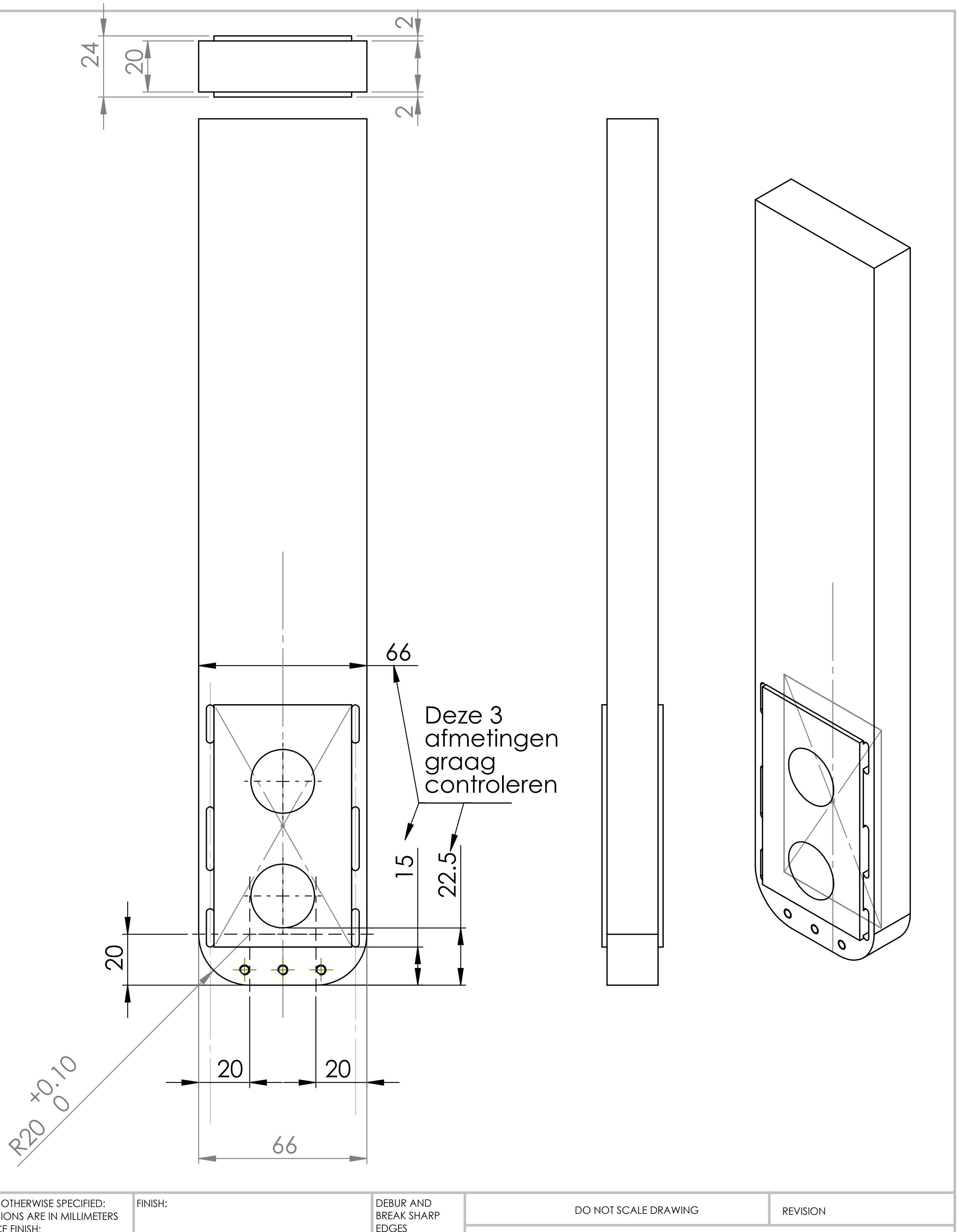

UNLESS OTHERWISE SPECIFIED: DIMENSIONS ARE IN MILLIMETERS SURFACE FINISH: TOLERANCES: LINEAR: ANGULAR:	FINISH:	DEBUR AND BREAK SHARP EDGES	DO NOT SCALE DRAWING / REVISION

	NAME	SIGNATURE	DATE
DRAWN			
CHK'D			
APPV'D			
MFG			
Q.A			

MATERIAL: Stainless steel 316L

WEIGHT:

TITLE:

Modified holder (1X)

DWG NO. original_holder

A4

SCALE:1:2

SHEET 1 OF 5

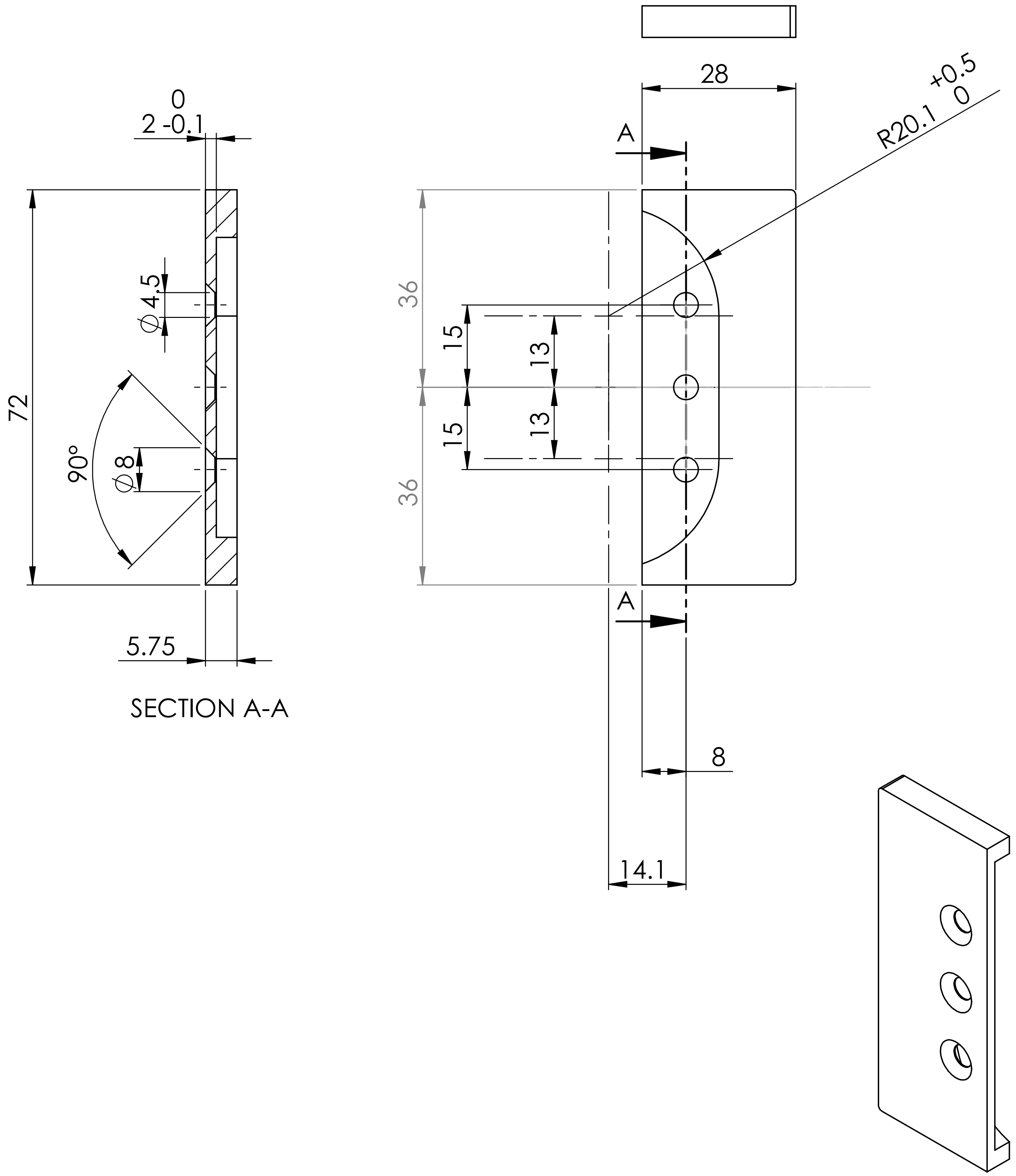

UNLESS OTHERWISE SPECIFIED:
DIMENSIONS ARE IN MILLIMETERS
SURFACE FINISH:
TOLERANCES:
LINEAR:
ANGULAR:

FINISH:

DEBUR AND BREAK SHARP EDGES

DO NOT SCALE DRAWING

REVISION

	NAME	SIGNATURE	DATE
DRAWN			
CHK'D			
APPV'D			
MFG			
Q.A			

TITLE:

Clamp plate (2X)

MATERIAL:

Stainless steel 316L

DWG NO.

original_holder

A4

WEIGHT:

SCALE:1:1

SHEET 2 OF 5

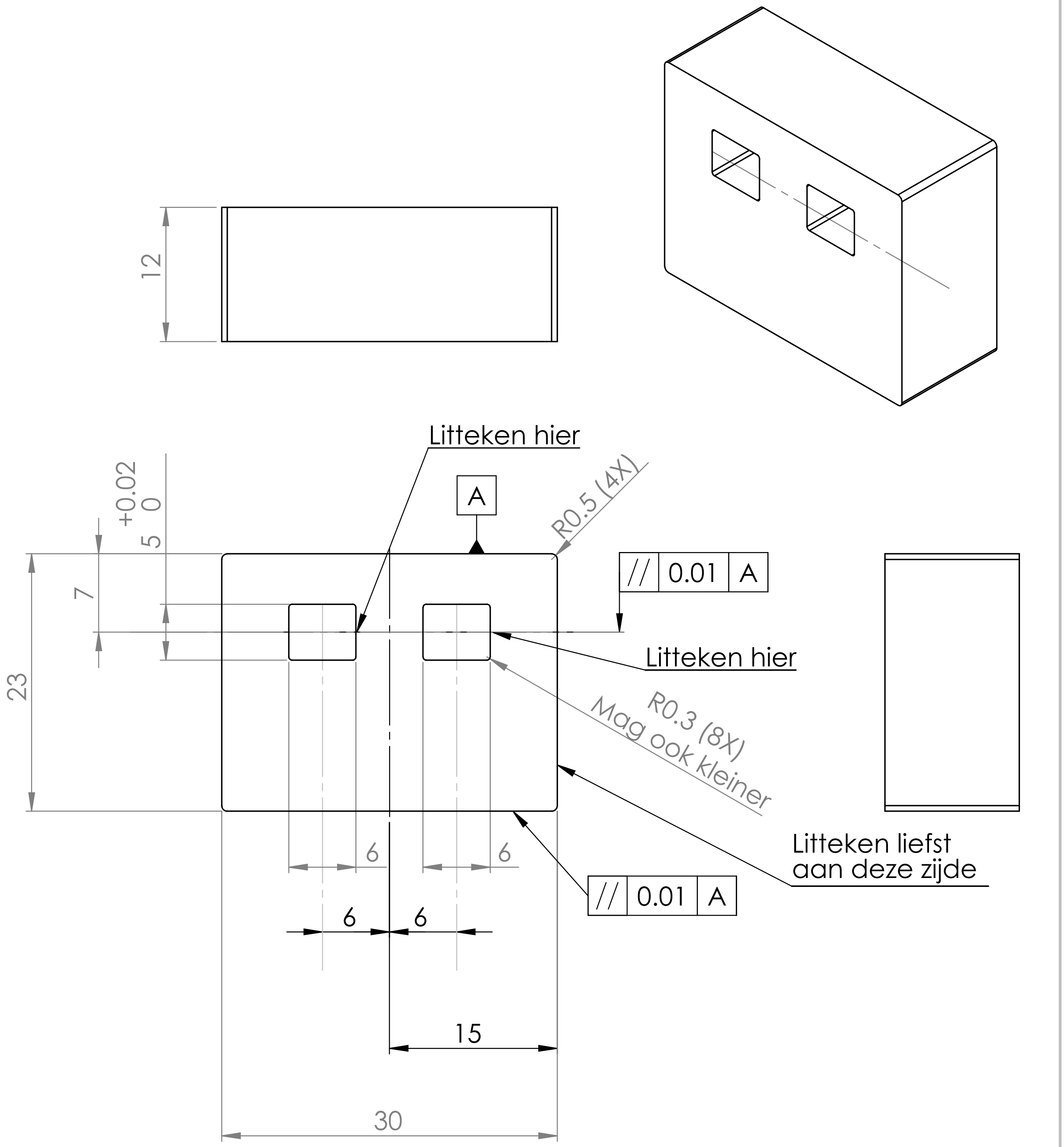

UNLESS OTHERWISE SPECIFIED:
DIMENSIONS ARE IN MILLIMETERS
SURFACE FINISH:
TOLERANCES:
LINEAR:
ANGULAR:

FINISH:

DEBUR AND BREAK SHARP EDGES

DO NOT SCALE DRAWING

REVISION

	NAME	SIGNATURE	DATE
DRAWN			
CHK'D			
APPV'D			
MFG			
Q.A			

TITLE:

Pushing block (1X)

MATERIAL:
Stainless steel 316L

DWG NO.
original_holder

A4

WEIGHT:

SCALE:2:1

SHEET 3 OF 5

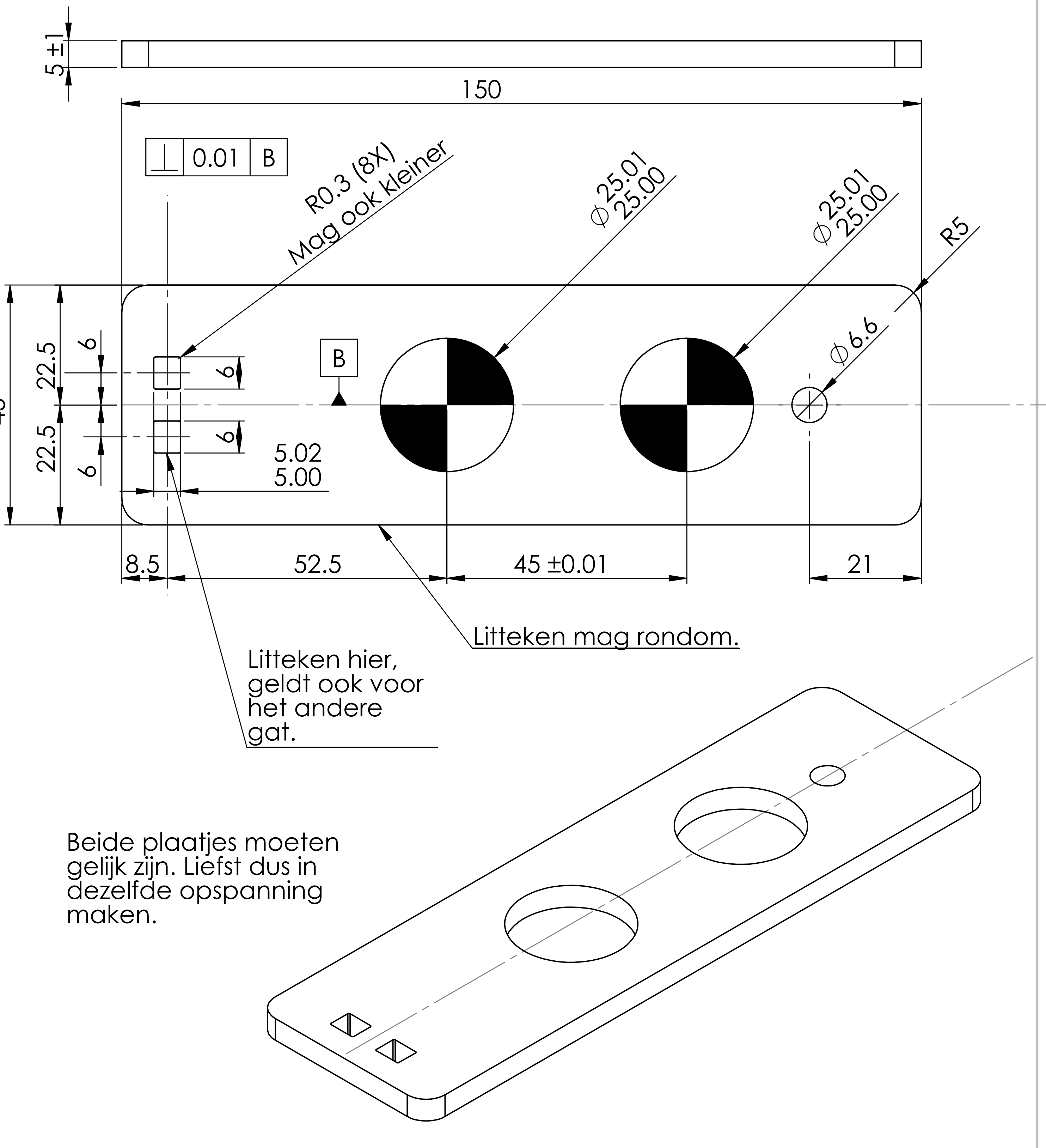

UNLESS OTHERWISE SPECIFIED: DIMENSIONS ARE IN MILLIMETERS SURFACE FINISH: TOLERANCES: LINEAR: ANGULAR:	FINISH:		DEBUR AND BREAK SHARP EDGES		DO NOT SCALE DRAWING	REVISION
	NAME	SIGNATURE	DATE		TITLE:	
DRAWN					Positioning plate (2X)	
CHK'D						
APPV'D						
MFG						
Q.A				MATERIAL: Stainless steel	DWG NO. original_holder	A4
				WEIGHT:	SCALE:1:1	SHEET 4 OF 5

Without pushing block

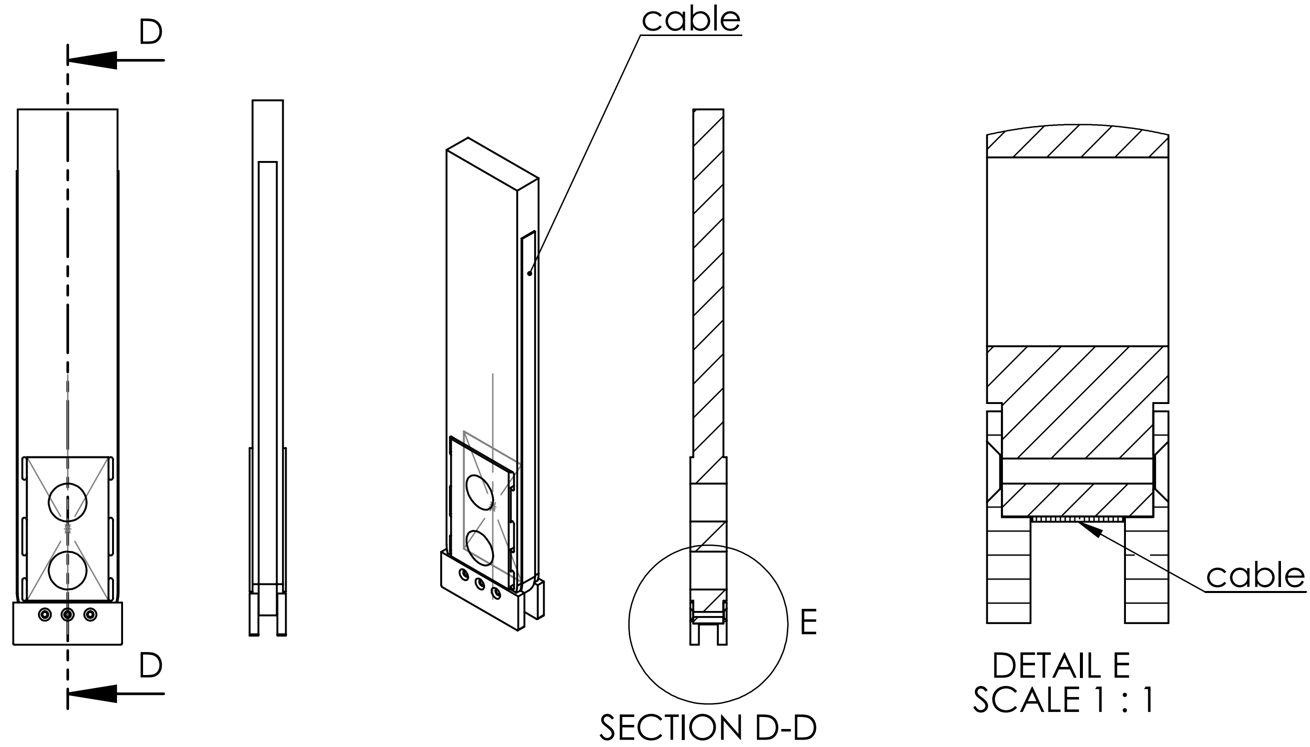

With pushing block and positioning plates

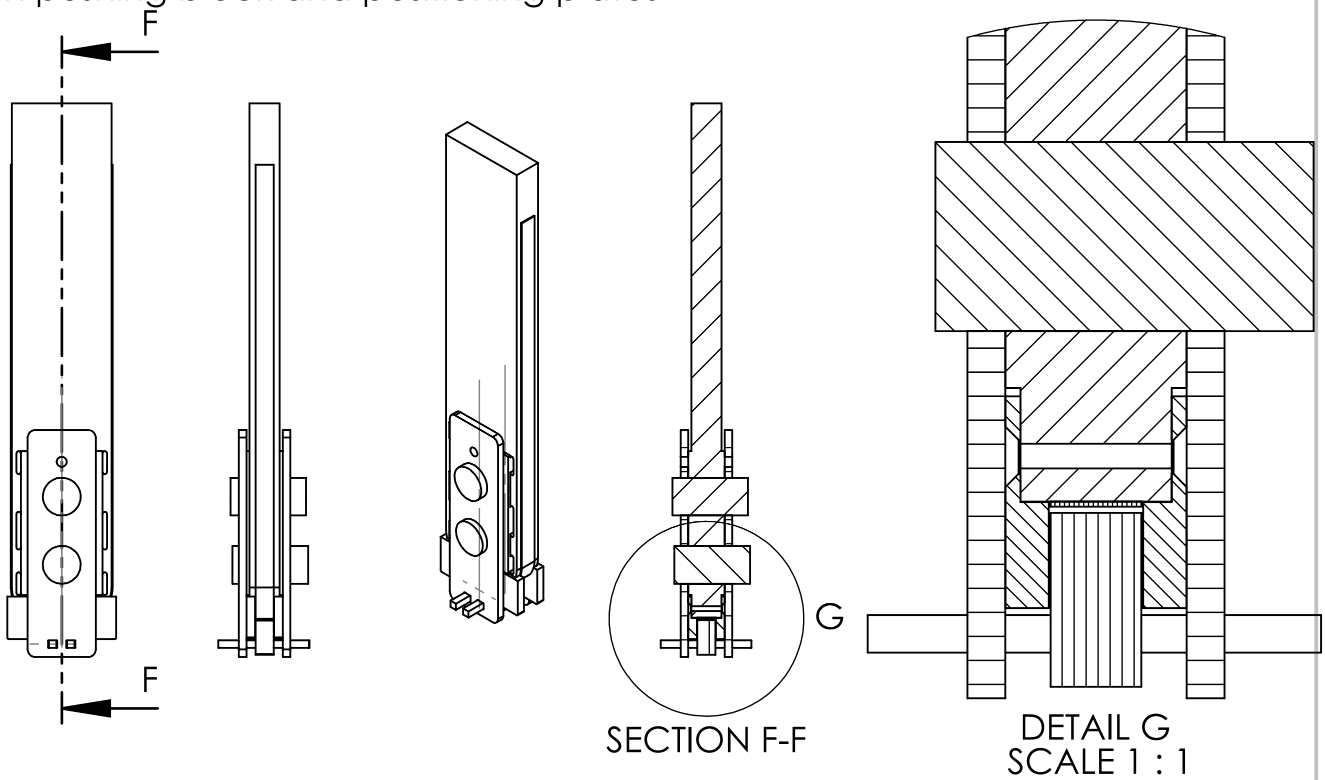

UNLESS OTHERWISE SPECIFIED: DIMENSIONS ARE IN MILLIMETERS SURFACE FINISH: TOLERANCES: LINEAR: ANGULAR:	FINISH:	DEBUR AND BREAK SHARP EDGES	DO NOT SCALE DRAWING	REVISION

	NAME	SIGNATURE	DATE			
DRAWN						
CHK'D						
APPV'D						
MFG						
Q.A				MATERIAL:		
				WEIGHT:		

TITLE:

Assembly

DWG NO. original_holder — A4

SCALE:1:5 — SHEET 5 OF 5

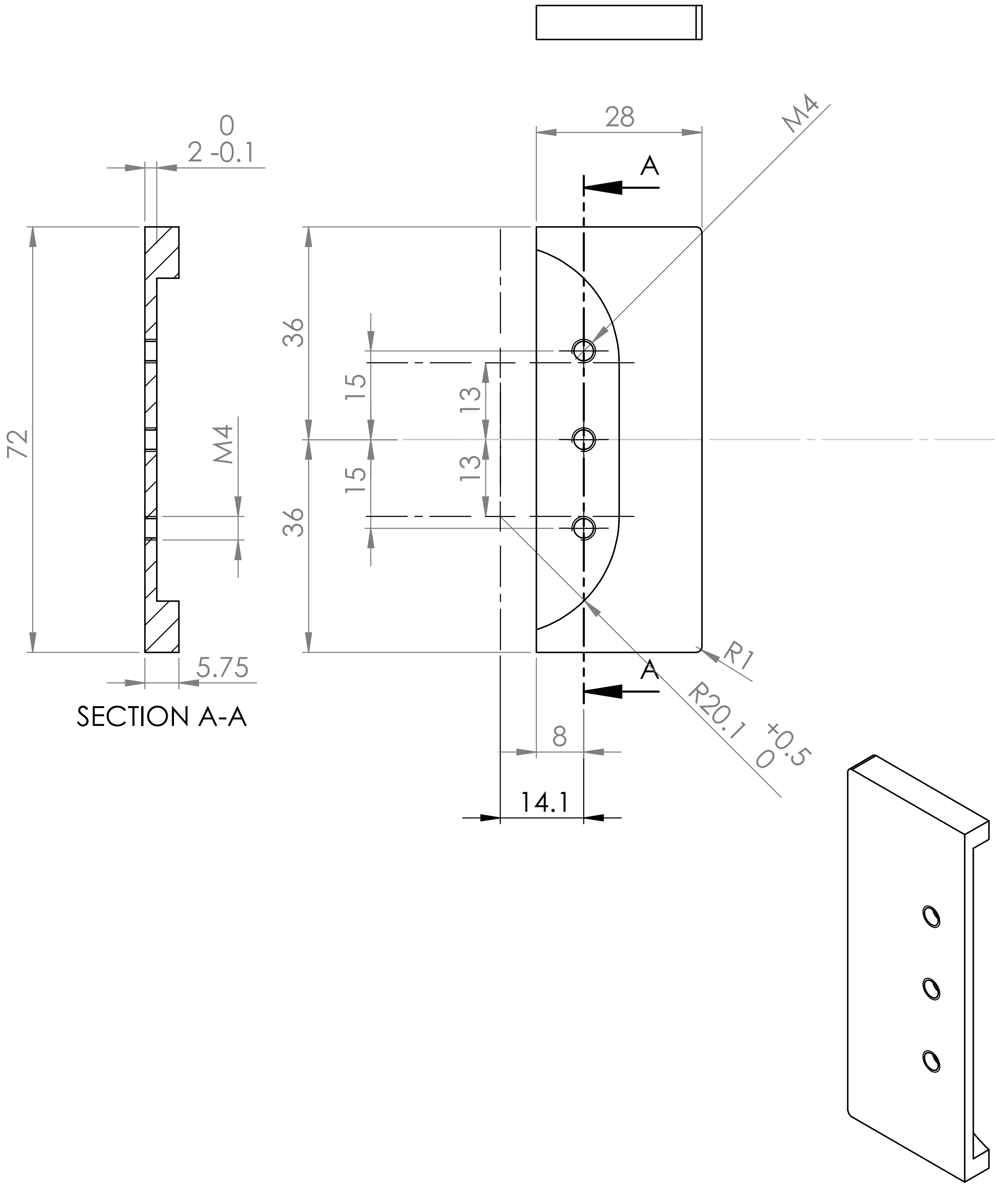

UNLESS OTHERWISE SPECIFIED: DIMENSIONS ARE IN MILLIMETERS SURFACE FINISH: TOLERANCES: LINEAR: ANGULAR:	FINISH:				DEBUR AND BREAK SHARP EDGES	DO NOT SCALE DRAWING	REVISION
	NAME	SIGNATURE	DATE			TITLE:	
DRAWN						Clamp plate met schroefdraad (3x)	
CHK'D							
APPV'D							
MFG							
Q.A				MATERIAL: Stainless steel 316L		DWG NO. clamp_plate_met_schroefdraad	A4
				WEIGHT:		SCALE:1:1	SHEET 1 OF 1

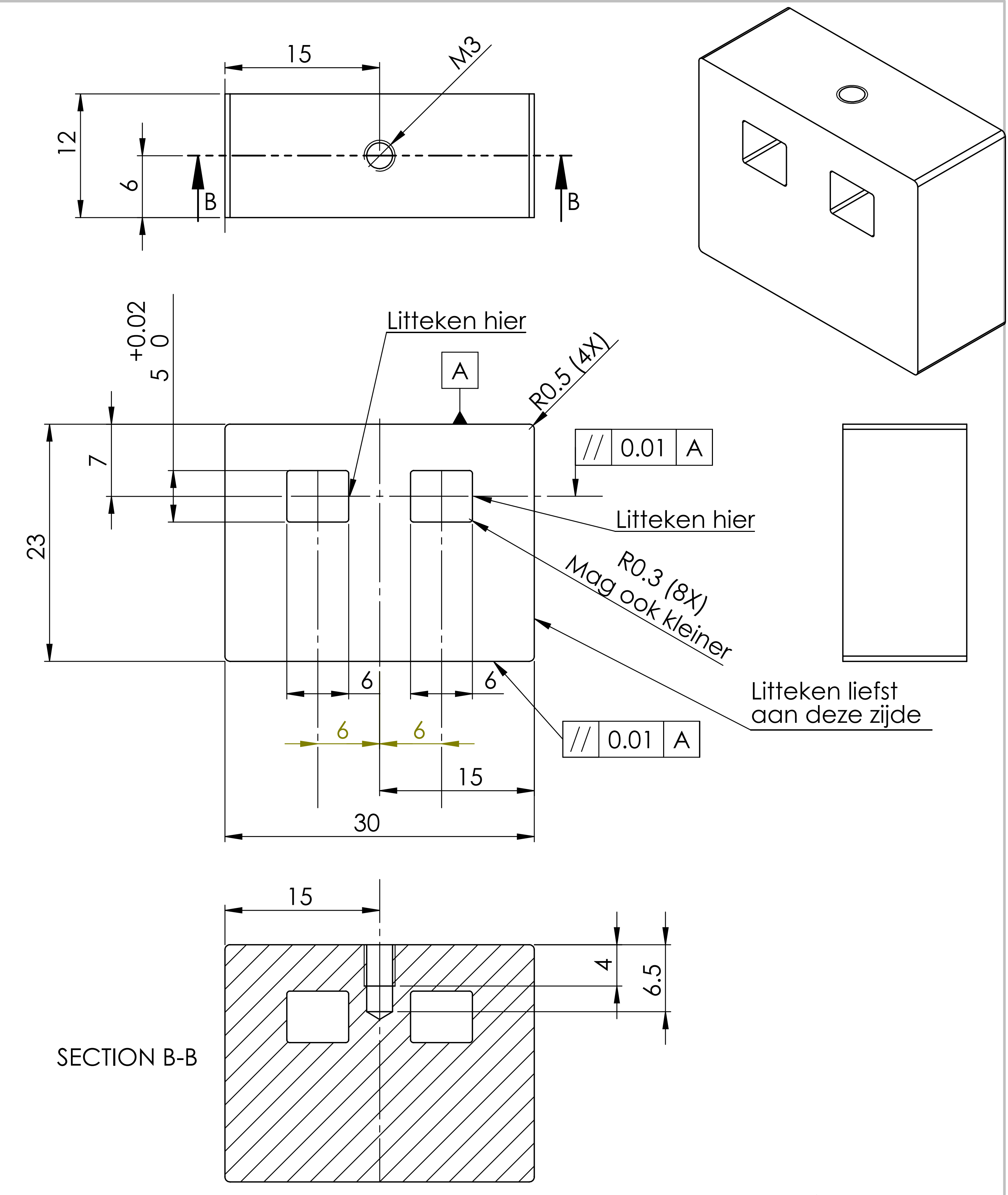

UNLESS OTHERWISE SPECIFIED:
DIMENSIONS ARE IN MILLIMETERS
SURFACE FINISH:
TOLERANCES:
LINEAR:
ANGULAR:

FINISH:

DEBUR AND BREAK SHARP EDGES

DO NOT SCALE DRAWING

REVISION

	NAME	SIGNATURE	DATE
DRAWN			
CHK'D			
APPV'D			
MFG			
Q.A			

MATERIAL:
Stainless steel 316L

WEIGHT:

TITLE:
Pushing block met schroefdraad (3X)

DWG NO. pushing_block_met_schroefdraad A4

SCALE:2:1

SHEET 1 OF 1

Bibliography

[1] H. ten Kate. *Large Hadron Collider and ATLAS: Superconductors for High Energy Physics*. Lecture slides for the course Applications of Superconductivity at Twente University. 2013.

[2] P. Lee. *The expanded ASC "Plots" page*. 2014. URL: http://fs.magnet.fsu.edu/~lee/plot/plot.htm.

[3] L. Bottura, G. de Rijk, L. Rossi, and E. Todesco. "Advanced Accelerator Magnets for Upgrading the LHC". In: *Applied Superconductivity, IEEE Transactions on* 22.3 (2012), p. 4002008. DOI: 10.1109/TASC.2012.2186109.

[4] A. Ball et al. *Future Circular Collider Study: Hadron Collider Parameters*. Specification FCC-1401101315-DSC. CERN, 2014.

[5] CERN. *EuCARD-2: Enhanced European Coordination for Accelerator Research & Development*. 2014. URL: http://eucard2.web.cern.ch/.

[6] M. K. Wu et al. "Superconductivity at 93 K in a new mixed-phase Y-Ba-Cu-O compound system at ambient pressure". In: *Phys. Rev. Lett.* 58 (9 1987), pp. 908–910. DOI: 10.1103/PhysRevLett.58.908.

[7] D. Dimos, P. Chaudhari, J. Mannhart, and F. K. LeGoues. "Orientation Dependence of Grain-Boundary Critical Currents in $YBa_2Cu_3O_{7-\delta}$ Bicrystals". In: *Phys. Rev. Lett.* 61 (2 1988), pp. 219–222. DOI: 10.1103/PhysRevLett.61.219.

[8] Y. Iijima et al. "Structural and transport properties of biaxially aligned $YBa_2Cu_3O_{7-x}$ films on polycrystalline Ni-based alloy with ion-beam-modified buffer layers". In: *Journal of Applied Physics* 74.3 (1993), pp. 1905–1911. DOI: 10.1063/1.354801.

[9] SuperPower Inc. *2G HTS Wire*. URL: http://www.superpower-inc.com/content/2g-hts-wire.

[10] X. Xiong et al. “Progress in High Throughput Processing of Long-Length, High Quality, and Low Cost IBAD MgO Buffer Tapes at SuperPower”. In: *Applied Superconductivity, IEEE Transactions on* 19.3 (2009), pp. 3319–3322. DOI: 10.1109/TASC.2009.2018816.

[11] H. ten Kate. *Pratical superconductors*. Lecture slides for the course Applications of Superconductivity at Twente University. 2013.

[12] M. Takayasu, F. Mangiarotti, L. Chiesa, L. Bromberg, and J. Minervini. “Conductor Characterization of YBCO Twisted Stacked-Tape Cables”. In: *Applied Superconductivity, IEEE Transactions on* 23.3 (2013), p. 4800104. DOI: 10.1109/TASC.2012.2234182.

[13] D. C. van der Laan. “Development of HTS Conductor on Round Core (CORC) cables for fusion applications at Advanced Conductor Technologies”. In: *1st Workshop on Accelerator Magnets in HTS, 21-23 May 2014, DESY* (2014).

[14] D. C. van der Laan, P. D. Noyes, G. E. Miller, H. W. Weijers, and G. P. Willering. “Characterization of a high-temperature superconducting conductor on round core cables in magnetic fields up to 20 T”. In: *Superconductor Science and Technology* 26.4 (2013), p. 045005. DOI: 10.1088/0953-2048/26/4/045005.

[15] W. Goldacker et al. “Roebel cables from REBCO coated conductors: a one-century-old concept for the superconductivity of the future”. In: *Superconductor Science and Technology* 27.9 (2014), p. 093001. DOI: 10.1088/0953-2048/27/9/093001.

[16] N. J. Long et al. “Development of YBCO Roebel cables for high current transport and low AC loss applications”. In: *Journal of Physics: Conference Series* 234.2 (2010), p. 022021. DOI: 10.1088/1742-6596/234/2/022021.

[17] G. Kirby et al. “Accelerator Quality HTS Dipole Magnet Demonstrator Designs for the EuCARD-2, 5 Tesla 40 mm Clear Aperture Magnet (unpublished)”. In: *Applied Superconductivity Conference 2014, Charlotte* (2014).

[18] J. van Nugteren et al. “Study of a 5 T Research Dipole Insert-Magnet using an Anisotropic ReBCO Roebel Cable (unpublished)”. In: *Applied Superconductivity Conference 2014, Charlotte* (2014).

[19] J. Ekin et al. “Transverse stress and fatigue effects in Y-Ba-Cu-O coated IBAD tapes”. In: *Applied Superconductivity, IEEE Transactions on* 11.1 (2001), pp. 3389–3392. DOI: 10.1109/77.919790.

[20] N. Cheggour et al. “Transverse compressive stress effect in Y-Ba-Cu-O coatings on biaxially textured Ni and Ni-W substrates”. In: *Applied Superconductivity, IEEE Transactions on* 13.2 (2003), pp. 3530–3533. DOI: 10.1109/TASC.2003.812390.

[21] N. Cheggour, J. Ekin, C. Thieme, and Y. Xie. “Effect of Fatigue Under Transverse Compressive Stress on Slit Y-Ba-Cu-O Coated Conductors”. In: *Applied Superconductivity, IEEE Transactions on* 17.2 (2007), pp. 3063–3066. DOI: 10.1109/TASC.2007.897918.

[22] T. Takao et al. “Characteristics of Compressive Strain and Superconducting Property in YBCO Coated Conductor”. In: *Applied Superconductivity, IEEE Transactions on* 17.2 (2007), pp. 3517–3519. DOI: 10.1109/TASC.2007.899654.

[23] D Uglietti, R Wesche, and P Bruzzone. “Effect of transverse load on the critical current of a coated conductor Roebel cable”. In: *Superconductor Science and Technology* 26.7 (2013), p. 074002. DOI: 10.1088/0953-2048/26/7/074002.

[24] L. Chiesa, N. Allen, and M. Takayasu. “Electromechanical Investigation of 2G HTS Twisted Stacked-Tape Cable Conductors”. In: *Applied Superconductivity, IEEE Transactions on* 24.3 (2014), pp. 1–5. DOI: 10.1109/TASC.2013.2284854.

[25] J Fleiter, A Ballarino, L Bottura, and P Tixador. “Electrical characterization of REBCO Roebel cables”. In: *Superconductor Science and Technology* 26.6 (2013), p. 065014. DOI: 10.1088/0953-2048/26/6/065014.

[26] W. Goldacker et al. “Status of high transport current ROEBEL assembled coated conductor cables”. In: *Superconductor Science and Technology* 22.3 (2009), p. 034003. DOI: 10.1088/0953-2048/22/3/034003.

[27] T. Takematsu et al. “Degradation of the performance of a YBCO-coated conductor double pancake coil due to epoxy impregnation”. In: *Physica C: Superconductivity* 470.1718 (2010), pp. 674 –677. DOI: 10.1016/j.physc.2010.06.009.

[28] C. Barth, N. Bagrets, K. P. Weiss, C. M. Bayer, and T. Bast. “Degradation free epoxy impregnation of REBCO coils and cables”. In: *Superconductor Science and Technology* 26.5 (2013), p. 055007. DOI: 10.1088/0953-2048/26/5/055007.

[29] D. C. van der Laan, J. W. Ekin, C. C. Clickner, and T. C. Stauffer. “Delamination strength of YBCO coated conductors under transverse tensile stress”. In: *Superconductor Science and Technology* 20.8 (2007), p. 765. DOI: 10.1088/0953-2048/20/8/007.

[30] Y. Yanagisawa et al. “Remarkable weakness against cleavage stress for YBCO-coated conductors and its effect on the YBCO coil performance”. In: *Physica C: Superconductivity* 471.1516 (2011), pp. 480 –485. DOI: 10.1016/j.physc.2011.05.003.

[31] W. Markiewicz et al. “Design of a Superconducting 32 T Magnet With REBCO High Field Coils”. In: *Applied Superconductivity, IEEE Transactions on* 22.3 (2012), pp. 4300704–4300704. DOI: 10.1109/TASC.2011.2174952.

[32] H. Park et al. “Mechanical and electric characteristics of vacuum impregnated no-insulation HTS coil”. In: *Physica C: Superconductivity (in press)* (2014). DOI: 10.1016/j.physc.2014.04.010.

[33] S. Matsumoto et al. “Generation of 24 T at 4.2 K using a layer-wound GdBCO insert coil with Nb_3Sn and NbTi external magnetic field coils”. In: *Superconductor Science and Technology* 25.2 (2012), p. 025017. DOI: 10.1088/0953-2048/25/2/025017.

[34] K. Mizuno, M. Ogata, and K. Nagashima. “An Innovative Superconducting Coil Fabrication Method with YBCO Coated Conductors”. In: *Quarterly Report of RTRI* 54.1 (2013), pp. 46–51. DOI: 10.2219/rtriqr.54.46.

[35] U. P. Trociewitz et al. “35.4T field generated using a layer-wound superconducting coil made of $(RE)Ba_2Cu_3O_{7x}$ (RE = rare earth) coated conductor”. In: *Applied Physics Letters* 99.20, 202506 (2011), p. 202506. DOI: 10.1063/1.3662963.

[36] Y. Yanagisawa et al. “Removal of degradation of the performance of an epoxy impregnated YBCO-coated conductor double pancake coil by using a polyimide-electrodeposited YBCO-coated conductor”. In: *Physica C: Superconductivity* 476.0 (2012), pp. 19 –22. DOI: 10.1016/j.physc.2012.01.025.

[37] G. Schwarz. “Thermal expansion of polymers from 4.2 K to room temperature”. In: *Cryogenics* 28.4 (1988), pp. 248 –254. DOI: 10.1016/0011-2275(88)90009-4.

[38] D. Chichili, J. Hoffman, and A. Zlobin. “Investigation of alternative materials for impregnation of Nb_3Sn magnets”. In: *Applied Superconductivity, IEEE Transactions on* 13.2 (2003), pp. 1792–1795. DOI: 10.1109/TASC.2003.812892.

[39] J Sandler et al. “Development of a dispersion process for carbon nanotubes in an epoxy matrix and the resulting electrical properties”. In: *Polymer* 40.21 (1999), pp. 5967 –5971. DOI: 10.1016/S0032-3861(99)00166-4.

[40] M. J. Biercuk et al. “Carbon nanotube composites for thermal management”. In: *Applied Physics Letters* 80.15 (2002), pp. 2767–2769. DOI: 10.1063/1.1469696.

[41] J. N. Coleman, U. Khan, W. J. Blau, and Y. K. Gunko. “Small but strong: A review of the mechanical properties of carbon nanotube-polymer composites”. In: *Carbon* 44.9 (2006), pp. 1624 –1652. DOI: 10.1016/j.carbon.2006.02.038.

[42] C. Wong and R. Bollampally. “Comparative study of thermally conductive fillers for use in liquid encapsulants for electronic packaging”. In: *Advanced Packaging, IEEE Transactions on* 22.1 (1999), pp. 54–59. DOI: 10.1109/6040.746543.

[43] N. Bagrets, E. Weiss, S. Westenfelder, and K.-P. Weiss. “Cryogenic Test Facility CryoMaK”. In: *Applied Superconductivity, IEEE Transactions on* 22.3 (2012), pp. 9501204–9501204. DOI: 10.1109/TASC.2011.2176902.

[44] Huntsman Advanced Materials. *Araldite Casting System, Araldite DBF Araldur HY 951*. 2005.

[45] Wikipedia. *Thermal Expansion*. URL: http://en.wikipedia.org/wiki/Thermal_expansion.

[46] The Engineering Toolbox. *Coefficients of Linear Thermal Expansion*. URL: http://www.engineeringtoolbox.com/linear-expansion-coefficients-d_95.html.

[47] Quantum Design. *PPMS (Physical Property Measurement System)*. May 2014. URL: http://www.lot-qd.de/uk/en/home/ppms/.

[48] N. Bagrets, W. Goldacker, S. I. Schlachter, C. Barth, and K.-P. Weiss. “Thermal properties of 2G coated conductor cable materials”. In: *Cryogenics* 61.0 (2014), pp. 8 –14. DOI: 10.1016/j.cryogenics.2014.01.015.

[49] C. Barth. “High Temperature Superconductor Cable Concepts for Fusion Magnets”. PhD Thesis. Karlsruhe Institute of Technology, 2013. DOI: 10.5445/KSP/1000035747.

[50] F. de Araujo and H. Rosenberg. “The thermal conductivity of epoxy-resin/metal-powder composite materials from 1.7 to 300 K”. In: *Journal of Physics D: Applied Physics* 9.4 (1976), p. 665. DOI: 10.1088/0022-3727/9/4/017.

[51] C. Tsai, H. Weinstock, and W. Overton Jr. “Low temperature thermal conductivity of stycast 2850FT”. In: *Cryogenics* 18.9 (1978), pp. 562 –563. DOI: 10.1016/0011-2275(78)90162-5.

[52] G. Willering, A. P. Verweij, J. Kaugerts, and H. ten Kate. “Stability of Nb-Ti Rutherford Cables Exhibiting Different Contact Resistances”. In: *Applied Superconductivity, IEEE Transactions on* 18.2 (2008), pp. 1263–1266. DOI: 10.1109/TASC.2008.920560.

[53] W. M. De Rapper, L.-R. Oberli, B. Bordini, E. Takala, and H. ten Kate. “Critical Current and Stability of High-J_c Nb_3Sn Rutherford Cables for Accelerator Magnets”. In: *Applied Superconductivity, IEEE Transactions on* 21.3 (2011), pp. 2359–2362. DOI: 10.1109/TASC.2010.2103549.

[54] C. Schmidt, A. Frank, W. Goldacker, A. Kling, and S. Terzieva. "Progress in assembling coated conductor cables by the Roebel technique (RACC)". In: *Physica C: Superconductivity* 469.1520 (2009). Proceedings of the 21st International Symposium on Superconductivity (ISS 2008), pp. 1422 –1426. DOI: 10.1016/j.physc.2009.05.050.

[55] X. Jin et al. "Study on the Mechanism of Preventing Degradation in the Performance of REBCO Coils". In: *Applied Superconductivity, IEEE Transactions on* 24.3 (2014), pp. 1–4. DOI: 10.1109/TASC.2013.2280714.

[56] W. Goldacker et al. "ROEBEL Assembled Coated Conductors (RACC): Preparation, Properties and Progress". In: *Applied Superconductivity, IEEE Transactions on* 17.2 (2007), pp. 3398–3401. DOI: 10.1109/TASC.2007.899417.

[57] H. ten Kate, B. ten Haken, S. Wessel, J. Eikelboom, and E. Hornsveld. "Critical Current Measurements of Prototype Cables for the CERN LHC up to 50 kA and between 7 and 13 Tesla Using a Superconducting Transformer Circuit". In: *11th International Conference on Magnet Technology (MT-11)*. Springer Netherlands, 1990, pp. 60–65. DOI: 10.1007/978-94-009-0769-0_9.

[58] G. Mulder, H. ten Kate, H. Krooshoop, and L. van de Klundert. "On the Inductive Method for Maximum Current Testing of Superconducting Cables". In: *11th International Conference on Magnet Technology (MT-11)*. Springer Netherlands, 1990, pp. 479–484. DOI: 10.1007/978-94-009-0769-0_82.

[59] W. Wessel. *Superconducting transformer for direct currents up to 50 kA*. Internal presentation at Twente University. 2011.

[60] H. ten Kate, W. Nederpelt, P. Juffermans, F. van Overbeeke, and L. van de Klundert. "A New Type of Superconducting Direct Current Meter for 25 kA". In: *Advances in Cryogenic Engineering*. Vol. 31. Advances in Cryogenic Engineering. Springer US, 1986, pp. 1309–1313. DOI: 10.1007/978-1-4613-2213-9_147.

[61] H. Weijers, A. Godeke, B. ten Haken, S. Wessel, and H. ten Kate. "Improved Superconducting Direct Current Meter for 25-50 kA". In: *Advances in Cryogenic Engineering*. Vol. 39. Advances in Cryogenic Engineering. Springer US, 1994, pp. 1147–1152. DOI: 10.1007/978-1-4615-2522-6_140.

[62] H. Boschman, A. Verweij, S. Wessel, H. ten Kate, and L. J. M. Van de Klundert. "The effect of transverse loads up to 300 MPa on the critical currents of Nb_3Sn cables [for LHC]". In: *Magnetics, IEEE Transactions on* 27.2 (1991), pp. 1831–1834. DOI: 10.1109/20.133551.

[63] W. van de Camp. "Critical current versus transverse stress and thermal stability of a RRP Nb_3Sn Rutherford cable". Master thesis. Twente University, 2012.

[64] S. Ebnesajjad. "Characteristics of Adhesive Materials". In: *Handbook of Adhesives and Surface Preparation*. Ed. by S. Ebnesajjad. Plastics Design Library. Oxford: William Andrew Publishing, 2011, pp. 137 –183. DOI: 10.1016/B978-1-4377-4461-3.10008-2.

[65] J. Fleiter, A. Ballarino, W. Goldacker, and A. Kario. "Characterization of Roebel Cables for Potential use in High-Field Magnets (unpublished)". In: *Applied Superconductivity Conference 2014, Charlotte* (2014).

[66] D. W. Hazelton, Y. Y. Xie, Y. Qiao, E. Zhang, and V. Selvamanickam. "SuperPowers Second Generation HTS Conductor Design for Stability and Low AC Losses". In: *AIP Conference Proceedings* 824.1 (2006), pp. 859–868. DOI: 10.1063/1.2192434.

[67] J. Ekin. *Experimental Techniques for Low-Temperature Measurements: Cryostat Design, Material Properties and Superconductor Critical-Current Testing*. OUP Oxford, 2006.